MINISTRY OF EDUCATION
FEDERAL UNIVERSITY OF RIO GRANDE DO SUL
GRADUATE PROGRAM IN MECHANICAL ENGINEERING

EVALUATION OF THE WSGG MODEL FOR COUPLED CALCULATIONS OF LAMINAR DIFFUSION FLAMES

by

Pedro Wink Guaragna

A Qualification Dissertation for the degree of
Master in Engineering

Porto Alegre, September 2022

EVALUATION OF THE WSGG MODEL FOR COUPLED CALCULATIONS OF LAMINAR DIFFUSION FLAMES

by

Pedro Wink Guaragna
Mechanical Engineer

A Qualification Dissertation submitted to the committee of the Graduate Program in Mechanical Engineering (PROMEC), from the Engineering School of the Federal University of Rio Grande do Sul (UFRGS), as part of the necessary requirements to obtain the degree of

Master in Engineering

Field of Study: Transport Phenomena

Advisor: Prof. Dr. Francis Henrique Ramos França
Co-advisor: Prof. Dr. Guilherme Crivelli Fraga

Evaluation Committee:

Prof. Dr. Fernando Marcelo Pereira ..... PROMEC / UFRGS

Prof. Dr. Felipe Roman Centeno ..... PROMEC / UFRGS

Prof. Dr. Amir Antônio Martins Oliveira Jr. ..... POSMEC / UFSC

Prof. Dr. Fernando Marcelo Pereira
Coordinator of PROMEC

Porto Alegre, September 2022

"Why do we fall, sir? So that we can learn how to pick ourselves up."

Michael Caine as Alfred Pennyworth,
Batman Begins

AKNOWLEDGMENTS

Esse trabalho não seria possível sem a ajuda de professores, colegas, amigos e familiares. Professores em especial aos meus orientadores Francis e Guilherme pela disposição, contribuições e dedicação durante a realização deste trabalho. Agradeço também ao colega Fredherico da Silva pelo apoio com o software CHEM1D, assim também ao colega Alexandre Selhorst pelo apoio em modelagens WSGG.

Gostaria de agradecer a toda equipe do Departamento de Engenharia Mecânica da UFRGS pelo auxílio institucional. Ao PROMEC, agradecimento especial pela dedicação e mobilização para manter as aulas e funcionamento durante a pandemia. Agradeço a STIHL que juntamente ao PROMEC foram flexíveis para que eu pudesse me dedicar mutuamente ao trabalho e ao estudo.

Aos meus amigos Carolina e Rafael que como sempre nos últimos 10 anos estiveram ao meu lado, me apoiando nos bons e maus momentos.

Por último e mais importante, deixo meu mais caloroso obrigado aos meus pais, Guilherme e Rosangela, que dedicaram suas vidas para criarem um ambiente amoroso e com oportunidades para eu me tornar quem sou hoje. Aos meus irmãos e irmã pelo companheirismo. Aos meus afilhados Felipe e Catarina por me ensinarem a ser criança novamente. A minha noiva Natália pelo amor e apoio que me deram energias para seguir em frente.

Para todos que de maneira direta ou indireta contribuíram para o sucesso de mais essa etapa da minha vida: muito obrigado!

RESUMO

A radiação nos meios participantes é um fenômeno que resulta do alargamento das linhas espectrais consequência de transições dos modos de energia entre vibração e rotação em nível atômico, sendo, portanto, um efeito altamente dependente da concentração de espécies e temperatura, e sua relevância em casos de alta temperatura foi demonstrado experimentalmente, teoricamente e numericamente. O presente estudo visa explorar diferentes abordagens para a solução da transferência de calor radiativa acoplada às reações químicas e equações de transporte de chamas de difusão laminar. Para isto, o software CHEM1D foi aplicado para o cálculo de chamas contra-fluxo unidimensionais. Embora a aplicação já tenha em seu código um modelo de gás cinza de limite óptico fino (OTA), o presente trabalho implementou o modelo do gás cinza (GG) e o modelo da soma ponderada de gases cinzas (WSGG), bem como o método de integração linha por linha (LBL). Para o modelo WSGG, diferentes correlações de coeficientes para absorção e ponderação disponíveis na literatura foram incluídas neste estudo. Comparações dessas quatro abordagens foram o foco desta dissertação mudanças na taxa de deformação (que representa a velocidade dos reagentes) e na diluição do CO_2 no lado do combustível. Devido à sua exatidão no cálculo da dependência espectral das propriedades radiativas, o LBL é considerado a solução de referência com a qual os três modelos foram comparados. As principais variáveis avaliadas foram o termo máximo da fonte de calor radiativo, a perda total de calor por radiação e a concentração da espécie de monóxido de carbono. Os modelos WSGG mostram-se em todos os casos apresentados melhor para estimar as variáveis propostas, com resultados de formulações deste modelo que contabilizam separadamente as espécies participantes tendo um desempenho geral aceitável. Após essas comparações, foi feito um estudo investigando os limites de extinção dos modelos e do LBL, com diluições sendo aumentadas até a extinção da chama devido às perdas radiativas para diferentes taxas de deformação. Os resultados são comparados com dados experimentais da literatura, e mostra-se que algumas formulações WSGG com maior complexidade embora tenham melhores resultados anteriormente, não possuem robustez para alcançar convergência em maior diluição de CO_2. Para as reações químicas foi utilizado um uma versão reduzida do GRI-MECH 1.2 com 19 espécies, incluindo N_2 e AR e com 84 reações.

Palavras-chave: Chamas não pré-misturadas; Modelos de radiação; Chama unidimensional; modelo de soma ponderada de gases cinzas; integração linha a linha.

ABSTRACT

Radiation in participating media is a phenomenon that results from the broadening of spectral lines consequence of the transitions of energy modes between vibration and rotation in atomic level, therefore being an effect highly dependent of species concentration and temperature, and its relevance in several high-temperature problems has been demonstrated experimentally, theoretically, and numerically. This present study aims to explore different approaches for the solution of the radiative heat transfer coupled with the chemical reactions and transport equations of laminar diffusion flames. For this endeavor, the CHEM1D software was extensively applied for the calculation of one-dimensional counter-flow flames. Although the application already has imbued in its code a thin optic limit grey-gas model (Optically Thin Approximation – OTA), the present work has implemented the Grey-Gas (GG) and the Weighted-Sum-of-Grey-Gases (WSGG) models as well as the Line-by-Line integration method (LBL). For the WSGG model, different correlations of coefficients for the pressure absorption and temperature dependence available in literature were included in this study. Comparisons of these four approaches were the focus of this dissertation for different calculation setups. These changes were in the strain rate (which stands as the velocity of the reagents) and in the dilution of CO_2 in the fuel side. Due to its exactness in calculating the spectral dependence of the radiative properties, the LBL is considered the benchmark solution to which the three models were compared. The main variables evaluated were the maximum radiative heat source term, the total radiative heat loss, and the species concentration of carbon monoxide. WSGG models show to be in every case presented better at estimating the proposed variables with results from formulations of this model that separately account for the participating species to have a well-rounded performance overall. Following these comparisons, it was investigated the extinction limits of the models and the benchmark, with dilutions being increased up until the flame extinguishes due to radiative losses for different strain rates. Results are compared with experimental literature data, and it is shown that some WSGG formulations with higher complexity although had better results previously, do not have robustness to achieve convergence in higher CO_2 dilution rates. For the chemical reaction, it was used a reduced version of GRI-MECH 1.2 with 19 species, including N_2 and AR, and 84 reactions.

Keywords: Non-premixed flames; Radiation models; One-dimensional flame; weighted-sum-of-gray-gases model; line-by-line integration.

CONTENTS

LIST OF FIGURES

LIST OF TABLES

LIST OF ACRONYMS AND ABBREVIATIONS

CHEM1D	Software for solving 1D flame structures
DOM	Discrete ordinates method
GG	Gray-gas model
HITEMP2010	Spectroscopic database
LBL	Line-by-line integration
OTA	Optically Thin Approximation
RTE	Radiative Transfer Equation
WSGG	Weighted-sum-of-grey-gases model

LIST OF SYMBOLS

Latin symbols

E	Emissive power [W/m²µm]
T	Temperature [K]
I	Radiation Intensity [W/m²µm]
t	Time [s]
V	Volume [m^3]
p	Pressure [N/m^2]
t	Time [s]
A	Area [m^2]
S	Radiation Path [m]

Greek symbols

η	Wavenumber [1/cm]
ω	Solid angle [sr]
σ	Stefan-Boltzmann constant [W/m^2K^4]
κ	Absorption coefficient [-]
ε	Emittance [-]

Subscripts

$(.)_{max}$	Maximum value
$(.)_{Tot}$	Total value
$(.)_a$	Participating species "*a*"
$(.)_i$	Gray gas "*i*"
$(.)_b$	Blackbody
$(.)_\eta$	Wavenumber
$(.)_l$	Angle "*l*"
$(.)_j$	Order "*j*" of a polynomial coefficient

Superscripts

$(.)^+$	From left to right direction
$(.)^-$	From right to left direction

1. INTRODUCTION

The radiative heat transfer process in participating media is a subject of great importance, especially for the energy generation industry, as in combustion processes thermal radiation is generally the main heat transfer mode. However, its reliable computation still is challenging. The radiative properties of absorbing-emitting species have a complex behavior as these are not regularly distributed regarding the wavelength, but rather in specified intervals, called bands, inside which they strongly oscillate. Moreover, radiation in participating media is a volumetric phenomenon, instead of a surface phenomenon, so changes in the temperature and species concentration of the gases throughout space must also be accounted for. Compromise between accuracy and computational costs must be accounted for when modelling the gas radiation in the combustion process.

The high gradient of temperature and species concentration participating in the heat transfer could present problems of numerical convergence. And, as mentioned before, for each wavelength of a participating gas there are millions of spectral lines to represent the radiative behavior. The most accurate solution for spectral aspect of a participating gas can be achieved by the line-by-line integration (LBL) of each wavenumber of the spectrum. This method is considered as the benchmark results as it is almost exact minor some deviations due to approximations in the calculation.

The weighted-sum-of-gray-gases (WSGG) model approximates the behavior of a gas by representing its spectrum with a few gray gases that occupy certain noncontiguous portions of the spectrum plus a transparent window. The absorption and emission-weighting coefficient associated to each gray gas must be determined, with different works in literature developing iterations of this model with fitting data, usually total emittances, based upon different scenarios. One of the most widely referred work is by Smith et al., 1982, where coefficients were fitted against emittance data computed from exponential wide-band model for typical combustion products of methane and fuel oil. For these fuels, the corresponding partial pressure ratios between water vapor and carbon dioxide are 2/1 and 1/1, respectively.

Other authors also developed correlations for the WSGG model, including Krishnamoorthy, 2010, who based his model for a methane and air, turbulent jet flame with partial pressure ratios varying between 1.5/1 to 4/1, while maintaining maximum error below 10% when compared to spectral line based WSGG (SLW) benchmark solutions. Dorigon et al., 2013, proposed new coefficients for partial pressure ratios of 2/1 and 1/1 based on the up-to-date HITEMP2010 spectral database and validated the results with line-by-line integration of

the whole spectrum in several cases of non-isothermal, non-homogeneous problems and results achieved were below 5% in maximum error.

In most cases, the validation and development of the WSGG correlations were made in decoupled calculations of the radiative transfer equation, where temperature and molar concentration data were predefined, either from experimental data or from empirical distribution. In real combustion applications, however, radiation is coupled to all other physical processes, and it thus affects scalars such as the temperature and the reaction rates and formation of species, as well as the propagation speed and extinction characteristics. On the other hand, changes in the aforementioned scalars influence the radiative properties of the medium and, as consequence, on the resulting radiation field.

Due to computational costs, spatially demanding simulations of flames are a challenge, especially if coupled with the RTE. The CHEM1D software developed by Somers, 1994, which solves one dimensional flame structures, proves a powerful tool for solving detailed chemistry flames coupled with the radiative problem. It calculates the transport, chemical kinetics and radiative heat transfer decoupled from flow equations. In the following section of this work, a review of most relevant papers available in literature in regard to coupled approaches to the radiation phenomenon are presented.

1.1 LITERATURE REVIEW

There are several works available in literature regarding spectral modelling of the radiative properties of a flame, which leads to the possibility of this work itself as it has a great focus on the comparison of several WSGG formulations available. Also, there are several works both experimental and numerical that assess the concentration of species and temperature field of counterflow flames. However, as the main purpose of the present study is to shed light on the coupled effect of radiation with the other physical processes, this literature review focus on the main previous studies that investigated this coupled effect.

In the work provided by Chan et al., 1998, a detailed mechanism of 49 species and 279 elementary reactions was applied together with narrow band models to account for the band-overlapping effects in a methane-air combustion counter-flow where the species of H_2O, CO_2, CO and CH_4 are visible to the radiative phenomenon. Besides the well-known extinction limit caused by high dissipation rate of the flame (overstretching), it was also identified that counter-flow flames in the condition of low scalar dissipation rates could also reach extinction due radiative losses. Also, in low to moderate dissipation rates, it was found that the thermal

radiation contributed to the temperature and NO_x formation results in significant differences to adiabatic solutions. Finally, it was also noted that preheating either air or fuel resulted in increment in the NO_x and CO formation.

Bundy et al., 2003, investigated the suppression of low strain rate non-premixed flames of methane and air in a counterflow configuration with minimum conduction losses. This was done experimentally with thin filament pyrometry to measure the flame temperature field. A study in the extinction was measured as function of the global strain rate for three different dilutants, CO_2, N_2 and CF_3Br added to the fuel and the oxidizer. The work performed therefore demonstrated the limits of dilution of these species before the radiative losses become preeminent enough to cause the extinction of the flame. It was seen that the main suppressor was the CF_3Br, followed by CO_2, and N_2 last.

Bidi et al., 2008, applied the Discrete Ordinate Method (DOM) to solve the Radiative Transfer Equation (RTE) with a formulation of the WSGG model in a coupled scenario of a turbulent premixed methane-air combustion in a cylindrical chamber. The coefficients for the WSGG were considered constant through the range of temperature and pressure-path length. A five-step reduced mechanism was used. In this case, numerical results of the coupled solution reached closer values to that of experimental cases than in calculations performed disconfirming the radiation effect. However, with the increasing ratio of the length by diameter of the chamber, the capability of the presented numerical solution to replicate experimental results declined, especially in terms of the species concentration. A possible explanation for it was the effect of accounting radiation that in this case broadened the high temperature zone affecting species concentration.

Centeno et al., 2015, applied two distinct formulations of the WSGG model, one with a constant ratio and other with a non-constant ratio of the concentrations of water vapor and carbon dioxide, in a turbulent non-premixed methane and air combustion. Also, the gray gas model (GG) was applied and compared to these two formulations of the WSGG. The results presented point that, although the temperature was heavily influenced by the radiation effect, the species formation were not so influenced. Moreover, the results for the WSGG models presented better accuracy to the experimental data compared to the GG model. However, the applied kinetic mechanism was a two-step global reaction, and the focus was on the main species that participate in the radiative process.

Hoerlle et al., 2015, evaluated simplified chemical kinetics in 1D and 2D numerical simulations of laminar diffusion flames of methane with dilution of carbon dioxide. It was observed that a 4-step mechanism presented good results for temperature and major chemical

species, however not so for minor species like CO and H_2. On the other hand, the Flamelet-Generated Manifold (FGM) technique demonstrated good results while gaining expressive computational gain.

Da Silva et al., 2020, used the CHEM1D software to study flamelets and explore different approaches to the radiation problem. Cases were studied in which the Optical Thin Approximation (OTA), a formulation of the WSGG with fixed coefficients and the LBL integration were evaluated and compared to experimental data regarding the velocity and temperature profiles, as well as the radiative heat flux. In addition, it was investigated the effect of dilution of CO_2 and N_2 in the fuel side for the OTA and WSGG models. The study showed that below a certain strain rate limit the one-dimensional solution could not correctly reproduce the experimental profiles compared due to heat losses in the sides of the burner. After this analysis, other studies exploring the simplification of the chemistry mechanism is explored by the writers reaching good assessment of the radiative quantities compared to the detailed cases even with the simplification in the chemistry provided by the FGM.

The literature for coupled calculations of radiation with the chemistry process is relatively scarce. In most developments, radiation is accounted for but not the focus of the study and there is little to no evaluation of the capabilities of the model selected for the solution. As it can be seen, the radiation can subject the flame to changes, especially in the temperature that leads to changes in the species formation.

1.2 OBJECTIVES

To solve the Radiation Transfer Equation, a spectral integration (regarding the wavenumber) is required to obtain the total radiative intensity. When considering participating species, like carbon dioxide and water vapor, this becomes a more complex endeavor as the absorption coefficient of both species presents a non-continuous behavior regarding the wavenumber. One may opt to solve the integral in its entirety, which leads to the method of the line-by-line integration (LBL). However, this leads to computational costs, in which some scenarios might be unfeasible specially when coupled with other demanding settings (i.e., three-dimensional domains, turbulent flows, detailed chemistry mechanisms, etc.).

Therefore, a solution for a compromise between time and accuracy comes as the adopting of models for solving the spectral integration. These models, of course, need validation, and a controllable one-dimensional flame that is replicable in laboratory is a powerful tool for comparing these models and analyzing their effects in the coupled effect of combustion.

The purpose of the present study is to evaluate different propositions of the WSGG model and compare them with the LBL method regarding the results calculated for the fields of temperature and species concentration, as well as the radiation field. Besides these methods, comparisons with other set ups are made, such as: calculations that neglect radiation; that solve the case decoupling the radiative from the chemistry kinetics; or use the optically thin approximation to account for the radiative transfer.

Therefore, the objectives are:

- Compare the WSGG models to the LBL in regard to the radiation field (Radiative Heat Source and Flux), the temperature profile and the species formation (H_2O and CO_2 as both are the participating species in the RTE modelling, and others of interest due to emission studies as NOx and CO).
- Evaluate the capacity of the models to predict the extinction due to low strain rates (in which radiative losses become more prominent).
- Evaluate the effects of CO_2 dilution regarding the radiation field and species concentration

1.3 OUTLINE OF THE WORK

This work is divided in five chapters. In this first chapter an introduction of models for the Radiative Transfer Equation (RTE) available in literature is presented, followed by the main studies published for coupled solutions of the radiation field and finally the objectives for work are explained.

Chapter 2 presents some fundamental concepts about the transport equations that describe the case of a counterflow flame, followed by concepts of radiative heat transfer in participating media as well as brief explanations regarding the different methods used in this work to integrate the RTE (benchmark LBL and the WSGG model).

In the third chapter it is demonstrated the methodology applied for solving the problem. The implementation of the different coefficients of the WSGG is briefly commented. The numerical modelling is presented followed by the description of the problem (boundary conditions and set up of the solvers). A study of dependence of the results regarding its mathematical modelling is discussed as well as verification of the implementation of the coefficients.

Chapter 4 presents the results found in this work. Firstly, the comparison of each implemented WSGG coefficient with the benchmark solution in a base case is presented. Then,

the most promising formulations of the WSGG are evaluated for different strain rates. Finally, these are evaluated at different CO_2 dilution and strain rates.

The fifth and final chapter is the conclusion giving an overview of the formulations and models used in this work and their performance in the proposed scenarios. Suggestions of future work are also presented. This chapter is followed by the bibliographical references and appendix with more results that were opted to be left out of the results section.

2. RADIATIVE TRANSFER EQUATION AND SPECTRAL MODELING

Energy radiates from one object to another under all conditions and all times. The source of the emitted radiation is a combination of electronic and molecular oscillations and transitions in the emitting material, as well as lattice vibrations. The energy radiates as an electromagnetic (EM) wave, regardless of whether there is matter or not along its path. Both the emitted and absorbed radiation are functions of the physical and chemical properties of the material as well as its energy level (as quantified by its temperature). The interaction between emitting and absorbing bodies via EM waves is the essence of radiative energy transfer [Howell et al., 2016]. Although radiation occurs through all wavelengths, the range of interest for engineering applications is from 0.1 μm to 100 μm, which comprehends the thermal portion of the spectrum, therefore the ultraviolet, the visible light and the infrared intervals.

2.1 BLACK BODY

The black body is an idealized body capable of emitting energy uniformly in all directions and wavelengths (or, analogously the wavenumber) and all incident radiation is integrally absorbed by it, that is to say no energy is reflected or transmitted. Therefore, the black body is a crucial concept in the study of radiation and most helpful for determining radiative properties of real surfaces when compared to them.

From the definition of black body some important aspects arise. Firstly, for a given temperature and wavenumber, no surface can emit more energy than the blackbody. Secondly, the radiation emitted by a blackbody is dependent only of its temperature and the wavelength, being independent of the direction, and therefore considered a diffuse emitter.

Consider a blackbody with a temperature T surrounded by a sensor that covers the whole hemisphere and captures the thermal radiation of wavenumber η within the range $d\eta$, as in Figure 2.1. Then, the blackbody hemispherical spectral emissive power, $E_{b,\eta}(W/m^2\mu m)$ which is described as the energy emitted by a black surface over time over an area and by an interval around a specific wavenumber is given by Planck's spectral distribution:

$$E_{\eta b}(\eta, T) = \frac{2C_1\pi\eta^3}{e^{(C_2\eta/T)} - 1} \tag{2.1}$$

in which C_1 = 0.59552137 x 10^{-16} W.m^2/sr and C_2 = 0.14387752 m.K are respectively the first and second radiation constants, T refers to the temperature, in K, and η indicates the wavenumber (it stands as the inverse from the wavelength: $\eta = 1/\lambda$).

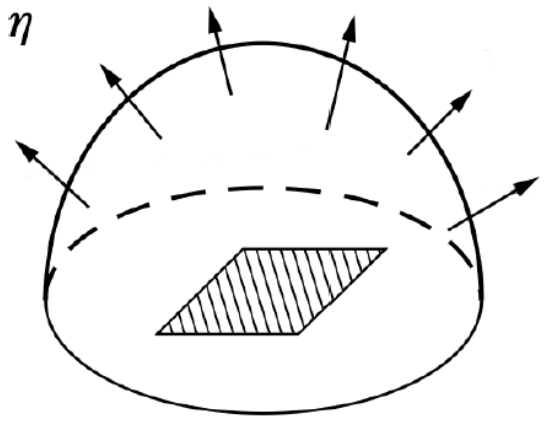

Figure 2.1 – Blackbody surrounded by a hemispherical detector [adapted from Howell et al., 2016].

The blackbody radiation intensity $I_{\eta b}$ can be directly related to the emissive power since the blackbody emits independently from the direction (that is to say $I_{\eta b} = E_{\eta b} / \pi$). Integrating over the whole spectrum leads to the Stefan-Boltzmann law and one can determine the total radiation intensity of the blackbody, I_b which now is only a function of temperature:

$$I_b(T) = \frac{E_b}{\pi} = \frac{\sigma T^4}{\pi} \tag{2.2}$$

where σ = 5.6704 x 10^{-8} W/m^2.K^4 is the Stefan-Boltzmann constant and E_b is the total emissive power of the blackbody.

2.2 SPECTRAL RADIATION INTENSITY

Consider an infinitesimal area which emits a radiation energy in a certain direction which can be described by its angles dθ and dφ, as it is shown in Figure 2.2. The solid angle $d\omega$ is the conical area that comprises the propagation of radiation from its origin to its destiny dA_n.

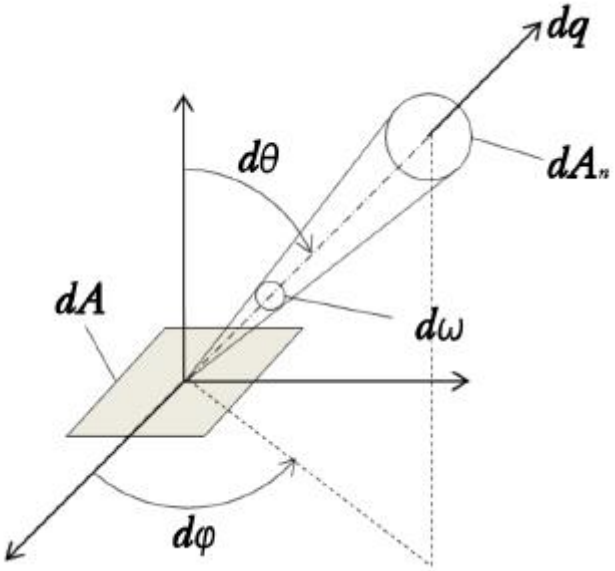

Figure 2.2 – Spectral intensity emitted by an infinitesimal area *dA* [adapted from Incropera et al., 2008].

The spectral radiation intensity I_η is then defined as the spectral radiative energy *dq* per unit projected area *dA* along a path *S*, per solid angle $d\omega$ around ω, per unit time interval *dt* at time *t*, and a small wavenumber interval $d\eta$ around η [Howell et al., 2016].

$$I_\eta(\eta, \theta, \varphi) = \frac{dq}{dA \cos\theta \, d\omega d\eta} \tag{2.3}$$

in which I_η is given in $W/m^2.\mu m.sr$, $dA.cos\theta$ is the projected area dA_n, and dω is the solid angle that is described as $sin\theta d\theta d\varphi$.

2.3 RADIATIVE ENERGY ALONG A PATH

The scenario presented and Equation 2.3 are valid only when considering that the medium the radiation traverses does not affect the energy intensity. In other words, there is no attenuation due to absorption, nor augmentation due to emission and even not scattering because of the medium. However, when the medium does interfere along the path, it is named radiation in participating media. Only the first two phenomena (emission and absorption) will be in this work as scattering is not as significant in methane combustion. These two mechanisms are important as they couple the radiative energy propagation with the thermodynamic state of the matter. Absorption is the description of how the radiative energy is converted to the internal

energy of the matter while radiative emission which is proportional to the internal energy of the matter.

2.3.1 Attenuation of Intensity due to Absorption

Considering an infinitesimal volume *dV* in which the spectral radiation intensity I_η is normally incident as shown in Figure 2.2.

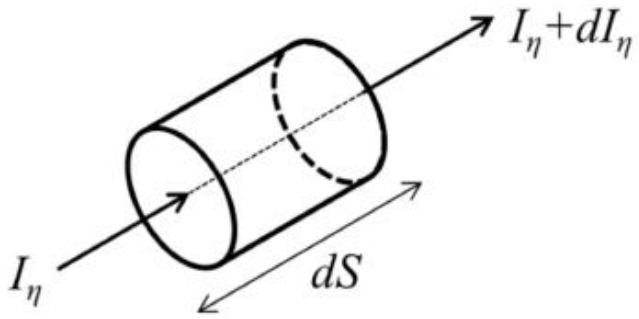

Figure 2.3 – Spectral radiation intensity normal to an absorbing infinitesimal volume [adapted from Howell et al., 2016].

The absolute amount of absorption dI_η has been observed to be directly proportional to the magnitude of the incident energy I_η as well as the distance *dS* the beam travels through the medium *dV* as pointed by Modest, 2003. This proportionality can be described as:

$$dI_\eta(S) = -\kappa_\eta(S) I_\eta(S) dS \tag{2.4}$$

Where κ_η which stands for this proportionality is the absorption coefficient. The negative sign is to indicate that intensity decreases due to this effect. The dependence of the variables to a given path S is an important one to indicate henceforth that each position the medium may be subject to changes in its temperature or species concentration or both, and this ultimately leads to changes in the radiative behavior.

In molecular gases, the absorption depends heavily on the number of receptive molecules per unit volume, therefore it is interesting to present the concept of a pressure absorption coefficient $\kappa_{p,\eta} = \kappa_\eta / p_a$ where p_a is the partial pressure of the participating species.

2.3.2 Augmentation of Intensity due to Emission

The change in intensity due to emission is also proportional to the distance traveled by the radiative beam and the local intensity of the medium [Modest, 2003]. For media that are in local thermodynamic equilibrium (LTE):

$$dI_\eta(S) = \kappa_\eta(S) I_{b,\eta}(S) dS \tag{2.5}$$

2.4 TOTAL EMITTANCE

Emissivity is defined as the ratio between the emitted radiation by a surface and the radiation emitted by the blackbody at the same temperature [Incropera et al., 2008]. Therefore, it is a dimensionless parameter defined as:

$$\varepsilon(T) = \frac{E_s(T)}{E_b(T)} \tag{2.6}$$

in which E_s is the real emission power of a surface.

In the case of a participating media, an analogous property may be defined, named emittance. As in general the spectral radiation emitted by real surface differs from Planck's distribution, emissivity can therefore have different values for different wavelengths and directions [Incropera et al., 2008]. One can define the variable of total emittance as the integration for the whole spectrum of the ratio between radiation emitted by the media and the spectral intensity of the blackbody:

$$\varepsilon(T) = \frac{\int_0^\infty I_{\eta b}\varepsilon_\eta(T)\, d\eta}{\int_0^\infty I_{\eta b} d\eta} \tag{2.7}$$

At a first moment, considering a gas with uniform temperature and composition, for example, a well-mixed furnace, then by applying the Kirchhoff's Law which assumes that emittance is equal to absorptance ($\varepsilon_\eta = \alpha_\eta$) at a directional and spectral level at any thermodynamic condition. The absorptance can be defined deriving from a balance of incident radiation that can either be absorbed, transmitted or reflected, which leads to, [Howell et al., 2016]:

$$\alpha_\eta = 1 - e^{(-\kappa_{p,\eta} p_a S)} \tag{2.8}$$

Using the relations presented in Equations (2.1), (2.2) and (2.8) and applying them to Equation (2.7), results in:

$$\varepsilon(T, p_a S) = \frac{\int_0^\infty I_{\eta b}\left[1 - exp\left(-\kappa_{p,\eta} p_a S\right)\right] d\eta}{\frac{\sigma T^4}{\pi}} \tag{2.9}$$

in which p_aS is the pressure path-length of the medium

2.5 Collision Broadening of a Spectral Line

The determination of radiative properties for molecular gases relies on quantum mechanical laws therefore it is convenient to refer the radiative process from the point of view of photons as it is the basic unit of radiative energy. Radiative emission releases photons, and absorption is the capture of photons.

The magnitude of a radiative energy transition is related to the frequency of the emitted or absorbed radiation. As the energy of the photon is $h\upsilon$ which h is the Planck's constant and υ is the frequency, an energy transition from one bound state to another happens at a fixed frequency. These are discrete transitions and result in the absorption of photons in definite frequencies or wave numbers, causing the appearance of dark lines in the transmission spectrum [Howell et al., 2016]. A scarce amount of energy would be absorbed from the entire incident spectrum by an absorption line; however, other effects cause the line to be broadened and consequently to have a finite wave number span around the transition wave number.

As pointed by [Howell et al., 2016] there are several important broadening mechanisms such as natural, Doppler, collision, and Stark broadening. However, for engineering applications involving infrared radiation collision broadening is the most relevant which happens when a collision between two or more particles, atoms, or molecules, disturb the energy level within a particle. The higher the pressure, the higher the spectral line broadening due to the higher the collision rate experienced by an atom or molecule with surrounding particles is increased.

The broadening of the line centered around the wavenumber $\eta_{i,j}$ for this case is described by a Lorentz profile:

$$\frac{C_{\eta,i,j}(\eta)}{S_{i,j}} = \frac{\gamma_C/\pi}{\gamma_C^2 + \left(\eta - \eta_{i,j}\right)^2} \tag{2.10}$$

in which $C_{\eta,i,j}$ is the absorption cross-section, in cm^2/molecule, $S_{i,j}$ is the line intensity, and γ_C is the line half-width at half-maximum line height for the collision broadening, and is given by [Howell et al., 2016]:

$$\gamma_C = \frac{1}{2\pi c_0} \frac{4\sqrt{\pi} D^2 p_a}{(M k_B T)^{1/2}} \tag{2.11}$$

where c_0 is the vacuum light velocity, D is the diameter of the atom or molecule, M is the particles mass, in kg, and k_B is the Boltzmann constant. As it can be seen from Eq. (2.11) the half-width is directly proportional to the partial pressure of the species and inversely proportional to the square root of the temperature, which indicates that this effect is especially important in not so elevated temperatures and where pressure is relevant. In the present study, temperatures do not surpass 2500 K and the total pressure is kept at 1 atm, which meets the scenarios presented by Wang and Modest, 2004, that concluded that the Lorentz profile returns good results for temperatures up to this values and pressures of at least 1 atm.

2.6 SPECTROSCOPIC DATABASES

Spectroscopic databases are a compilation of experimental results for parameters function of the wavenumber that are relevant to the spectral radiation. These include the energy difference between the initial and final state υ_i, given as a vacuum wavenumber, the energy of the lower state E_i, the line self-broadening $\gamma_{self,i}$, the broadening caused by air $\gamma_{air,i}$, and the temperature dependence coefficient n_c.

There are several spectral databases available in literature and they differ in parameters such as reference temperature, number of spectral lines per species, and species in the catalog. In order to solve the RTE through the line-by-line method, this study utilizes the HITEMP-2010 database [Rothman et al., 2010], which itself is a derivation from the HITRAN [Rothman et al., 1995]. This spectral database contains 114.241.164 spectral lines for H_2O, and 11.193.608

spectral lines for CO_2. The HITEMP-2010 also provides data for three other species, namely, CO, OH and NO; however, this work considered these species as non-participating in the thermal radiation.

The line intensity can be calculated from the following equation, [Rothman et al., 2010]:

$$S_i(T) = S_i(T_{ref})\frac{Q(T_{ref})}{Q(T)}\frac{e^{(-C_2E_iT)}}{e^{(-C_2E_iT_{ref})}}\frac{\left[1-e^{(-C_2\upsilon_iT)}\right]}{\left[1-e^{(-C_2\upsilon_iT_{ref})}\right]} \tag{2.12}$$

where T_{ref} is the reference temperature, in this case 298K, and Q is the sum of all energy states, such as vibrational, and rotational, and depends on the molecule characteristics. Only Q needs to be calculated while all other quantities are readily available. The routine for calculating Q is provided within the database. The next important quantity to be calculated is the line half-width at half-maximum. Henceforth named γ_i, it can be determined using the equation that follows:

$$\gamma_i(p,T) = \left(\frac{T_{ref}}{T}\right)^{n_c}\left[\gamma_{air,i}(p_{ref},T_{ref})(p-p_a) + \gamma_{self,i}(p_{ref},T_{ref})p_a\right] \tag{2.13}$$

in which the reference pressure p_{ref} is 1 atm.

Finally, considering the Lorentz profile mentioned earlier for describing the line broadening, the spectral cross-section can be described by the following equation [Howell et al., 2016]:

$$C_\eta = \sum_{i=\eta-\Delta\eta}^{I=\eta+\Delta\eta}\frac{S_i(T)}{\pi}\frac{\gamma_i}{\gamma_i^2+(\eta-\eta_i)^2} \tag{2.14}$$

where $\Delta\eta$ (cm^{-1}) is the spectral span around η.

2.7 The Absorption Coefficient

With knowledge of the absorption cross-section and the other parameters in last section, one can readily obtain the absorption coefficient:

$$\kappa_\eta(\eta,T,p,Y) = N(T,p)YC_\eta(\eta,T,p,Y) \tag{2.15}$$

in which N is the molecular density given in molecule/cm^{2}m, and Y is molar fraction of the species. The former is expressed by:

$$N(T,p) = \frac{pN_a}{R_{ug}T} \tag{2.16}$$

where N_a is the Avogradro's number, and R_{ug} is the universal gas constant.

2.8 RADIATIVE TRANSFER EQUATION (RTE)

Considering the infinitesimal volume of Figure 2.2 and applying an energy balance on it, accounting for both the attenuation and augmentation of the radiation intensity as it crosses its trajectory, the Radiative Transfer Equation (RTE) arises. Combining Eqs. 2.3 and 2.4 and neglecting the scattering, this equation can be written as [Howell et al., 2016]:

$$dI_\eta(S) = -\kappa_\eta(S)I_\eta(S)dS + \kappa_\eta(S)I_{b,\eta}(S)dS \tag{2.17}$$

Which can be differentiated by the path-length:

$$\frac{dI_\eta(S)}{dS} = -\kappa_\eta(S)I_\eta(S) + \kappa_\eta(S)I_{b,\eta}(S) \tag{2.18}$$

Mathematically, the RTE is a first order differential equation in regards to the spectral intensity for a given path-length S and therefore, in order to solve it, it is necessary to know the spectral intensity in any given point of the trajectory. To obtain the total radiative heat transfer, the RTE must be integrated on the whole spectrum and in all spatial directions. This can be time demanding and one can opt to apply a model to replicate the spectral integration, which is the case with the Gray-Gas (GG) and Weighted-Sum-of-Gray-Gases (WSGG) models. The integration of the whole spectrum is known as the line-by-line integration (LBL). These three methods for solving the RTE will be further discuss in this work as they are part of the study, although there should be noted that are other methods for solving the RTE. A method for solving the directional part of the RTE will be discuss next.

It should be noted that there are other methods for solving the spatial directions of the RTE, such as *spherical harmonics method*, *finite volume method* or *Monte Carlo method*. The

discrete ordinate method was selected as the RTE is intrinsically conservative by solving with it since the radiative energy balance is satisfied. This factor is crucial when radiation is coupled with other heat transfer mechanism in the global energy equation.

2.8.1 Discrete Ordinate Method (DOM)

The method of the Discrete Ordinate Method (DOM) was originally proposed by Chandrasekhar, 1960, and is based upon the discrete representation of the directional dependence of the radiation intensity. In this way, the RTE is solved for a set of directions that cover in their entirety of the 4π unit sphere (for a one-dimensional case, and for the three-dimensional case the solid angle) [Modest, 2003].

Therefore, considering the domain presented in Figure 2.4, the RTE is rewritten for each directional ordinate and the integrals are approximated with numerical quadrature for all discrete directions.

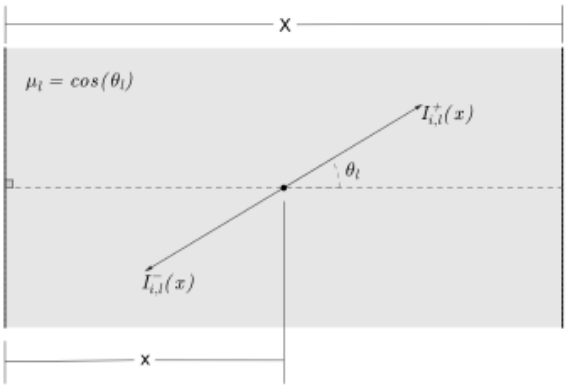

Figure 2.4 – One-dimensional domain [adapted from Selhorst et al., 2020].

Equation (2.18) can be rewritten as two different equations, one for the forward directions of the ordinates and another for the backward direction:

$$\mu_l \frac{\partial I^+_{\eta,l}(x)}{\partial x} = -\kappa_\eta(x) I^+_{\eta,l}(x) + \kappa_\eta(x) I_{b,\eta}(x) \qquad (2.19a)$$

$$-\mu_l \frac{\partial I^-_{\eta,l}(x)}{\partial x} = -\kappa_\eta(x) I^-_{\eta,l}(x) + \kappa_\eta(x) I_{b,\eta}(x) \qquad (2.19b)$$

in which μ_l is the cosine of angle θ_l and $I_{\eta,l}^+$ and $I_{\eta,l}^-$ are the radiation intensity in the forward and backward direction for $\mu_l > 0$ and, $\mu_l < 0$ respectively.

Equation 2.8 is a set of first order linear equations dependent on $I_{\eta,l}(x)$, thus, it only requires one boundary condition for each equation. This requirement is fulfilled by assuming that the walls of the domain behave like a blackbody, and therefore the fulfilling condition can be written as:

$$I^{+}_{\eta,l}(x=0) = I_{b,\eta}(x=0) \tag{2.20a}$$

$$I^{-}_{\eta,l}(x=X) = I_{b,\eta}(x=X) \tag{2.20b}$$

After solving Equations 2.19 for solving the RTE, the radiative heat flux, and the radiative heat source can be obtained. As mentioned before, this also requires a solution for the spectral integration.

2.9 METHODS FOR SPECTRAL INTEGRATION OF THE RTE

Three different methods for solving the spectral integration of the RTE were applied in this work, one being the integration itself and the other two applying a model to reduce computational cost of integrating across all the spectral lines.

2.9.1 Line-by-line (LBL) integration

The line-by-line (LBL) method usually stands as the benchmark solution due to the accuracy that can be achieved by performing a discretization on the wavenumber until a well-established convergence criterion. This high accuracy is product of solving the RTE for each absorption coefficient related to its respective wavenumber. However, since the databases from which the spectral properties are computed are obtained through experimental methods, the obtention process itself gather some errors, and therefore the LBL solution are not exact.

After solving the RTE using Equation 2.19, the radiative heat flux, and radiative heat source can be obtained as:

$$q''(x) = \sum_{l=1}^{L} \int_{\eta=0}^{\infty} \left\{ 2\pi \mu_l g_l \left[I^{+}_{\eta,l}(x) - I^{-}_{\eta,l}(x) \right] \right\} d\eta \tag{2.21a}$$

$$-\nabla q''(x) = \sum_{l=1}^{L} \int_{\eta=0}^{\infty} \left\{ 2\pi g_l \kappa_\eta \left[I^{+}_{\eta,l}(x) + I^{-}_{\eta,l}(x) \right] - 4\pi \kappa_\eta I_{\eta,b}(x) \right\} d\eta \tag{2.21b}$$

where g_l is the quadrature weight in the l direction, L is half the number of angle division and κ_η is determined solving Eq. 2.15 with the spectroscopic database.

2.9.2 Weighted-Sum-of-Gray-Gases (WSGG) Model

Instead of solving the RTE for each wavenumber, the weighted-sum-of-gray-gases (WSGG) model represents the spectrum in its entirety with only a few gases with uniform pressure absorption coefficient, plus a transparent window. Each *i*-th gas assumes a portion of the total radiation intensity in each direction. Therefore, the total sum of radiation intensity of the gases is:

$$I(S) = \sum_{i=1}^{I} I_i(S) \tag{2.22}$$

where I_i is the partial intensity corresponding to the *i*-th gray gas, given in W/m^2. Returning to Equation 2.18 and applying the WSGG model leads to:

$$\frac{dI_\eta(S)}{dS} = -\kappa_{p,i} p_a(S) I_i(S) + \kappa_{p,i} p_a(S) a_i(S) I_b(S) \tag{2.23}$$

where $a_i(S)$ is the weighting function that corresponds to a fraction of the blackbody. In most formulations the pressure absorption coefficient is constant, whereas the other variables p_a, a_i, and I_b are computed locally. This makes the WSGG model suitable for cases of non-homogeneous, and non-isothermal.

Therefore, the dependence of the absorption coefficient has on the wavenumber and on the thermodynamic state (temperature and molar concentrations) are decoupled. Integrating Equation 2.9 over the spectrum with the WSGG model, the total emittance becomes:

$$\varepsilon(T, p_a S) = \sum_{i=1}^{I} a_i(T)\left[1 - exp\left(-\kappa_{p,\eta} p_a S\right)\right] \tag{2.24}$$

Usually, WSGG coefficients are determined through fitting data with Equation 2.24 as this equation allows for obtaining both the pressure absorption coefficients of each gray gas as well as the temperature dependent coefficients, which can be represented by polynomial functions:

$$a_i(T) = \sum_{j=1}^{J} b_{i,j} \left(\frac{T}{T_{ref}} \right)^j \tag{2.25}$$

where, in the above equation, $b_{i,j}$ is the polynomial coefficient of the j-th order for the i-th gray gas. The temperature coefficients are calculated as above only for the gray gases. In order for the radiation energy to remain conserved, the transparent window is calculated as:

$$a_0(T) = 1 - \sum_{i=1}^{I} a_i(T) \tag{2.26}$$

The determination of these coefficients varies from author to author, with each using fitting data that best responded to their benchmark comparisons. Again, using the DOM for solving the spatial directions, Equation 2.23 becomes:

$$\mu_l \frac{\partial I_{i,l}^{+}(x)}{\partial x} = -\kappa_{p,i} p_a(x) I_{i,l}^{+}(x) + \kappa_{p,i} p_a(x) a_i(x) I_b(x) \tag{2.27a}$$

$$-\mu_l \frac{\partial I_{i,l}^{-}(x)}{\partial x} = -\kappa_{p,i} p_a(x) I_{i,l}^{-}(x) + \kappa_{p,i} p_a(x) a_i(x) I_b(x) \tag{2.27b}$$

As previously stated, the walls are considered blackbodies, and the boundary conditions undergo a small change to adapt for the model. The conditions become:

$$I_{i,l}^{+}(x = 0) = a_i(T_{x=0}) I_b(x = 0) \tag{2.28a}$$

$$I_{i,l}^{-}(x = X) = a_i(T_{x=X}) I_b(x = X) \tag{2.28b}$$

Like the LBL integration, after solving the Equations (2.24a) and (2.24b), the radiative heat flux and radiative heat source can be calculated [Howell et al., 2016]:

$$q''(x) = \sum_{l=1}^{L}\sum_{i=0}^{I}\left\{2\pi\mu_l g_l\left[I_{i,l}^{+}(x) - I_{i,l}^{-}(x)\right]\right\} \quad (2.29a)$$

$$-\nabla q''(x) = \sum_{l=1}^{L}\sum_{i=1}^{I}\left\{2\pi g_l \kappa_{p,i} p_a(x)\left[\left[I_{i,l}^{+}(x) + I_{i,l}^{-}(x)\right] - 2a_i I_b(x)\right]\right\} \quad (2.29b)$$

As with the LBL, the energy balance is assured. Also of importance, the transparent window, *i*=0, is only accounted for when obtaining the radiative heat flux.

2.9.2.1 Fixed-*MR* WSGG formulations

Most WSGG correlations available in the literature are for fixed molar ratio between water vapor, X_{H_2O}, and carbon dioxide, X_{CO_2}. That is to say that although the mole fractions of these two species may vary along the radiative path, the ratio between them is kept constant. For these formulations, good emittance fittings can be obtained by setting a linear dependence of κ_i on the partial pressure of the participating mixture while expressing the weighting coefficient as a polynomial function of the temperature, exactly as presented in Eq. 2.25.

Ergo, the development of fixed molar ratio WSGG formulations reduces to finding values of $\kappa_{p,i}$ and $b_{i,j}$ for varying *S* and *T* and for sets of mole fractions that maintain the $X_{H_2O}/X_{CO_2} = constant$, this is done by fitting Eq. 2.24 to Eq. 2.9. Typically, fixed-*MR* correlations have been proposed for *MR = 2.0*, which is characteristic of stoichiometric methane combustion, and *MR = 1.0,* that is a value closely found in combustion of oil. Although recent works in the literature have expanded the available correlations for other mole ratio values (for cases of oxy-fuel combustion, for example), this present work only applies fixed formulations with these two molar ratios.

2.9.2.2 Varying-*MR* WSGG formulations

It is possible to account for variations in the mole ratio by incorporating a dependence of the WSGG correlations on *MR* within $\kappa_{p,i}$, $b_{i,j}$, or both. As standard approach, one assumes a polynomial dependence of these quantities on the mole ratio, which can be generalized as:

$$b_{i,j} = \sum_{m=0}^{M} c_{i,j,m} MR^m \tag{2.30}$$

$$\kappa_{p,i} = \sum_{n=0}^{N} d_{i,j,n} MR^n \tag{2.31}$$

where $c_{i,j,m}$ and $d_{i,j,n}$ are constants added to the model, and *M* and *N* may vary depending on the correlation. Parameters for the transparent window are obtained in the same manner described previously.

Since complexity is higher for these formulations, they require additional emittance fittings for obtaining the new constants. This likely increases the overall error of the fittings since the regressive method needs to accommodate more data, and there are works available in literature, such as Kangwanpongpan et al., 2012, that has shown that for calculations where mole ratio is constant the performance is worse than for fixed-*MR* formulations. Moreover, no single correlation available in the literature is applicable to the entire range of possible *MR* values, and, in fact, it has been shown that using correlations outside their range yields considerable errors.

2.9.2.3 Interpolation of fixed-*MR* WSGG formulations

Another method for accounting for variations on the mole ratio in the WSGG model is to interpolate between fixed-*MR* correlations. Both linear and stepwise interpolations have been added and tested in this work, although it should be noted that, traditionally, linear interpolation has been generally better accepted since employing a stepwise methodology tends to lead to non-physical results.

2.9.2.4 The superposition WSGG model

This method allows the implementation of the model for mixtures of an arbitrary number of species, each one at an arbitrary concentration. In the superposition model, each species is modeled by its own set of gray gases and the RTE is solved for the permutations of the gray gases corresponding to each species, with the overall gray gas absorption and weighting coefficients defined through statistical arguments. Consider a H_2O-CO_2 mixture, with the

indexes i_w and i_c respectively assigned to the gray gases associated to each species, the radiative transfer equation in the superposition WSGG model is written as:

$$\frac{dI_{i_w i_c}}{dS} = -\left(\kappa_{i_w} + \kappa_{i_c}\right) I_{i_w i_c} + \left(\kappa_{i_w} + \kappa_{i_c}\right)\left(a_{i_w} \times a_{i_c}\right) I_b \tag{2.32}$$

in which $I_{i_w i_c}$ stands for the partial radiative intensity pertaining to the mixture's gray gas that is formed by the combination of i_w and i_c, with $\left(\kappa_{i_w} + \kappa_{i_c}\right)$ and $\left(a_{i_w} \times a_{i_c}\right)$ being the absorption and weighting coefficients respectively. Because WSGG correlations for individual species normally consist of three to four gray gases, this implicates a number of RTE solutions to determine radiation many times larger than for standard WSGG model since the calculation of the total intensity in this formulation requires simultaneous summations over the total number of H_2O and CO_2 gray gases.

In addition, it should be noted that the accuracy of this method is closely related to the quality of WSGG correlations for the individual species. The superposition method is tested in this work using sets of correlations for pure water vapor and carbon dioxide proposed by different authors.

2.9.3 Gray-Gas (GG) Model

The gray-gas model assumes that the spectral variations of the radiative properties of the media are negligible for the whole spectrum of the wavenumber. That is to say that $\kappa_\eta = \kappa$ [Howell et al., 2016]. Therefore, one can directly rewrite the RTE in its spectrally integrated form:

$$\frac{dI(S)}{dS} = -\kappa I(S) + \kappa I_b \tag{2.33}$$

For the calculation of the absorption coefficient it can be assumed that it has a constant value or that is a function of temperature and species concentration of the medium. In this work, the latter option was opted with coefficients proposed by Peters and Rogg, 1993. Equation 2.18 therefore becomes:

$$\mu_l \frac{\partial I_l^+(x)}{\partial x} = -\kappa(x) I_l^+(x) + \kappa(x) I_b(x) \quad (2.34a)$$

$$-\mu_l \frac{\partial I_l^-(x)}{\partial x} = -\kappa(x) I_l^-(x) + \kappa(x) I_b(x) \quad (2.34b)$$

Like previous methods, after solving the Equations (2.34a) and (2.34b), the radiative heat flux and radiative heat source can be calculated:

$$q''(x) = \sum_{l=1}^{L} \{2\pi\mu_l g_l [I_l^+(x) - I_l^-(x)]\} \quad (2.35a)$$

$$-\nabla q''(x) = \sum_{l=1}^{L} 2\pi g_l \kappa \left[[I_l^+(x) + I_l^-(x)] - 2I_b(x) \right] \quad (2.35b)$$

2.9.4 Optically Thin Approximation

This is the simplest method available in this work and considers the Gray-Gas hypothesis for the spectral model, whereas the absorption coefficient does not depend on the wavenumber, and neglects absorption, with only emission being responsible for the radiative heat transfer. Therefore, the RTE does not need to be solved. The radiation source term is given by:

$$-\nabla q''(x) = -4\sigma k_p (T^4 - T_\infty^4) \quad (2.36)$$

Which T_∞ is the room temperature and σ is the Stefan-Boltzmann constant. The term k_p is the mean Planck absorption coefficient for the grey-medium and can be obtained from:

$$k_p = \sum_{i=1}^{I} p_i k_{p,i} \quad (2.31)$$

Where $k_{p,a}$ is the Planck absorption coefficient for each gas i. The actual number of gray-gases employed can vary and in this work was investigated the solution for two gases (CO2 and H2O) with coefficients taken from Peters and Rogg, 1993.

3. NUMERICAL METHOD AND METHODOLOGY

3.1 ONE-DIMENSIONAL COUNTER-FLOW FLAME FORMULATION

The software used for carrying the simulations is the CHEM1D code developed by the Eindhoven University. CHEM1D solves the transport equations for the conservations of mass, chemical species, and energy according to the formulation proposed by de Goey et al., 1999, with assumptions of laminar flame and low Mach number.

Since the calculations are for a one-dimensional analysis, a stretch rate *K* is introduced to account for the effects of multidimensionality not present in the 1D scenario. This stretch rate stands for a relative rate of the mass change *M(t)* within an infinitesimal volume *V(t)* of the flame and moves with the local velocity of the flame:

$$M(t) = \int_{V(t)} \rho dx \tag{3.1}$$

with *u* being the flow velocity in the *x* direction and ρ being the specific mass.

$$K = \frac{1}{M}\frac{dM}{dt} \tag{3.2}$$

In the following equations, the terms involving *K* account for the deviation of the one-dimensional behavior. Therefore, neglecting the curvature of the flame, the conservation of total mass stands as:

$$\frac{\partial(\rho u)}{\partial x} = -\rho K \tag{3.3}$$

The conservation of mass can also be defined for a given chemical species *i*. Therefore, in terms of its mass fraction Y_i, the equation can be written as:

$$\frac{\partial(\rho u Y_i)}{\partial x} = \frac{1}{Le_i}\frac{\partial}{\partial x}\left(\frac{\lambda}{c_p}\frac{\partial Y_i}{\partial x}\right) + \dot{\omega}_i - \rho K Y_i \tag{3.4}$$

where Le_i is the Lewis number which associates the mass diffusion with the thermal diffusion of the mixture, while $\dot{\omega}_i$ stands for the reaction source term, and λ being the thermal conductivity coefficient (in W/m.K), c_p being the specific heat constant at constant pressure of the mixture: $c_p = \sum_{i=1}^{N} c_{p,i} Y_i$, with *N* being the total number of species in the mixture.

Further simplification of the transport model can be achieved with the use of a constant Lewis number, resulting in faster computational times. Following Smooke and Giovangigli, 1991, the thermal conductivity coefficient λ and the dynamic viscosity μ can be approximated as temperature based functions of the form:

$$\frac{\lambda}{c_p} = 2.58 \times 10^{-5} \left(\frac{T}{298}\right)^{0.69} \tag{3.5}$$

$$\frac{\mu}{c_p} = 1.67 \times 10^{-5} \left(\frac{T}{298}\right)^{0.51} \tag{3.6}$$

The conservation equation is in terms of the total specific enthalpy of the mixture, *h*. The effects of the chemical reactions are accounted through means of:

$$h = \sum_{i=1}^{N} Y_i h_i \tag{3.7}$$

$$h_i = h_{i,f}^0 + \int_{T_{ref}}^{T} c_{p,i}(T) dx \tag{3.8}$$

in which $h_{i,f}^0$ is the specific enthalpy of formation at the reference temperature T_{ref}.

Considering constant pressure and neglecting viscous dissipation, the energy equation is written as:

$$\frac{\partial(\rho u h)}{\partial x} = \frac{\partial}{\partial x}\left(\frac{\lambda}{c_p}\frac{\partial h}{\partial x} + \sum_{i=1}^{N} h_i \frac{\lambda}{c_p}\left(\frac{1}{Le_i} - 1\right)\frac{\partial Y_i}{\partial x}\right) - \rho K h + \dot{q}_R \tag{3.9}$$

with $\dot{q}_R$ being the source term for radiative heat losses. On the left side of the equation is the energy transport due to advection. On the right side, the terms in the parenthesis are the

conductive heat flux due to the temperature gradients (Fourier's Law) and the mass diffusion (considering Fick's Law). Information regarding the radiative term comes from solving equations 2.21b (in the case of the LBL) or 2.29b (in case of the WSGG). Temperature is obtained by relating it to the enthalpy:

$$\Delta h = c_p \Delta T \tag{3.10}$$

To better account for the stretch rate *K*, a conservation of the stretch is included. Its equation is written as:

$$\frac{\partial(\rho u K)}{\partial x} = \frac{\partial}{\partial x}\left(\mu \frac{\partial K}{\partial x}\right) - \rho K^2 + (\rho a^2)_{ox} \tag{3.11}$$

where *x* is the spatial coordinate perpendicular to the flame surface, *u* is the flame velocity and the subscript *ox* stands for oxidant. The term *a* represents the strain rate at the oxidant side, and is written as:

$$a = -\frac{\partial u}{\partial x} \tag{3.12}$$

which, therefore, can be interpreted as the velocity gradient of the flow.

Finally, to close the system of the conservation equations the ideal gas state equations is applied with constant pressure assumption. Therefore, it only depends on the temperature:

$$\rho = \frac{p_0 MW}{R_u T} \tag{3.13}$$

With p_0 being the pressure of the system, MW being the molecular weight of the mixture and R_u is the universal gas constant, 8.314 J/(K.mol)

The conservation equations (3.4), (3.9) and (3.11) and the radiative equations (2.19), (2.27) or (2.34) (depending on the method) presented in the previous section are subject to the following boundary conditions:

$$u(x=0)=0$$

$$Y_i(x\to -L)=Y_{i,fuel} \qquad Y_i(x\to +L)=Y_{i,ox}$$

$$h(x\to -L)=h_{fuel} \qquad h(x\to +L)=h_{ox}$$

$$K(x\to -L)=a\sqrt{\rho_{ox}/\rho_{fuel}} \qquad K(x\to +L)=a$$

$$I^{+}_{\eta,l}(x=0)=I_{b,\eta}(x=0) \qquad I^{-}_{\eta,l}(x=X)=I_{b,\eta}(x=X)$$

Finally, mass conservation is ensured by correcting the mass fraction of N_2.

3.2 DESCRIPTION OF PROBLEM AND CALCULATION SET-UP

The problem analyzed in this study consist in the radiative heat transfer coupled with the chemical reactions and fluid dynamics for a one-dimensional counter-flow laminar flame. The position *x=0* of the domain represents the mid-point where the fuel jet meets with the oxidant (stagnation point), where the fuel enters the domain from the left boundaries (negative *x*-values, positive flow velocity) and the oxidant from the right boundaries (positive *x*-values, negative flow velocity). Figure 3.1 presents a drawing of the problem described.

The length *L* of the mathematical domain was set at 4 (four) centimeters in both directions. For lower values of the strain rate, the flame presents itself thicker in the *x* direction, therefore this value of *L* was chosen to ensure that the boundaries of the mesh did not affect the gradients of the temperature and velocity. The boundaries are set at 298 K and the system is at atmospheric pressure. It should be noted that since the total pressure is kept at 1 atm, one can infer that the partial pressure of the species is equal to their molar fraction.

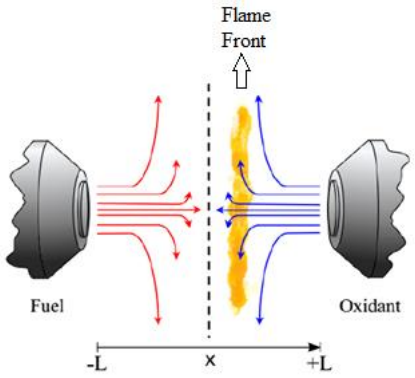

Figure 3.1 – Representation of a counter-flow flame. Adapted from Da Silva et al., 2020.

The fuel consists of methane either pure or with dilutions of carbon dioxide. These dilutions range from 2 to 80%. Due to the computational costs, the LBL method was calculated

only at specific percentages: 0, 20, and 50 and from 70-80%. The oxidant consists of dry air with molar concentration of 0.21 of oxygen gas and 0.79 of nitrogen gas. The strain rate, which is a dimensionless quantity that defines the velocity of the fuel and the oxidant streams, is also an important factor on the analysis of the effect it causes on the radiative properties of the flame. This parameter was also varied ranging from 10 s^{-1} to 100 s^{-1}. Again, due to the computational cost, the LBL method was calculated for the strain rates of 10, 20, 28, 30, 32, 40, 60, 80 and 100. These higher values of dilution (70-80%) and the range of strain rate were selected in order to compare with experimental data provided in the literature by Bundy et al., 2003, which presents results of critical dilution values of CO_2 for flame extinction limits at different strain rates.

The accuracy of the radiation models are evaluated by means of comparison with the line-by-line integration. The main quantities evaluated were the radiative heat flux, the volumetric rate of radiative heat generation, given as the negative of the divergent of the radiative heat flux, and the total radiative heat loss, which is the volume integrated radiative heat source. Since the radiative transfer equation is calculated coupled with the other flow and chemical equations, the temperature field and the molar fractions of water vapor, carbon dioxide and carbon monoxide were also evaluated.

It is more frequently seen in literature in comparisons of an applied WSGG formulation with the LBL (or other benchmark) the results in terms of the relative and normalized error for each volume of the domain when analyzing the radiative properties. However, this “point-by-point” basis is impractical for coupled calculations, since any changes in the gradients of temperature and species concentration or in the flow speed leads to changes in the overall length of the flame and of its discretization. Therefore, comparing two or more cases in a point-by-point analysis would require interpolating the results of all cases to a same volume discretization, which might already lead to more error, and then compare properties that are highly dependent on scalars that will not be the same in each volume. Therefore, the methods of comparison proposed in this work are to evaluate the relative error for the maximum values of each of the above-mentioned properties and graphically analyze if the models can correctly predict the trends in the gradients of the properties.

The software employs a fully implicit modified Newton technique for solving reactive flows with the finite volumes method. For the transport equations, the terms of advection are discretized employing the exponential method and the diffusive terms are discretized by the central differences method. In all cases it was applied the detailed mechanism DRM 19

proposed by Kazakov et al., 1995, which consists of 19 species. The Lewis number was set to unity for the calculation of the diffusion of the species in the mixture.

The mesh is adaptive with an algorithm based on the temperature and chemical species gradients so that resolution increases in the steep gradients regions. The solver was limited to 10000 maximum iterations and convergence criteria was of the residuals being below the 10^{-7}.

3.3 IMPLEMENTATION OF WSGG FORMULATIONS AND MESH DEPENDENCE STUDY

The first step in this study was to expand the tools available in the software CHEM1D for solving the radiative heat transfer equation. The first method added was the LBL integration. The routine of calculation for the LBL requires receiving as input from the other subroutines of within the solver the number of volumes, their positions, and their values of temperature and molar fractions of water vapor and carbon dioxide. Together with the databases for the HITEMP-2010, the calculation of the spectral lines occurs as described in chapter 2. Then the radiative heat source and flux are calculated. The result for the source term is imported to the energy equation solver, calculations continues, and repeat themselves until the convergence criteria is reached.

The second step was the introduction of the WSGG model and its different formulations. In total, there were 17 different formulations of the WSGG model implemented into the software. Two routines in Fortran were written, one for models that directly calculates the absorption coefficient of the mixture between water vapor and carbon dioxide, and another one that utilizes the superposition method, that first calculates the coefficients separately then concatenates the values. Considering the former routine, the coefficients were fitting by the authors according to specific values of molar ratio between the species and different available fitting data. As explained in the previous chapter, four different calculation schemes for the molar ratio were applied:

- "Fixed", where the coefficients are established for a certain molar ratio and does not account for variations of it neither in the pressure absorption coefficient nor in the temperature dependence coefficient.
- "Polynomial" or varying-*MR*, where the temperature dependence coefficient accounts for molar ratio variations by means of a polynomial curve fitting with the correlations, while the pressure absorption coefficient can also have a polynomial curve fitting or not.

- “Linear”, where there are different sets of correlations of both coefficients for different specific molar ratio and the model takes as input the value of the molar ratio of the evaluated volume and interpolates the coefficients for the adjacent molar ratio sets available in the model.
- “Stepwise”, similar to the “Linear” model, but instead of a linear interpolation of closest available sets, the model calculates the coefficients based upon the adjacent higher set.

The routine that applies the superposition method calculates individually the pressure absorption and temperature dependence coefficients for water vapor and carbon dioxide and then combines the results. The resulted coefficients are then applied to the calculations of radiative heat source and flux.

Table 3.1 presents all the variations of the WSGG applied in this study together with a characterization of the method for calculating the coefficients, the proposed range of applicability (molar ratio and temperature) and the method the author used for estimating the coefficients (the reference emittance data).

Table 3.1 – WSGG formulations applied in this work.

Main author and year	Name in this work	Coef. Calc.	MR range	Temp. range [K]	Reference ε data
Smith, 1982	Smi1982	Fixed	1 or 2	600-2400	EWB
Krishnamoorthy, 2010	Kri2010	Fixed	1 or 2	-	Perry
Yin, 2010	Yin2010	Fixed	1 or 2	500-3000	EWB
Yin, 2010	Yin2010	Stepwise	0.25 – 4	500-3000	EWB
Yin, 2010	Yin2010	Linear	0.25 – 4	500-3000	EWB
Johansson, 2011	Joh2011	Polynomial	0.125 – 2	500-2500	SNB
Kangwanpongpan, 2012	Kan2012	Fixed	1 or 2	400-2500	HITEMP2010
Kangwanpongpan, 2012	Kan2012	Linear	0.125 – 4	400-2500	HITEMP2010
Kangwanpongpan, 2012	Kan2012	Polynomial	0.125 – 4	400-2500	HITEMP2010
Dorigon, 2013	Dor2013	Fixed	1 or 2	400-2500	HITEMP2010
Yin, 2013	Yin2013	Fixed	1 or 2	500-3000	EWB
Bordbar, 2014	Bor2014	Polynomial	0.01 – 4	300-2400	HITEMP2010
Cassol, 2014	Cas2014	Superposition	-	400-2500	HITEMP2010
Coelho, 2017	Coe2017	Superposition	-	400-2500	HITEMP2010
Shan, 2018	Sha2018	Fixed	1 or 2	500-2500	SNB
Shan, 2018	Sha2018	Stepwise	0.125 – 4	500-2500	SNB
Shan, 2018	Sha2018	Linear	0.125 – 4	500-2500	SNB
Selhorst (wide), 2020	Sel2020	Polynomial	0.125 – 4	300-2500	HITEMP2010
Bordbar, 2020	Bor2020	Superposition	-	300-2400	HITEMP2010

The reference emittance data obtained for the correlations selected come or from exponential wide-band model (EWB), or from emissivity curves available in literature such as the one made available by Hottel et al., 2007 (Perry), or from statistical narrow-band model (SNB) or from the HITEMP2010.

Models with a "fixed" formulation were applied in this work individually, therefore as each would be a model of its own. In total, 27 models were applied and compared to the LBL (20 formulations plus 7 "extra" correlations from the fixed models).

In the work presented by Selhorst et al., 2020, it was presented two different formulations of the WSGG, and both where here applied. The second one, called "narrow", is categorized as a mixture of polynomial and stepwise formulation for having the two sets of coefficients depending on the molar ratio. One range is for 0.125 to 1 and the second is from 1 to 4 parts of water vapor to carbon dioxide.

3.3.1 Results for the adiabatic case

Below Figure 3.2 presents the calculated fields of temperature and species concentration for an adiabatic case that is without losses due to the radiative heat transfer. As it is a counter-flow flame, the gradients are steeper than well-mixed furnaces. These scalars are presented here first without the effect of radiation for later comparisons as how the iterative process affects them. The setting is of a strain rate of 20 s^{-1} and 0% dilution of CO_2 in the fuel side.

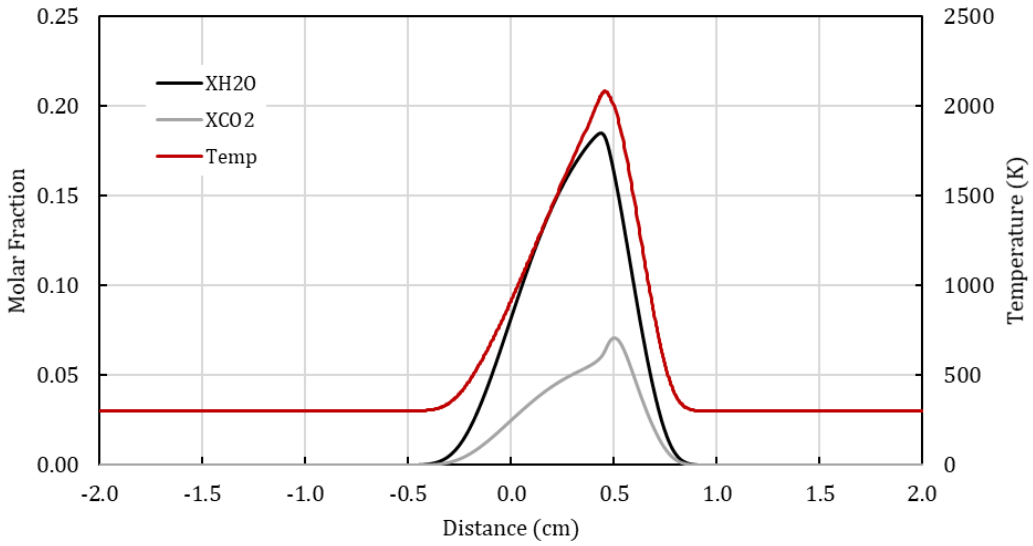

Figure 3.2 – Results for temperature, water vapor and carbon dioxide in an adiabatic calculation. Strain rate of 20 s^{-1} and no dilution.

This setup will be named as “base case” as in next sections comparisons will be made with this case and different setups.

As mentioned earlier, there are two other views of interest for the participating species concentration: the molar ratio and the sum of species. Therefore, Figure 3.3 presents both results together with the concentration of carbon monoxide.

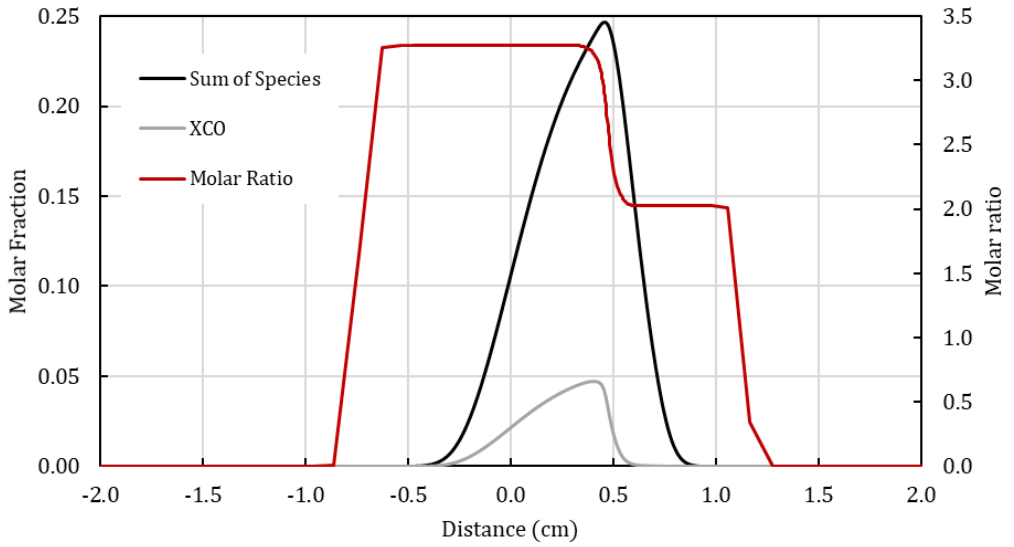

Figure 3.3 – Results for sum of species, carbon monoxide and molar ratio in an adiabatic calculation. Strain rate of 20 s^{-1} and no dilution.

As one of the present study objectives is to determine how the WSGG models compare with the LBL in different scenarios, Figure 3.4 presents the calculated fields of species for a strain rate of 40 s^{-1} in continuous line for reference the previous result from Figure 3.5 is shown in dotted lines. The same is replicated for the formation of carbon monoxide and the other two scalars of the participating species. Figure 3.6 presents these values for the strain rate of 40 s^{-1} with the previous results as dotted lines. Therefore, as it can be seen from these results, in adiabatic counterflow flames the increase of the strain rate does not generally lead to a significant change in the maximum values of the scalars, but rather on their gradients as the length of the flame is diminished. The difference in maximum temperature for instance is around 20 K.

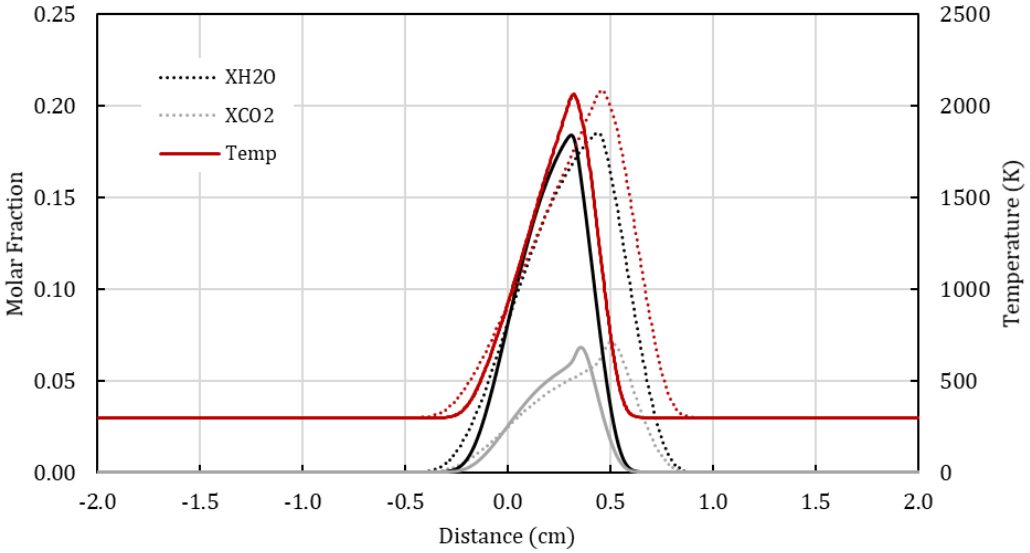

Figure 3.4 – Results for temperature, water vapor and carbon dioxide in an adiabatic calculation. Strain rate of 40 s^{-1} as continuous lines and 20 s^{-1} as dotted lines.

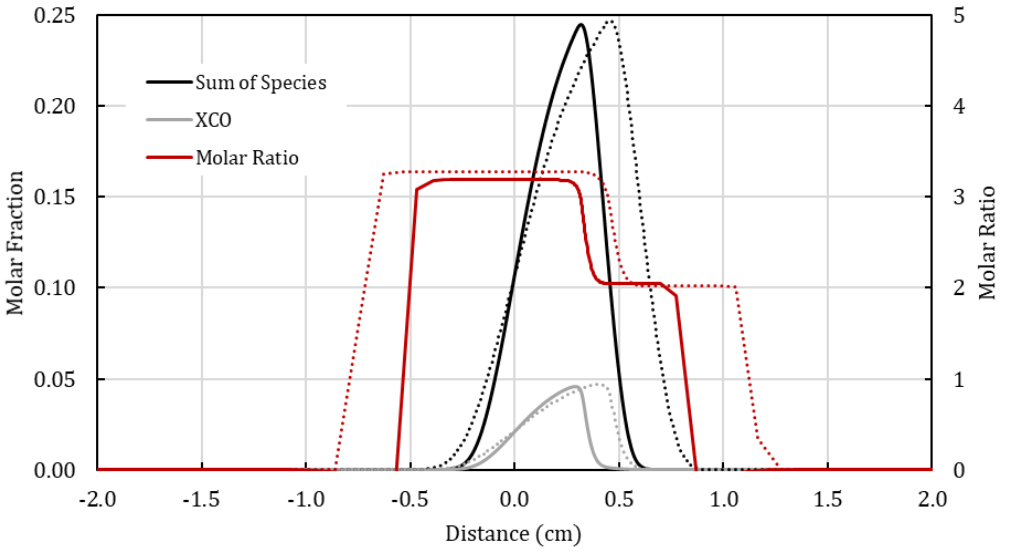

Figure 3.5 – Results for sum of species, carbon monoxide and molar ratio in an adiabatic calculation. Strain rate of 40 s^{-1} as continuous lines and 20 s^{-1} as dotted lines.

Another scenario that is discussed in this work is the different proportions of CO2 dilution in the fuel side, which is a subject of great interest in biofuel combustion. Figure 3.7 presents the scalar fields for a dilution of 50% of CO_2 and strain rate of 20 s^{-1} and again as the previous figures, the standard result is also presented as dotted lines.

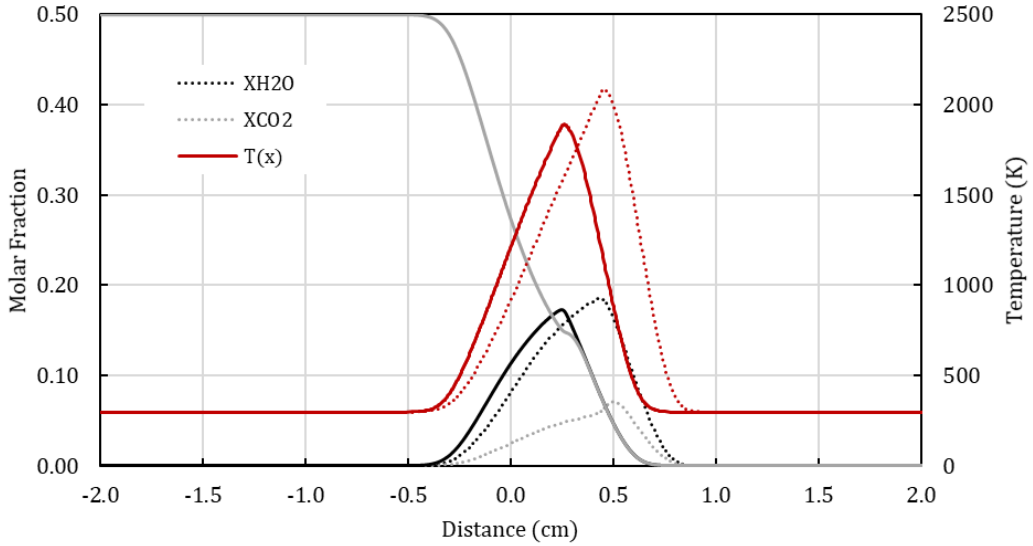

Figure 3.6 – Results for temperature, water vapor and carbon dioxide in an adiabatic calculation. Dilution of 50% CO2 as continuous lines and no dilution as dotted lines.

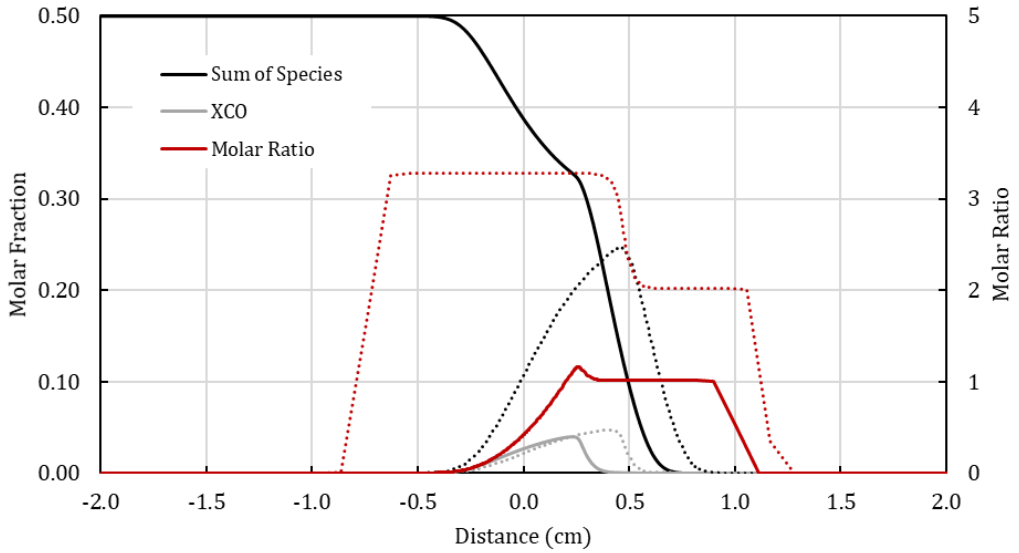

Figure 3.7 – Results for sum of species, carbon monoxide and molar ratio in an adiabatic calculation. Dilution of 50% CO2 as continuous lines and no dilution as dotted lines.

3.4 MESH CONVERGENCE

To ensure that the results were not affected by the discretization of the computational domain, a study of the quality of the mesh was performed. Two verifications were made, first for the total number of volumes, and, with the resulting mesh, for the number of the discrete directions used in the RTE integration.

3.4.1 Spatial discretization

Three different meshes were applied to the same case, a counter-flow methane-air combustion without radiative losses (adiabatic). The meshes M1, M2 and M3 had respectively, 400, 200 and 100 volumes each. Values evaluated to determine the mesh quality were the maximum values of temperature, velocity, and carbon monoxide. Other results, such as species for water vapor and carbon dioxide, were also included in this analysis but there was no noticeable difference in their formations.

The methodology for mesh analysis was the Grid Convergence Index (GCI), first presented by Roache, 1994 and updated by Celik et al., 2008. The main purpose of the GCI is to report the results of the mesh convergence study uniformly and present an estimation of the error related to the solution. Although it can be calculated with two set of meshes, ideally three meshes should be used to estimate if the results are within an asymptotic curve of convergence. Therefore, the GCI is an estimation of the calculated results and the asymptotic value of a mesh with infinite number of volumes.

For the most refined mesh, M1, the GCI should be calculated as:

$$GCI_{12} = \frac{F_s|\varepsilon_{12}|}{(r^p - 1)} \tag{3.11}$$

in which F_s is a factor of safety; for the case of three meshes, it equals 1.25, for two meshes 3. The r is the refinement factor between the meshes, therefore it is valued as 2 (as M1 was twice the volumes of M2, which in turn was twice the volumes of M3). The relative error ε_{12} is calculated by:

$$\varepsilon_{12} = \frac{(f_2 - f_1)}{f_1} \tag{3.12}$$

where f_1 is the solution of the evaluated criteria for mesh 1, and f_2 is the solution for the intermediary mesh. Also, from Eq. (3.11), p is the convergence order, given as:

$$p = \frac{\ln((f_3 - f_2)/(f_2 - f_1))}{\ln r} \tag{3.13}$$

finally, after calculating the GCI_{12} and GCI_{23} for a solution, one can verify wherever the solution is towards the asymptotic range by:

$$\chi = \frac{GCI_{23}}{r^p GCI_{12}} \tag{3.14}$$

which, the closer it is to unity, the closer the solution is to the asymptotic range of convergence.

The Table 3.2 presents the results of the evaluated variables for the mesh study for the three cases.

Table 3.2 – Maximum temperature, velocity and molar fraction of species for three different meshes.

Mesh		T_{max} [K]	V_{max} [cm/s]	$X_{H2O,max}$ [%]	$X_{CO2,max}$ [%]	$X_{CO,max}$ [%]
M1	400	2082.9	103.6	18.53	7.099	4.701
M2	200	2082.6	102.0	18.53	7.095	4.702
M3	100	2081.7	98.7	18.52	7.100	4.698

As mentioned earlier the results for carbon dioxide and water vapor were closely similar between each case. Therefore, they are better presented in the form of a graph. Figure 3.1 presents the formation of carbon dioxide and water vapor for the case of M1 together with the mesh distribution for all three cases.

Due to the discretization parameters all three meshes concentrate the elements at the region with the higher values of combustion products and temperature. The three meshes were evaluated with the GCI method and the results are presented in Table 3.3.

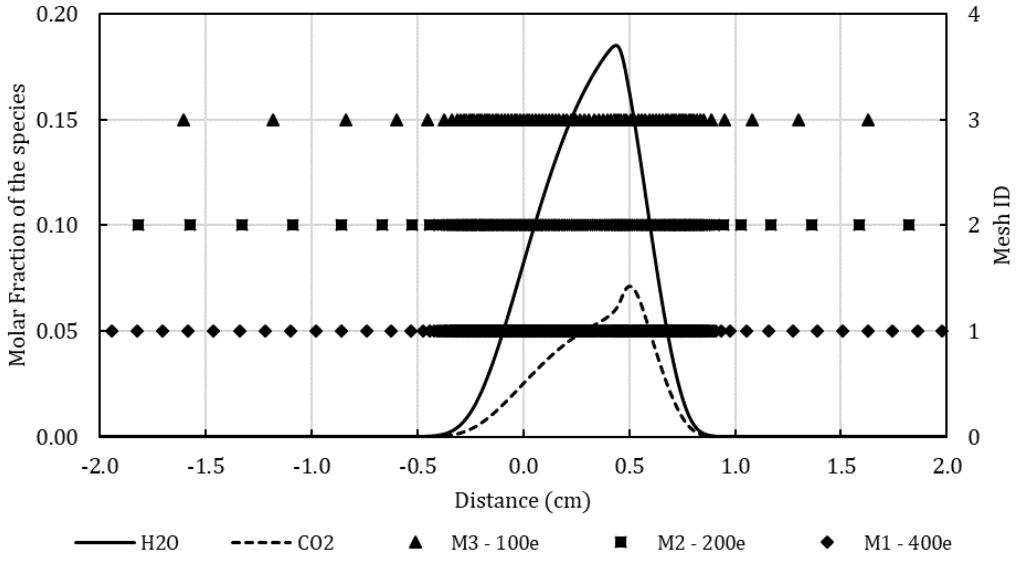

Figure 3.8 – Mesh comparison and results for water vapor and carbon dioxide in an adiabatic calculation.

Therefore, all values presented good results for the mesh convergence study. Although the higher results were with the maximum velocity, with a 2% estimated difference to mesh independence result, the main factors in this study relate to temperature and species concentration as they have direct influence in the radiative heat transfer.

Table 3.3 – GCI and convergency factor.

	T_{max}	V_{max}	$X_{H2O,max}$	$X_{CO2,max}$	$X_{CO,max}$
GCI_{12} [%]	$5.85x10^{-5}$	$2.01x10^{-2}$	$1.24x10^{-4}$	$2.24x10^{-3}$	$1.30x10^{-5}$
GCI_{23} [%]	$7.80x10^{-6}$	$4.04x10^{-2}$	$1.65x10^{-4}$	$2.94x10^{-3}$	$1.24x10^{-4}$
χ	1.0001	1.0160	1.0000	1.0006	0.9999

3.4.2 Directional discretization

Using the resulting mesh of 400 volumes, both the LBL method and the WSGG model with correlations as proposed by Dorigon et al., 2013, were applied, and it was performed a comparison of the total number of directions used in solving the Discrete Ordinates Method (DOM). For this, the disposition of the volumes, the temperature and the species molar fractions from the base case presented in last section were used in a RTE solver made available by the LRT-UFRGS (Laboratory of Thermal Radiation). This in-house RTE code uses several Fortran routines together to solve the radiative heat flux and heat source fields along a one-dimensional

domain bounded by two walls, with the possibility of selecting the radiative boundary condition of them. This in-house code was used as the main reference in the implementation of the WSGG and LBL solvers in the CHEM1D software.

It was calculated the radiative heat source and heat flux with total angle divisions of 20, 16, 12, 8 and 4. The difference between the first and the last case was of up to 4% maximum for the heat flux and 2.5% for the heat source. Due to computational costs, it was opted to use 12 angle divisions instead of 20, and with this configuration it was noted a difference of 0.9% for the heat flux and 0.7% for the heat source.

4. RESULTS AND DISCUSSION

In this chapter, the results obtained in this work are presented. Firstly, it is presented the LBL integration in 6 (six) different scenarios that are the combination of three strain rates (10, 20 and 40 s^{-1}) and three carbon dioxide dilutions (0, 20% and 50%). The selected values of strain rate are in order to show the expected results to the scalars with the change in this factor. Secondly, for the setups mentioned above, the benchmark is compared to all implemented WSGG formulations, with the most significant results presented in graphs. Not all formulations achieved convergence in the coupled calculation and therefore only those that did are presented in this study.

The third analysis is an overview of the results of the most promising correlations for a several values of strain rate and carbon dioxide dilution. The fourth analysis discussed here is the capacity of the LBL integration and the WSGG models to calculate the proposed case with increasing dilution of CO_2. The purpose of this study is to compare with experimental data for flame extinction due to radiative losses and increased presence of an inert gas (in this case CO_2).

4.1 RESULTS OF BENCHMARK AND COMPARISON WITH DECOUPLED CALCULATIONS

In the next sections for each flame set up, the results for the LBL integration coupled with the other combustion calculations are presented. These results are compared with the decoupled LBL solution of the scalars field of an adiabatic flame with similar set up. Each section is for a specific dilution and strain rate. The last section contains a summary of all cases in the form of a table. The purpose of this section is to evaluate the differences aggregated between the decoupled and coupled methods of calculating the radiative quantities. The dotted lines represent the results for the cases adiabatic flame (as previously shown in Chapter 3 and presented once again for convenience).

4.1.1 Dilution of 0% and Strain rate of 20 s^{-1}

Figure 4.1 presents the results of temperature and participating species concentration for the LBL integration method for a strain rate of 20 s^{-1} and no dilution of carbon dioxide.

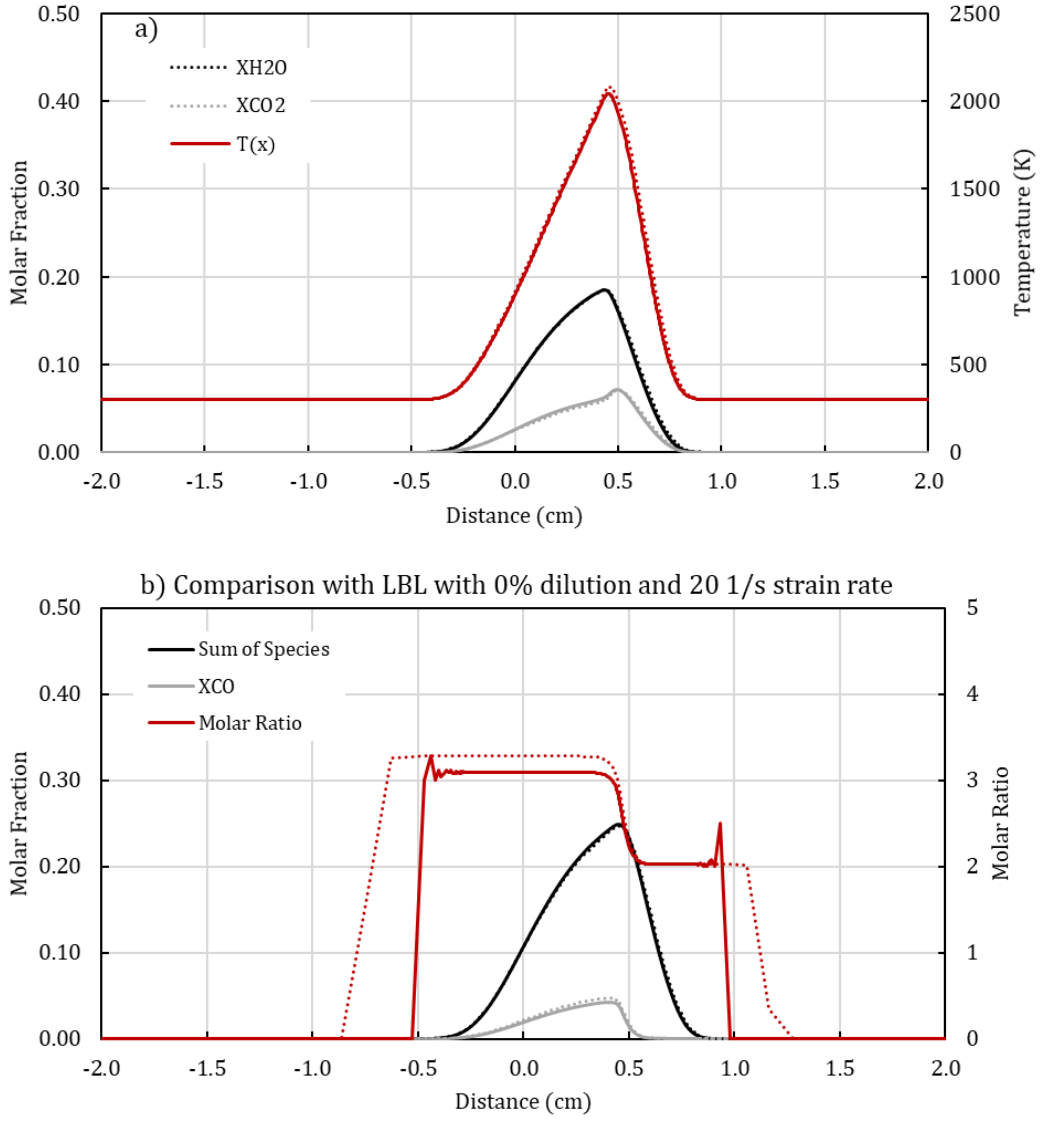

Figure 4.1 – For a dilution of 0% of CO_2 and strain rate of 20 s^{-1}: (a) Results of the LBL for temperature, H_2O and CO_2. (b) Results of the LBL for molar ratio, sum of species and CO.

Two main results can be taken from these results. The first is the difference in temperature, in which by including radiative losses amounts to almost 40 K. Although in the scope of a combustion with temperatures reaching as high as 2050 K, this difference is expected to be significant as temperature is accounted for in the RTE directly in the power of four and indirectly in the absorption coefficient of the participating gases.

The second result of interest is the maximum molar fraction of carbon monoxide that has decreased in as much as 10.3% when radiation is included. This might be a direct influence of the temperature decrease. It is interesting also to note that, although the LBL results point for a narrower range of the molar ratio, the partial pressure range remains roughly the same. This

means that the region of -0.5cm to 1.0cm roughly remains the region where the radiative transfer is more important. The maximum value of water vapor remains unchanged (by less of 0.1%), while the maximum molar fraction of carbon dioxide increased 1.2% from the decoupled case to the coupled one. The latter result together with the decrease in temperature should even out the radiation quantities as they are proportional to the partial pressure and temperature.

Figure 4.2 presents the results of the radiative heat source and radiative heat flux for the LBL integration. A comparison is made with a decoupled calculation using the scalars of the results without radiative losses from the previous graph.

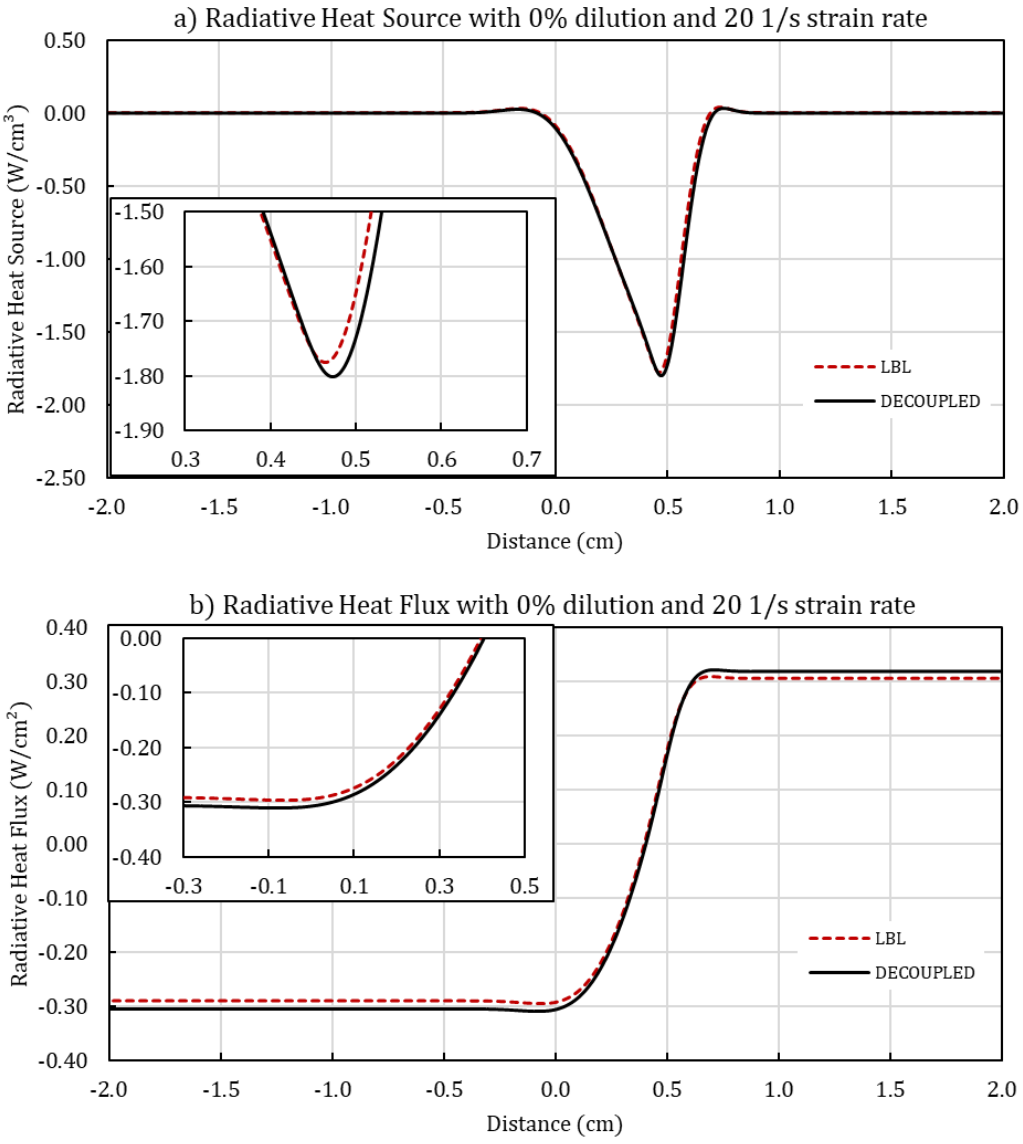

Figure 4.2 – For a dilution of 0% of CO_2 and strain rate of 20 s^{-1}: (a) Results of the LBL for radiative heat source. (b) Results of the LBL for radiative heat flux.

As it can be seen, the increase in carbon dioxide (of 1.2%) together with the decrease in temperature (of 1.9%) resulted in a difference not quite pronounced for radiative heat source, where the coupled case had a slightly lower minimum value with a decrease in absolute value of 1.5%.

4.1.2 Dilution of 20% and Strain rate of 20 s^{-1}

Figures 4.3 and 4.4 presents the comparison for the case of a strain rate of 20 s^{-1} and 20% of dilution. The former is the species concentration and temperature and the latter is for the radiative quantities.

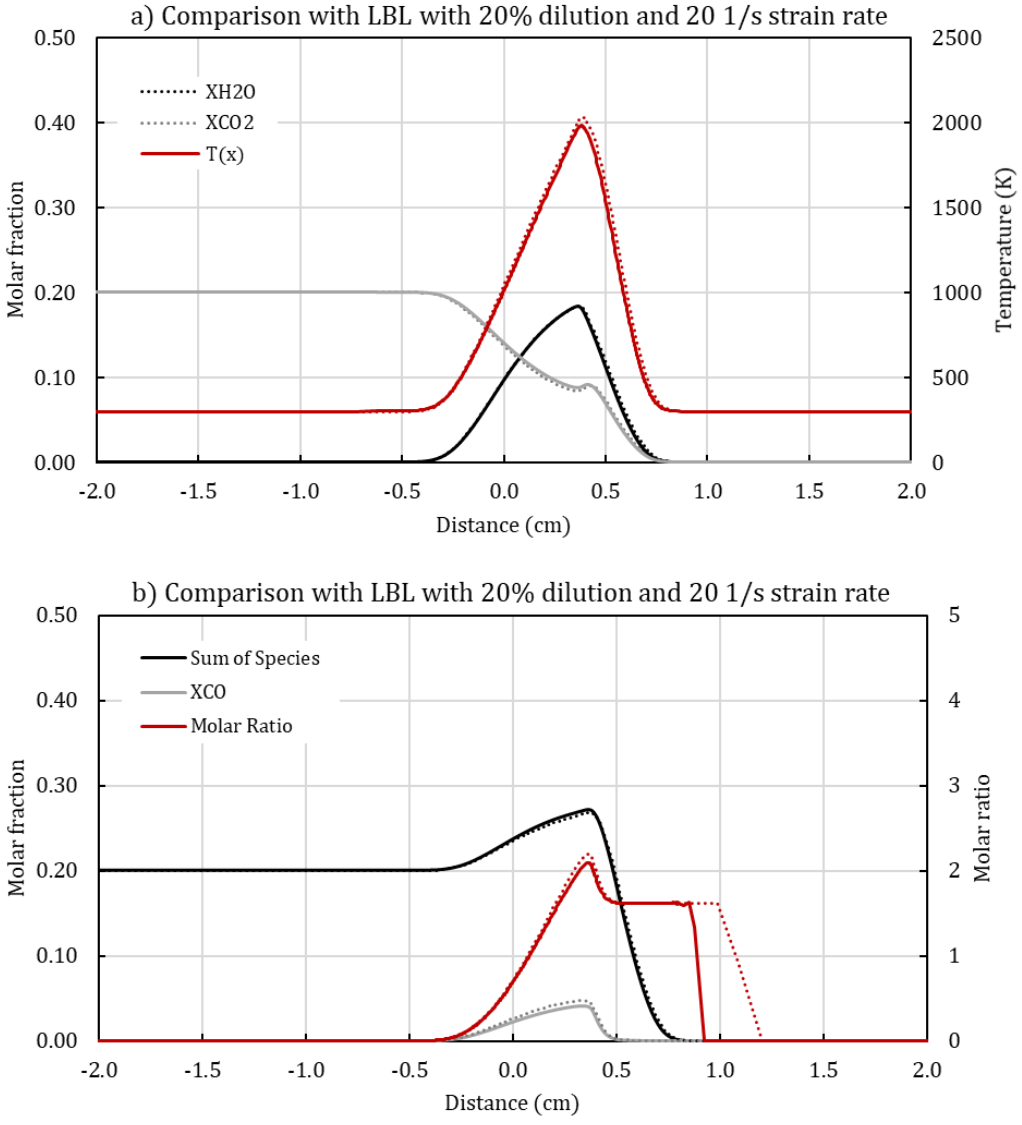

Figure 4.3 – For a dilution of 20% of CO_2 and strain rate of 20 s^{-1}: (a) Results of the LBL for temperature, H_2O and CO_2. (b) Results of the LBL for molar ratio, sum of species and CO.

As expected, due to content of carbon dioxide the in the fuel side, the molar ratio in the region of the flame diminished from a little over three in the fuel side and two in the oxidant side to rising a little over two in the fuel side and 1.6 in the oxidant side.

In later comparisons, the quantity of 20% dilution of carbon dioxide will be an important mark of comparison between fixed models of the WSGG as the average molar ratio is around 1.5, which stands as the halfway between correlations for molar ratio of 1 and of 2.

The addition of carbon dioxide does not seem to have a great affect in the formation of carbon monoxide, as the maximum value only increased by less than 3%. The overall temperature difference between the coupled LBL cases with and without dilution was of 63 K, which also resulted in a 3% difference. Also, the maximum molar fraction of carbon dioxide is reduced in 14.5% from the decoupled case.

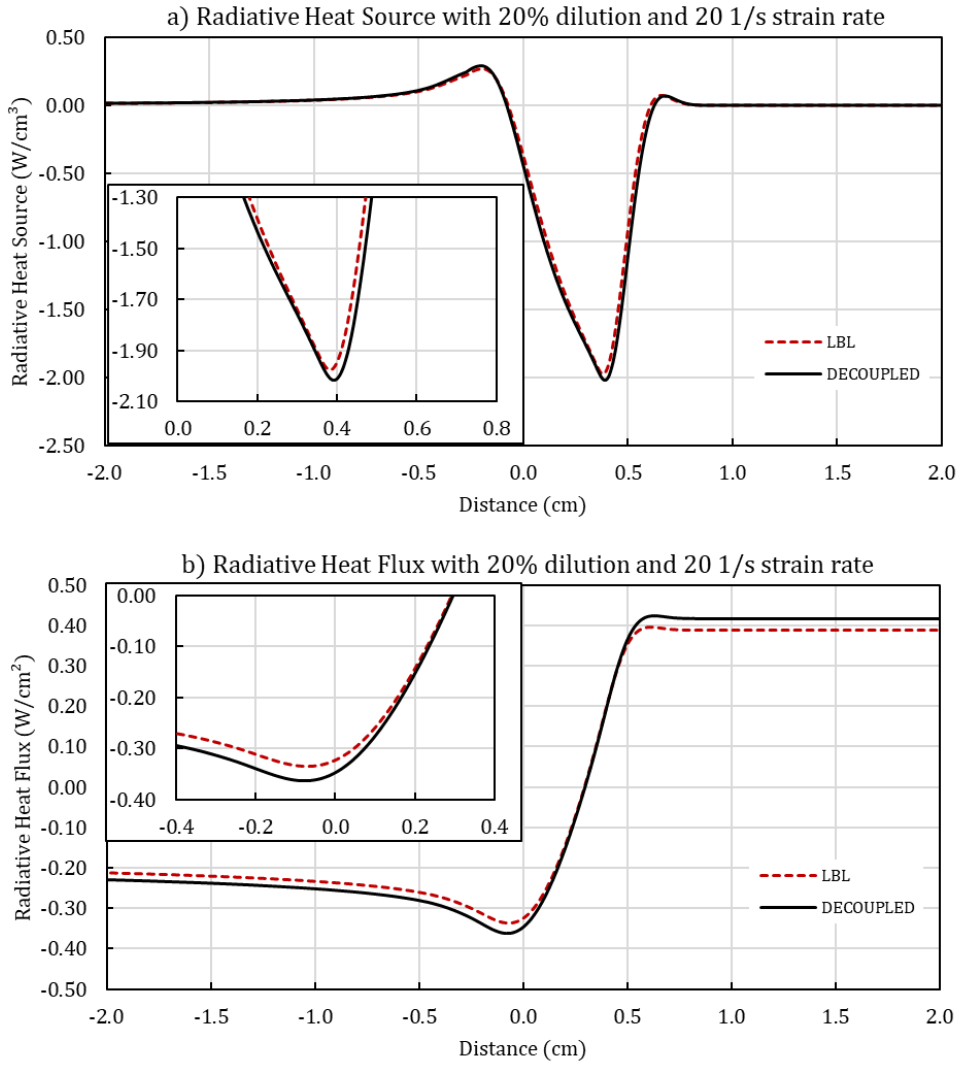

Figure 4.4 – For a dilution of 20% of CO_2 and strain rate of 20 s^{-1}: (a) Results of the LBL for radiative heat source. (b) Results of the LBL for radiative heat flux.

It was perceived an increase in the difference between the coupled and decoupled methods regarding the field of radiative heat flux. The previous case has a difference of 4% while this one has 7%. The dilution of CO_2 increased the radiation quantities, and this factor seems to lead to an increase in also the error associated in solving the radiation field decoupled from the other combustion processes.

4.1.3 Dilution of 50% and Strain rate of 20 s^{-1}

Figure 4.5 and 4.6 presents the results for the same strain rate but with a dilution of 50%.

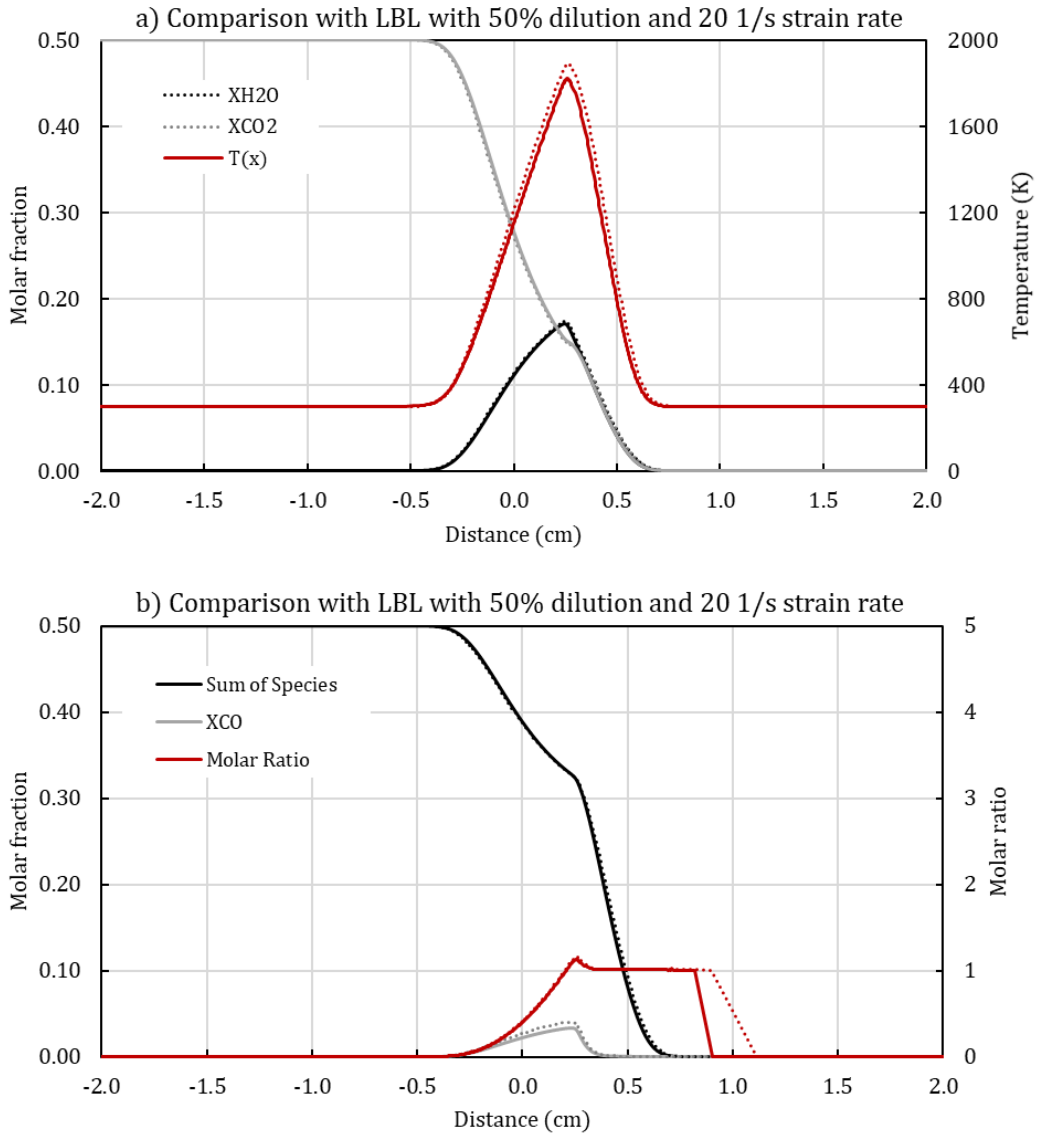

Figure 4.5 – For a dilution of 50% of CO_2 and strain rate of 20 s^{-1}: (a) Results of the LBL for temperature, H_2O and CO_2. (b) Results of the LBL for molar ratio, sum of species and CO.

The difference in temperature in this scenario compared to the base case can be perceived to have increased. This is expected, because carbon dioxide is a direct agent in the radiative field, therefore increasing it would increase the radiative losses in the system. The difference amounts to almost 70 K. The decrease in the maximum molar fraction of carbon monoxide is also more perceivable for the coupled case which has 19% less carbon monoxide formation.

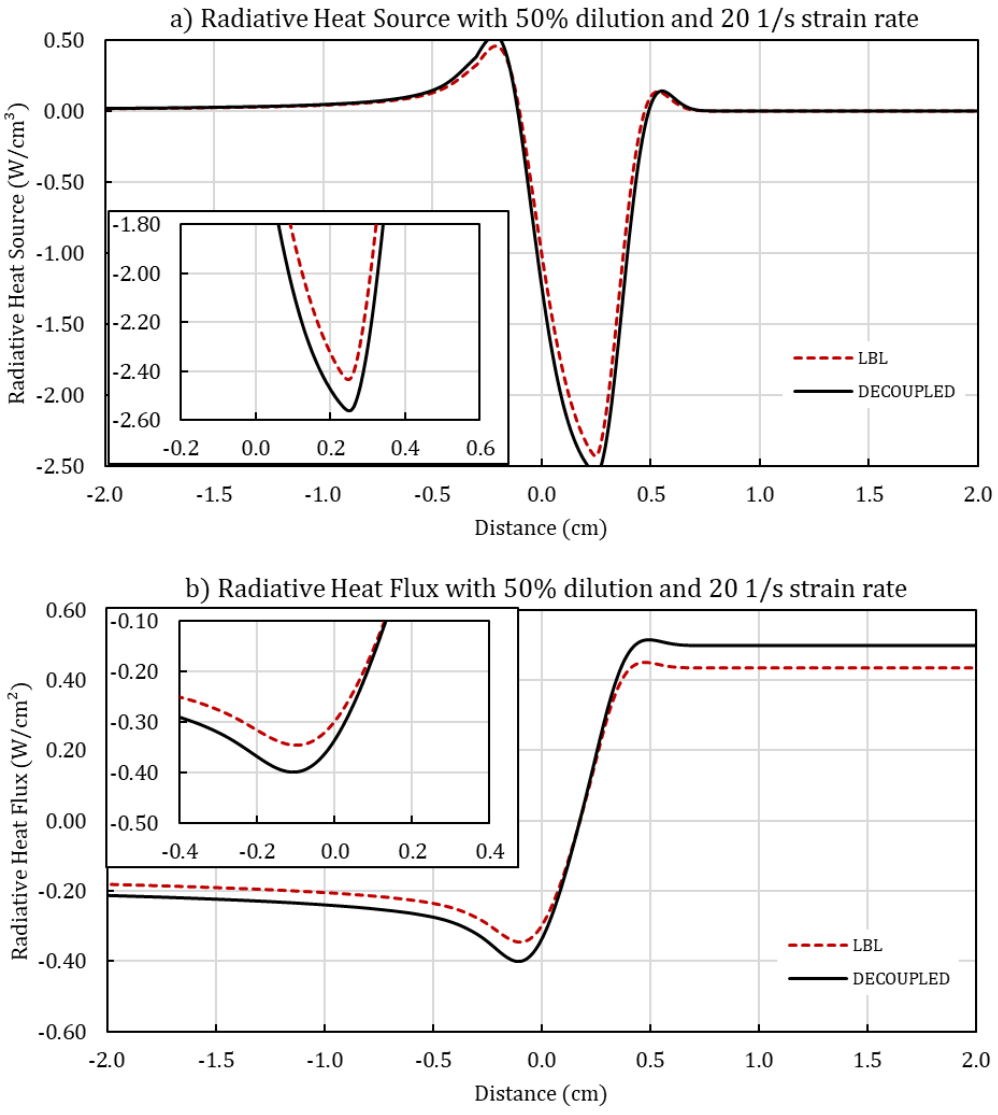

Figure 4.6 – For a dilution of 50% of CO_2 and strain rate of 20 s^{-1}: (a) Results of the LBL for radiative heat source. (b) Results of the LBL for radiative heat flux.

The difference in the heat source between this case and the base case is of around 5%, while for the heat flux this difference amounts to 13.7%. As it was verified for the previous cases, the radiative heat flux is more affected by the decoupling of the RTE than is the radiative heat source term.

4.1.4 Dilution of 0% and Strain rate of 40 s^{-1}

Figure 4.7 presents the results of the cases calculated for a strain rate of 40 s^{-1} for the temperature and species formation. Figure 4.8 presents the results for the radiative quantities between the decoupled and coupled calculations.

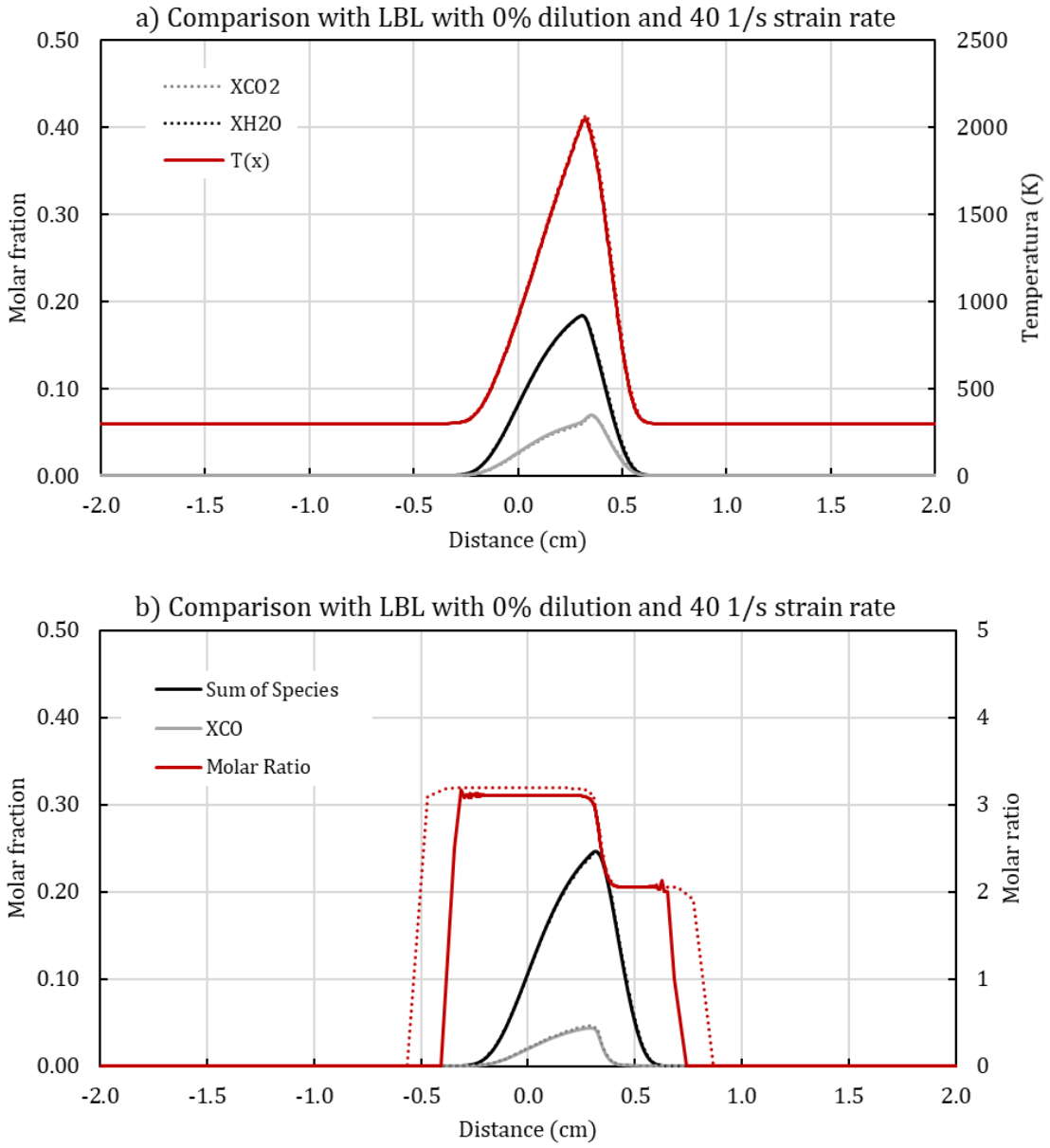

Figure 4.7 – For a dilution of 0% of CO_2 and strain rate of 40 s^{-1}: (a) Results of the LBL for temperature, H_2O and CO_2. (b) Results of the LBL for molar ratio, sum of species and CO.

It can be seen that the increase in the strain rate diminished the difference between the species formation and temperature from the coupled to the decoupled calculation. The reduction of the

maximum value of carbon dioxide for this strain rate and no dilution is of 4.7%, while for the same case with a strain rate of 20 s^{-1} this difference was of over 10%. The same reduction between cases happens for the temperature, that is only 21 K lower in the coupled case.

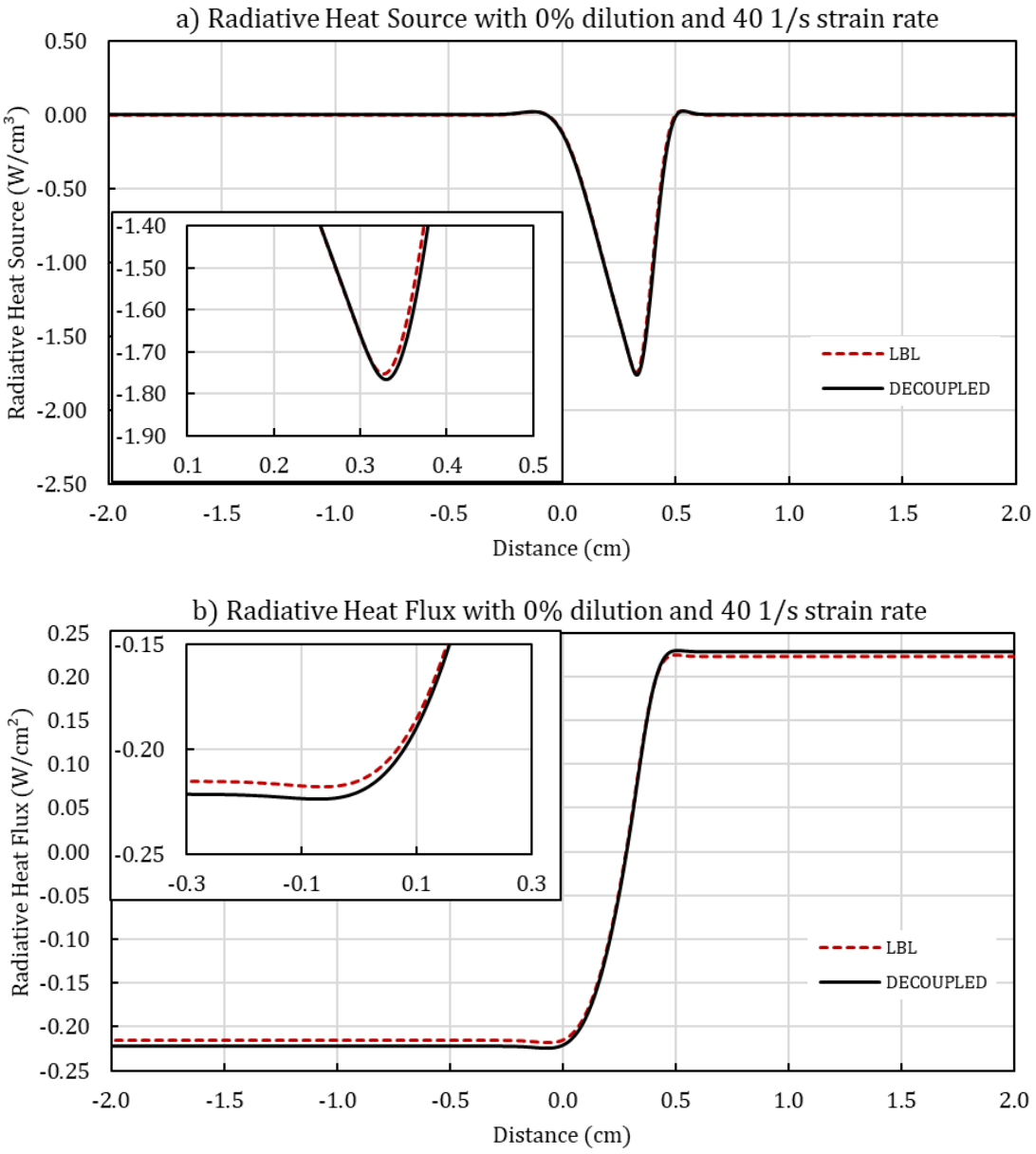

Figure 4.8 – For a dilution of 0% of CO_2 and strain rate of 40 s^{-1}: (a) Results of the LBL for radiative heat source. (b) Results of the LBL for radiative heat flux.

As expected from the results of the species and temperature, the radiation field also is more similar between the decoupled and coupled calculations. The radiative heat source and heat flux for the decoupled case has errors of 0.8% and 2.5%, respectively, when compared to the

calculation with the LBL integrated in the CHEM1D. For the case of no dilution, the strain rate of 20 s^{-1} these errors were of 1.5% and 4.0% respectively.

Another interesting result is that although the minimum value of the radiative heat source has remained roughly the same for both strain rates, the heat flux has greatly decreased with the increase of the strain rate compared to the base case. This is expected as the source term is the divergent of the flux.

Other strain rates higher than 20 s^{-1} were also calculated. The results have the same trend as the one presented for the strain rate of 40 s^{-1}, that is a lower gap between decoupled and coupled cases and reduction of the influence of the radiative losses in regard to the formation of species, especially the carbon monoxide. A compilation of the main results for these higher strain rates is presented in a later section.

4.1.5 Dilution of 0% and Strain rate of 10 s^{-1}

Strain rates lower than 20 s^{-1} were also studied in this work. Figure 4.9 presents the results of the species and temperature for a strain rate of 10 s^{-1}. Following the previous results, these are shown together with the same case for a decoupled calculation of the radiation quantities. Figure 4.10 presents the mentioned properties.

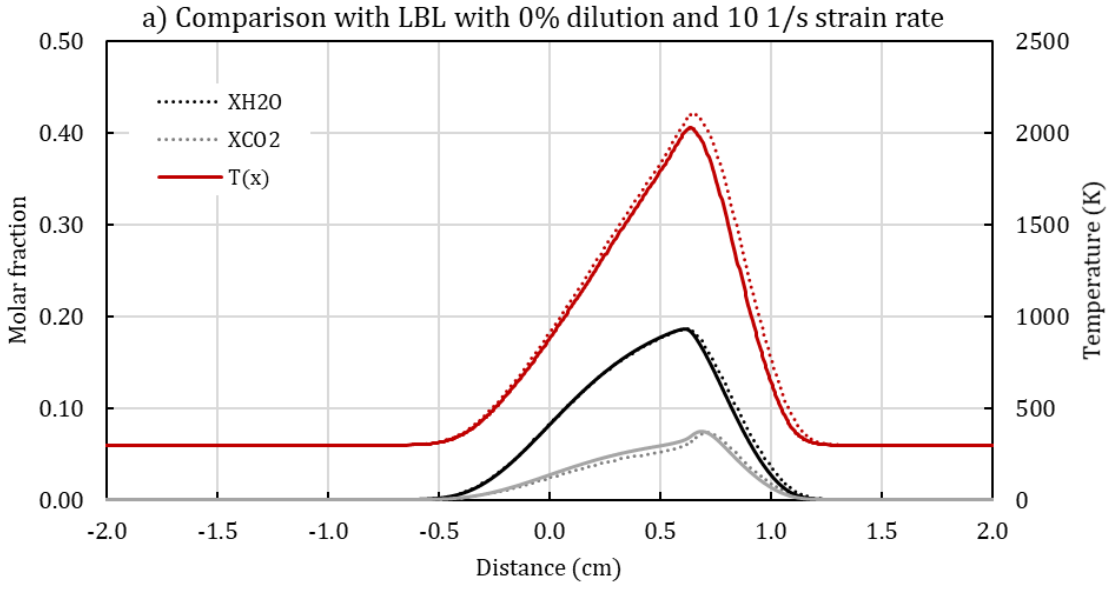

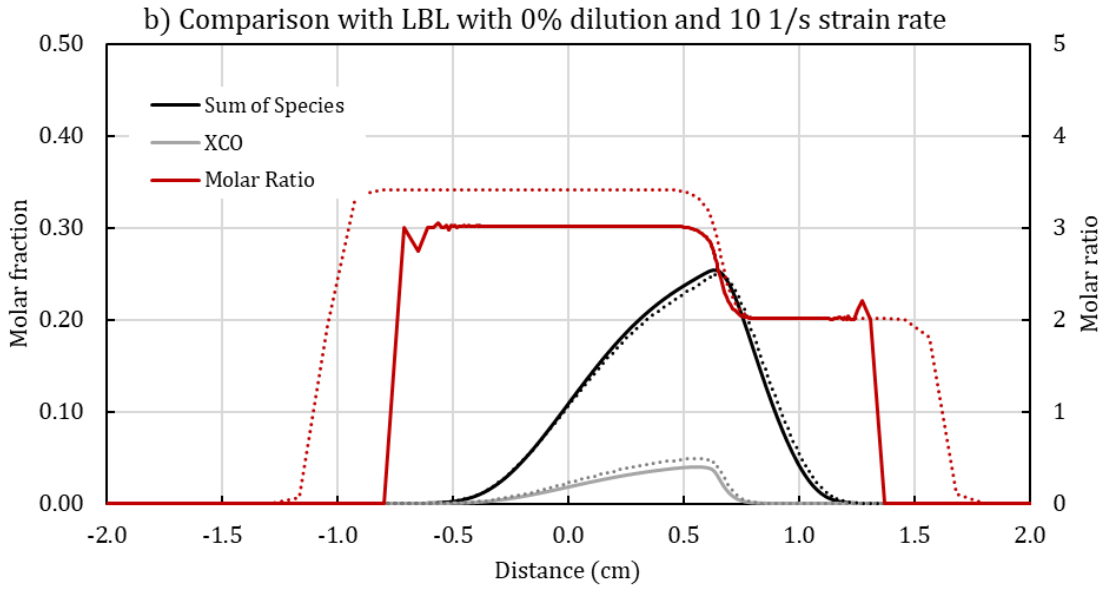

Figure 4.9 – For a dilution of 0% of CO_2 and strain rate of 10 s^{-1}: (a) Results of the LBL for temperature, H_2O and CO_2. (b) Results of the LBL for molar ratio, sum of species and CO.

The reduction of the strain rate produces a greater difference for the maximum temperature of both the decoupled and coupled calculations. For the decoupled case, the temperature reaches as high as 2100 K, while for the iterative case this same strain rate results in a temperature of 2026 K. This is resulted from the fact that the decoupled is first calculated as an adiabatic case and then radiative field is calculated from the resulting species and temperature. Therefore, because radiation plays a more important role in the heat losses for lower strain rates, this higher difference is expected.

Along with that, the error in the calculation of the molar fraction of carbon monoxide is also increased. The coupled case has a maximum CO molar fraction of 0.04 while for the decoupled calculation it is 0.049. That is a 22% difference between the results.

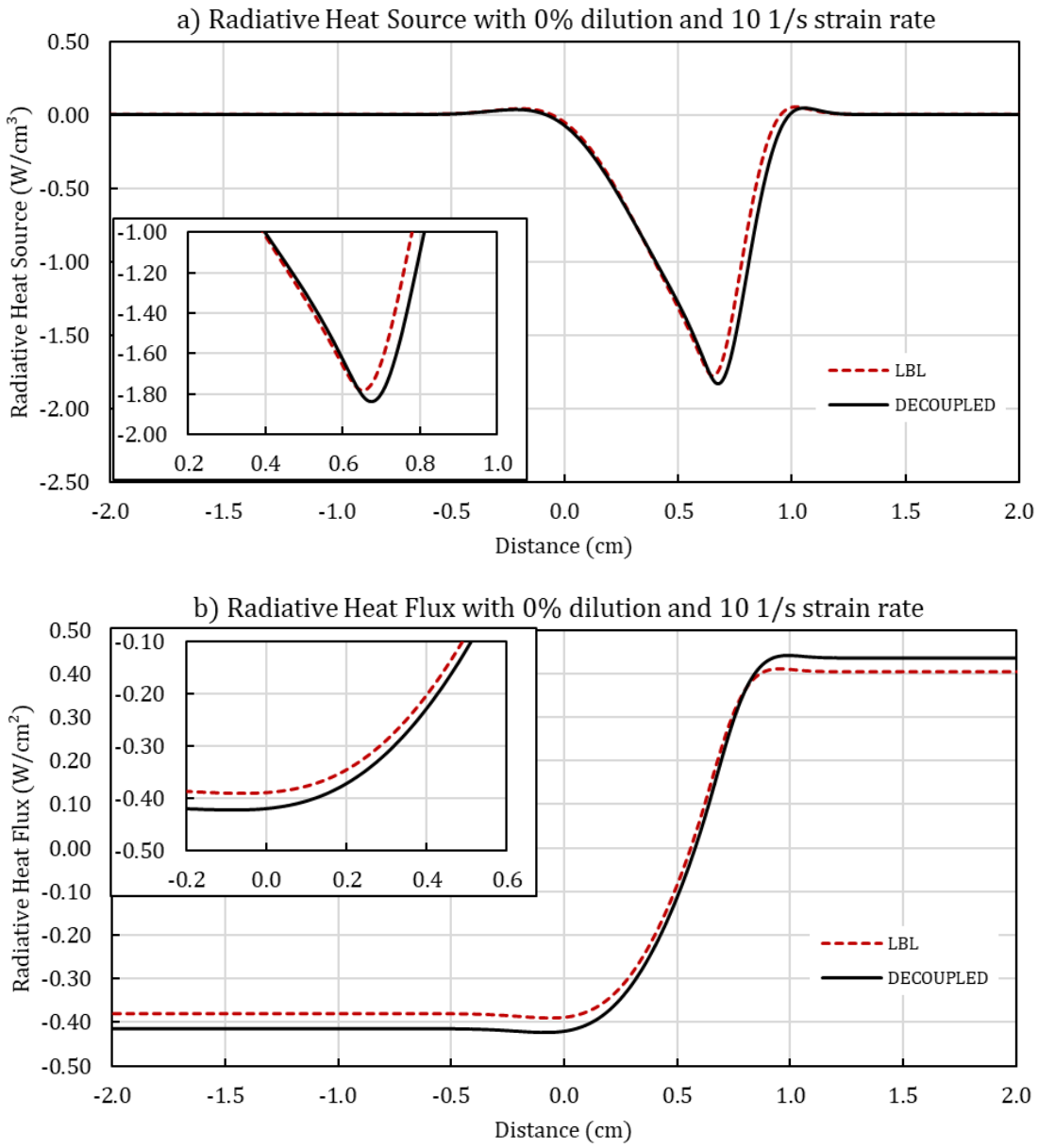

Figure 4.10 – For a dilution of 0% of CO_2 and strain rate of 10 s^{-1}: (a) Results of the LBL for radiative heat source. (b) Results of the LBL for radiative heat flux.

When compared to the results presented for the strain rate of 20 s^{-1} the radiative heat source has kept roughly its minimum value (that stands for the maximum heat loss) while the radiative heat flux has increased significantly. However, the radiative loss is higher in lower strain rates due to the flame itself being thicker as the strain rate decreases. Therefore, the net radiative loss of the flame is higher, although the maximum temperature is lower.

4.1.6 Compiled results

Below the results from the cases presented in this section and other cases calculated in this work for the LBL integrated and decoupled. These results are compiled for different strain rates and carbon dioxide dilutions in order to understand the effect of these factors in the main observed variables as well as the effect on the difference between the two methods.

This work compared the species concentration by two different quantities: the maximum molar fraction of a species and the total mass of the species along the domain. In regards to comparing the two different methods, it was noted that evaluating the maximum value of a species or its total formation resulted in the similar observations, specifically for the CO molar fraction; therefore, only maximum values will be discussed for this species concentration. For example, although it was seen that by decreasing the strain rate the maximum molar fraction of water vapor remains roughly the same but the total formation of it increases, both methods captured this behavior. This change in the total formation of H_2O is due to the flame being thicker and therefore having more space to burn the reagents.

For the maximum molar fraction of water vapor the difference was less than 0.5% between the decoupled and coupled cases for the lowest strain rate calculated. For carbon dioxide, the difference between the decoupled and coupled cases was at maximum 3.3% for a strain rate of 5 s^{-1}. The main quantity affected by decoupling the solution of the RTE was the carbon monoxide. Figure 4.11 presents the results of maximum molar fraction of carbon monoxide for different strain rates.

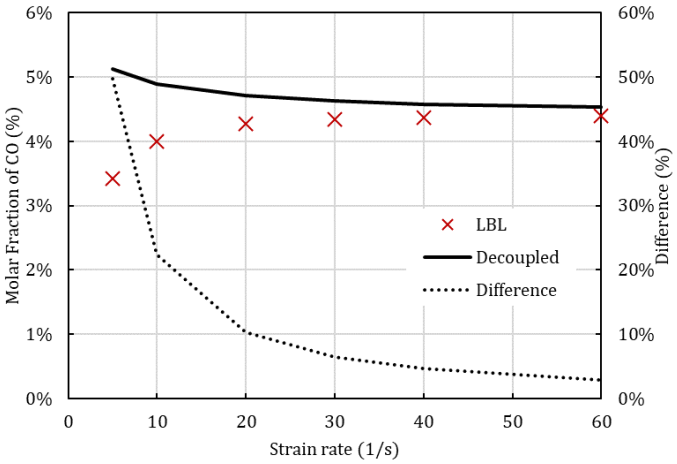

Figure 4.11 – Maximum molar fraction of Carbon Monoxide.

As the strain rate reduces, the decoupled case has a higher molar fraction of carbon monoxide calculated, with almost 50% of relative difference when compared to the integrated calculation of the LBL. This is because the effects of radiation become more prominent as the flame is thicker and emits more radiation as the broadening of spectral lines increases due to the more energetic state of higher temperatures.

When considering the calculation of the heat loss, there is a small but noticeable difference in the approaches. Figure 4.12 illustrates the maximum heat loss difference and the total heat loss.

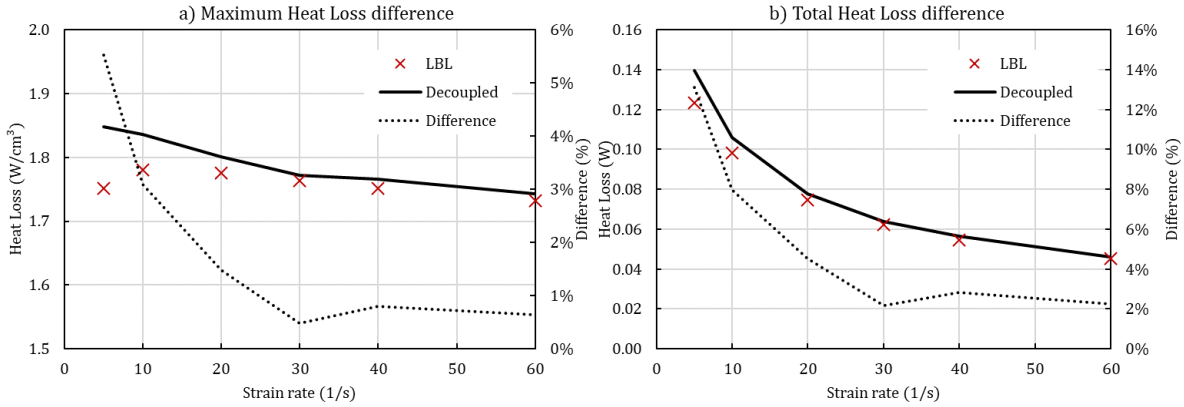

Figure 4.12 – For different strain rates: (a) Maximum Heat Loss. (b) Total Heat Loss.

Comparing the maximum heat loss between calculation approaches, only for lower strain rates the decoupled method differs significantly from the coupled calculation, going over 5% for the lowest strain rate and on a different trend. However, as it can be seen from the total heat loss, the decoupled method manages to roughly accompany the trend, but, as the strain rate decreases, the difference increases.

In the species formation of both participating species the difference between the decoupled and coupled method resulted in less than 1.2% for CO_2 dilution of 50%, with results for other dilutions by less than 0.9% for water vapor. Since carbon dioxide is being added to the system, there is no difference in the maximum molar fraction of carbon dioxide. Figure 4.13 presents the results for the molar fraction of carbon monoxide. The difference between methods increases with the dilution, reaching almost 20% for a fuel dilution of 50% of CO_2. This is expected, since the temperature is higher in the decoupled case. Figure 4.14 presents the results of the maximum and total heat loss the flame as function of the dilution.

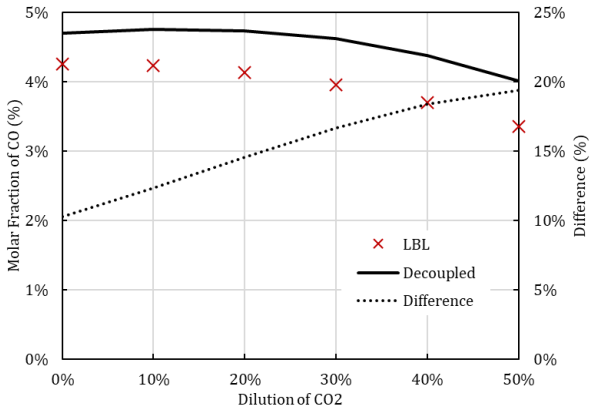

Figure 4.13 – For different dilution of CO_2: maximum molar fraction of CO.

An interesting result is presented as the mark of 10% of carbon dioxide dilution. Although the maximum heat loss is increasing along the dilution, this configuration has the lowest total heat loss between the compared cases. Although the temperature decreases around 30K with this added inert, this might yet indicate possible advantages in thermal efficiency with small additions of carbon monoxide.

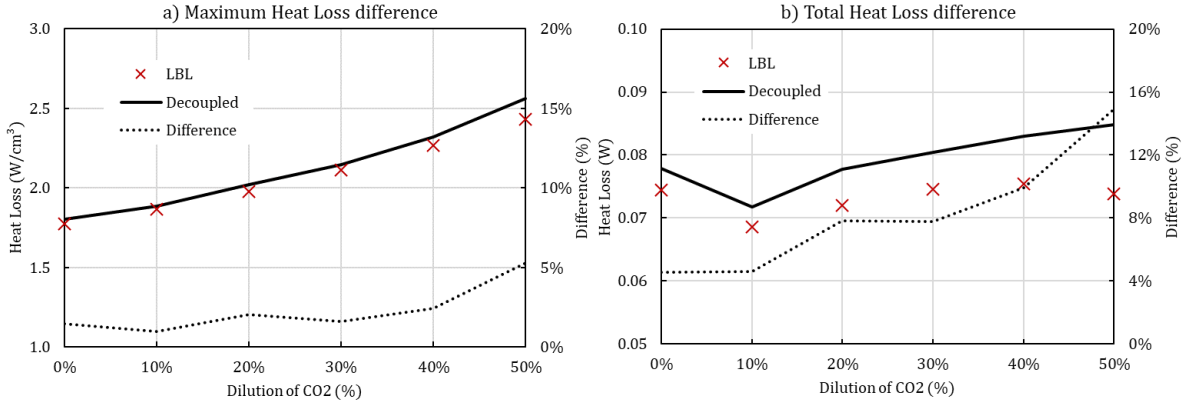

Figure 4.14 – For different dilutions: (a) Maximum Heat Loss. (b) Total Heat Loss.

Therefore, although most works in the literature develop evaluation of spectral models in decoupled scenarios, that is to say, from predefined species and temperature, it was seen in this section that there are differences in results between decoupling the RTE from the other transport and chemical equations of the flame. Differences can reach as high as 13% for radiative quantities and as high as 50% for molar fraction of CO. Carbon monoxide is known as a pollutant and today's regulations in regions such as USA and Western Europe have stricter limits for such species to be emitted in combustion process.

4.2 Results of the WSGG and Comparison with the Benchmark

This section presents the results of spectral models for different set-ups of dilution and strain rate. These are grouped according to the formulation used to develop them. At the end of each set up there is an overview of all methods used. The first setup is the base case of strain rate 20 s^{-1} and 0% dilution of CO_2 in the fuel side, followed by 20% and 50% dilution. The last setup is strain rate 10 s^{-1} and 0% dilution. Strain rates of 40 s^{-1} or higher does not present great relevance in terms of radiative heat transfer and was opted to be left out of this section.

4.2.1 Dilution of 0% and Strain rate of 20 s^{-1}

This section presents results for the strain rate of 20 s^{-1} and no dilution that is the setup known in this work as the base case. It was opted to left out results obtained with a fixed molar ratio of 1:1 because the average molar ratio for this case is closer to the 2:1 ratio.

4.2.1.1 GG and OTA models

Figure 4.15 is a comparison of the LBL integration with the Optically Thin Approximation and the Gray-Gas model. For this and all future graphs of the radiative heat source, the results of the LBL are presented as a red dashed line.

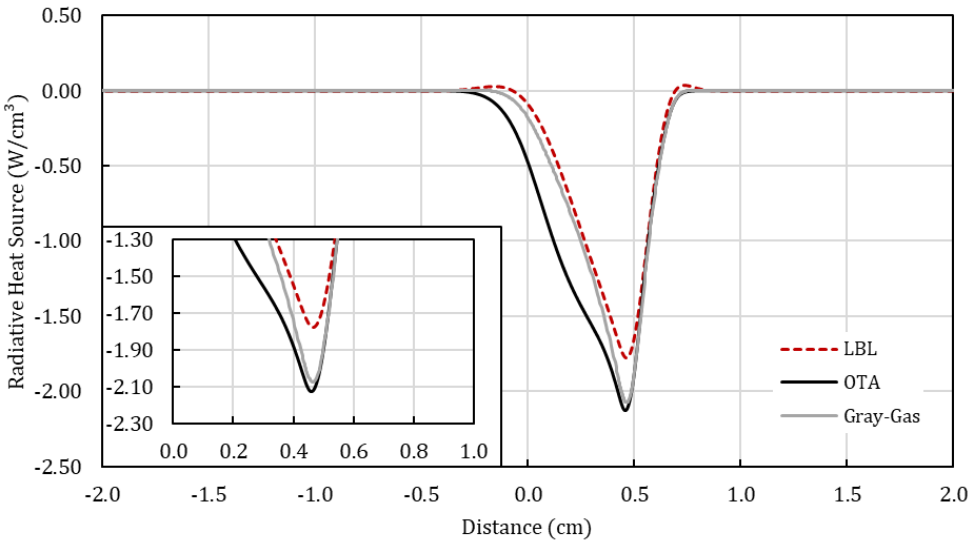

Figure 4.15 – Results of GG and OTA for a 0% dilution and 20 s^{-1} strain rate.

Both models overestimate the radiative heat source. The GG model has a slightly lower maximum heat loss when compared to the OTA model and it has over 16% of error when compared to the LBL. This difference increases when evaluating the total heat loss in the system that is 18% for the gray-gas model.

The OTA not only overestimates the maximum heat loss, but the overall profile is not accurately captured. While the valley of the curve has an error of almost 20%, this increases to 49% in total heat released to from the flame, because in the region of 0 to 0.5 cm the model highly overestimates the radiative heat loss.

4.2.1.2 WSGG formulations with fixed molar ratio of 2:1

Figure 4.16 presents the results for models with correlations for a fixed molar ratio of 2:1. The results are separated according to year of publication for better visualization. In general, these results are closer to the benchmark than the one calculated with a fixed molar ratio of 1:1. This is expected since the average molar ratio is closer to 2 than to 1. The correlation with best accuracy is Yin2013, which has a total radiative heat loss 7% higher than the one calculated by the LBL integration. The maximum value has a 1.2% error.

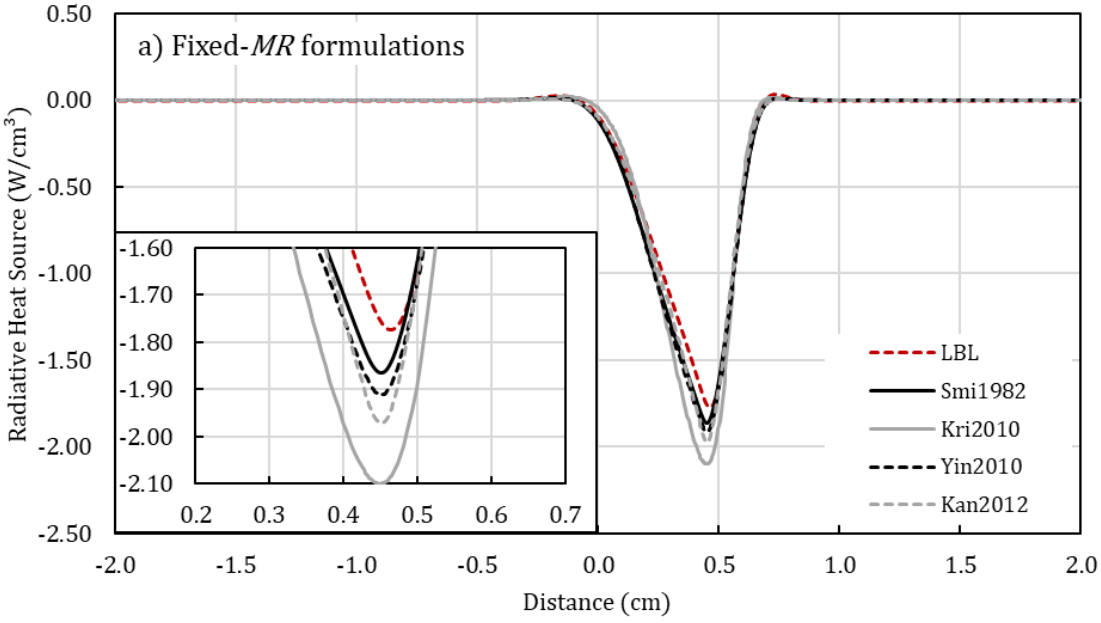

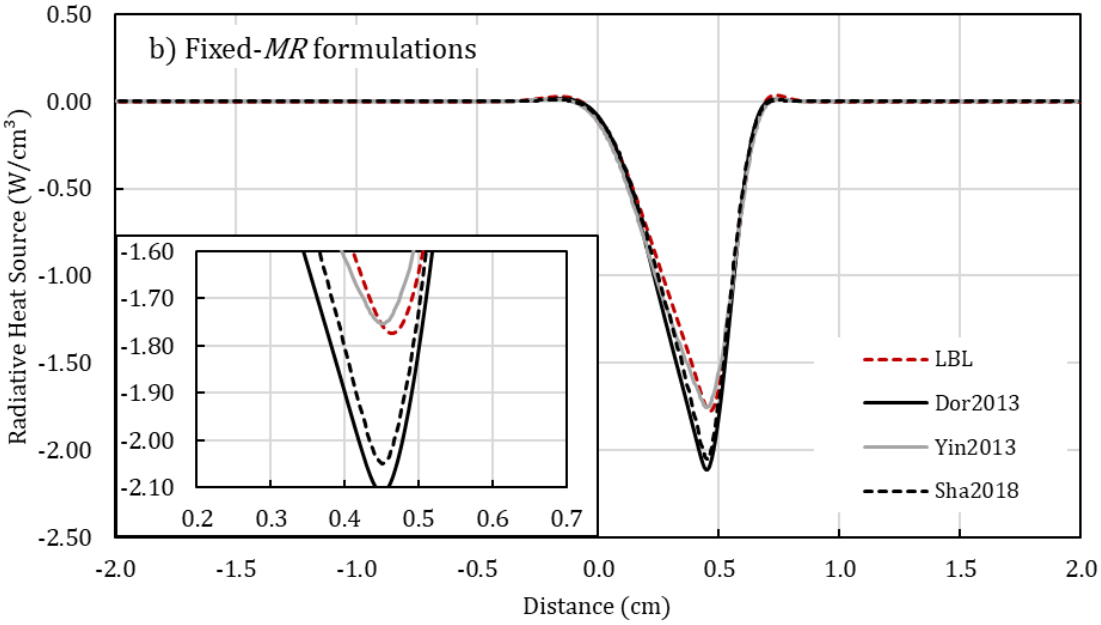

Figure 4.16 – Results of WSGG with molar ratio 2:1 for a 0% dilution and 20 s^{-1} strain rate.

From all these models, the one with the highest inaccuracy in this scenario is the one proposed by Dor2013 that overestimates the total heat loss by 15.6% and the maximum value by 18.9%. It is an interesting result as the model was developed with the HITEMP-2010 database, the same as the LBL solution.

4.2.1.3 WSGG stepwise formulations

This section and next ones consider formulations of the WSGG model that account for variations in the molar fraction ratio. Figure 4.17 illustrates the comparison for stepwise formulation.

Two models in particular have a strange unphysical behavior when reaching higher temperatures (and therefore higher radiative losses): Kan2012 and Sha2018. This is because of the stepwise scheme of both formulations. The first has a change when the molar ratio transition around the 3:1 ratio (looking at Figure 4.2 show that that happens around 0.4 cm). The latter has a transition around the 2.5:1 ratio (therefore, roughly after the first one). The stepwise formulation Yin2010 also has a transition that happens around the central point of the domain. This transition is when the sum of species goes above 0.1 atm.

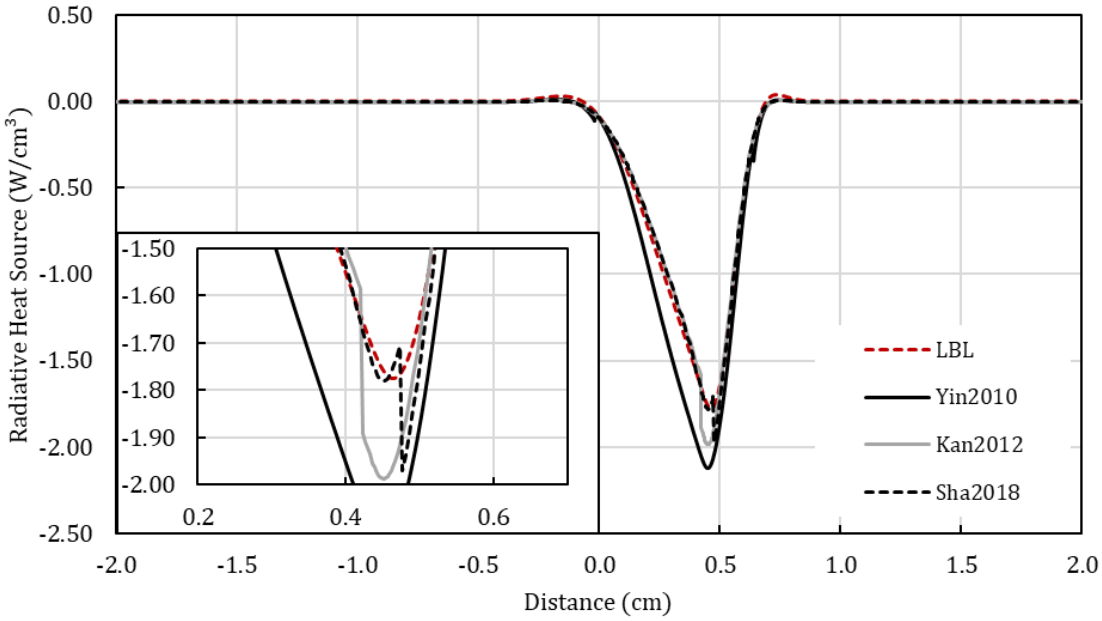

Figure 4.17 – Results of WSGG stepwise formulation for a 0% dilution and 20 s^{-1} strain rate.

Disregarding those abrupt transitions, the models in this section presented good results when compared to previous formulations. Kan2012 achieved an error of 0.02% in the total radiative heat loss while the maximum value has it around 12%.

4.2.1.4 WSGG linear formulations

Figure 4.18 presents the results for correlations with linear interpolation of the coefficients obtained at different molar ratio values. The coefficients here are the same as the stepwise formulation, what changes is the calculation scheme of κ_i and a_i.

The models appear to be improved with the change in the calculation scheme, especially Yin2010. Solved with the interpolation method for the molar ratio has an error of 3.2% for the maximum value and 5.4% for total radiative heat loss, compared to the previous presented values of 19.7% and 24.5% respectively.

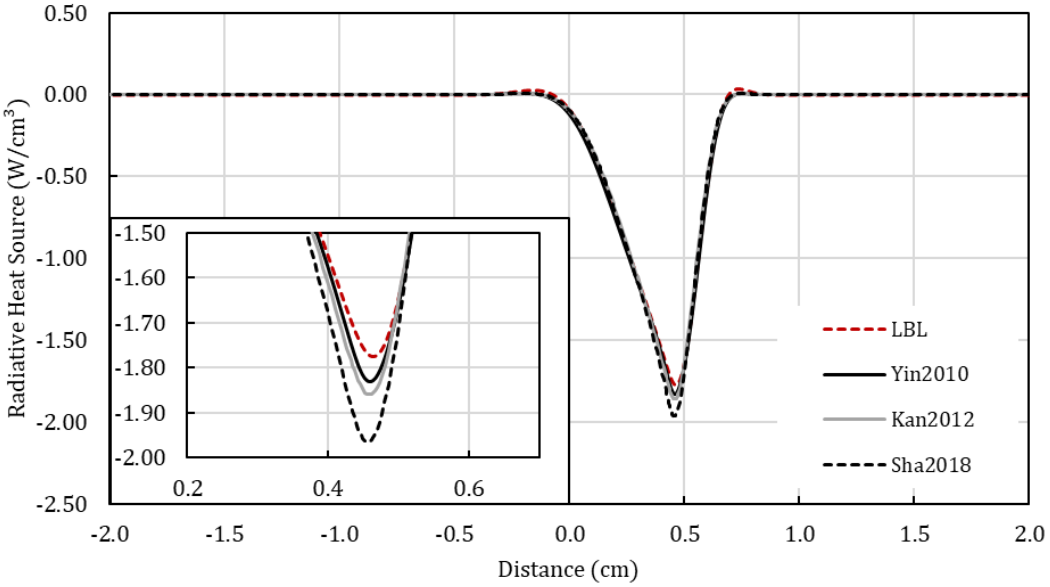

Figure 4.18 – Results of linear formulation WSGG for a 0% dilution and 20 s^{-1} strain rate.

However, although the other two models do not present the rather abrupt changes in gradient as verified in the previous section, the total radiative heat loss calculated now has increased inaccuracy. For Kan2010 this resulted in 1.8% and for Sha2018 it is of 4.8%. For the maximum radiative heat source all three models presented improvement when compared to the LBL.

4.2.1.5 WSGG polynomial formulations

Figure 4.19 presents the results of the calculations using formulations that apply a polynomial function to determine the dependence of the molar ratio in the weighting coefficient. As with previous cases, they are benchmarked to the LBL integration. Although there is again a model proposed by Kanwangpongpan et al., 2010, the coefficients are not the same as previous formulations, although the method for curve fitting remains the same. This is due to the change in the scheme of calculation for this formulation.

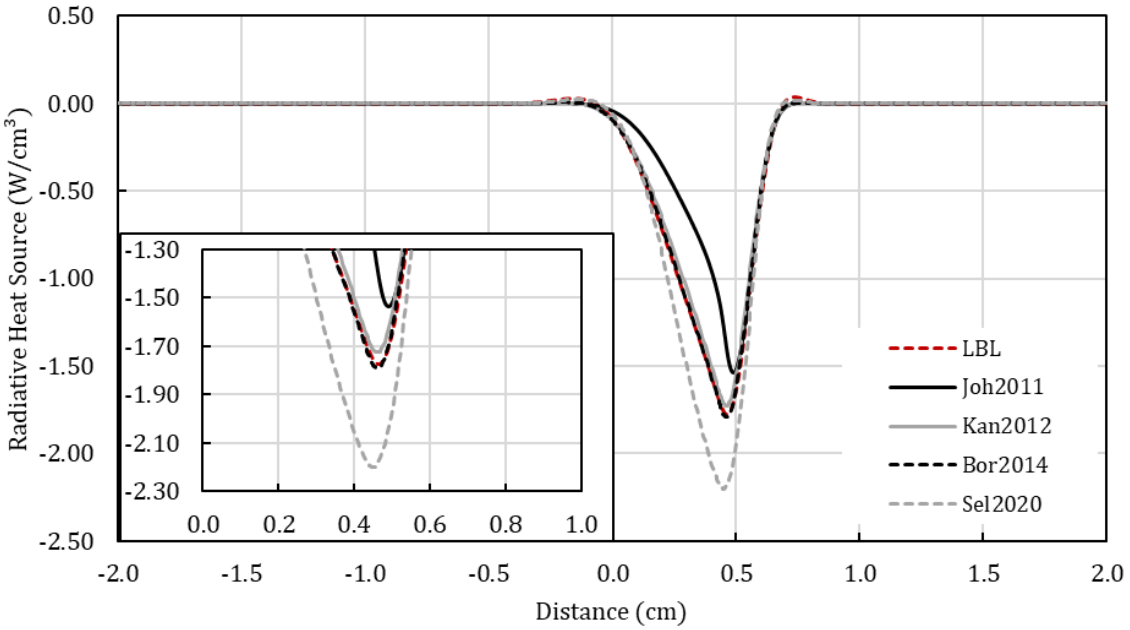

Figure 4.19 – Results of polynomial formulation WSGG for a 0% dilution and 20 s^{-1} strain rate.

An eye-catching result from this presented graph is noted from the model proposed by Bordbar et al., 2014. The maximum absolute value for the radiative heat source is 0.9% higher than the one calculated by the LBL integration. The total heat loss due to participating species was calculated with the model as 0.0747 W, which is 0.3% higher than the one by the benchmark. Although the coefficients proposed by Selhorst et al., 2020 are more recent and use the HITEMP-2010 database and benchmarked it with the LBL integration, its result for this scenario didn't perform as well as the other models. The radiative heat source term amounted to 24% of error while the total heat loss was 22%. It should be noted that in the work presented by these authors, more than one set of coefficients are available for use: one set for a wide range of molar ratio and another that have two different values of coefficients for molar ratios lower or higher than 1:1. For this work, only results with the first set (wide range) was applied and calculated in all scenarios. The other set in first analysis did not presented better results so it was opted to be left out.

4.2.1.6 WSGG superposition method

Figure 4.20 presents the results for models with the superposition formulation. As mentioned earlier, this method of calculating the gray gas radiative properties consists in

separately defining the coefficients for water vapor and carbon dioxide and then combining them using probabilistic arguments.

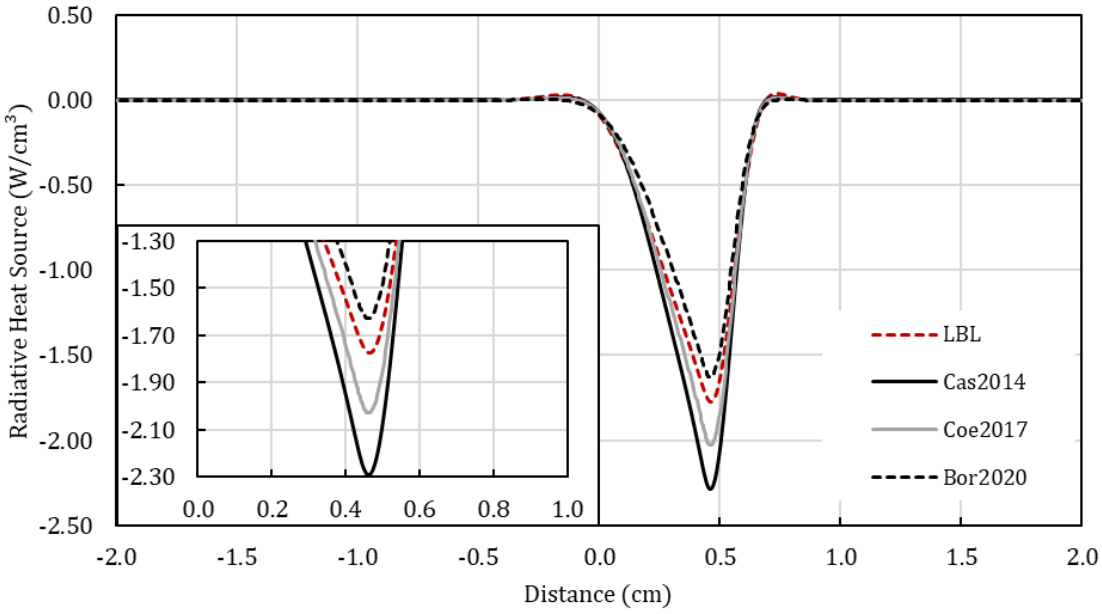

Figure 4.20 – Results of superposition WSGG for a 0% dilution and 20 s^{-1} strain rate.

Two models are roughly close to the benchmark, with one overestimating the radiative loss and another underestimating it. The former is the one proposed by Coe2017, which has an error of 14.3% and 8.4% for the maximum heat loss and total heat loss respectively. The latter is Bor2020 and has an inaccuracy of 8.2% and 11.8% for these properties, respectively.

4.2.1.7 Compiled results

Table 4.1 presents a summary of all results for this set up of calculation. The minimum radiative heat source value (or the point of highest radiative heat loss), the total radiative heat loss (over the domain) and the maximum value of carbon monoxide molar fraction are shown for the LBL method. The results for the models of this section are shown as relative error regarding the benchmark. One should note that these are not in absolute value, and a negative error represents that the model underestimates the result by the benchmark. Since models with a fixed molar ratio method have results for both molar ratios of 1:1 and 2:1 it was decided to present only the results of the latter in this table since it was seen that the average molar ratio for this case is closer to this.

Table 4.1 – Compiled results for 0% dilution and 20 s^{-1} strain rate. Models with both maximum and total heat loss below 10% are highlighted.

Model	Method	$\dot{Q}_{max}$	Q_{total}	$X_{CO,max}$
LBL	Integration	1.775	0.0745	0.0426
Adiabatic	-	-	-	10.3%
OTA	-	19.7%	49.3%	-3.3%
Gray Gas	1 gas	16.8%	18.1%	-1.5%
Smi1982	**MR 2:1**	**5.0%**	**10.0%**	**-0.8%**
Kri2010	MR 2:1	18.3%	13.4%	-1.5%
Yin2010	MR 2:1	7.7%	12.0%	-1.0%
Kan2012	MR 2:1	11.1%	6.4%	-0.6%
Dor2013	MR 2:1	18.9%	15.6%	-1.5%
Yin2013	**MR 2:1**	**-1.2%**	**7.0%**	**-0.4%**
Sha2018	MR 2:1	15.4%	9.1%	-0.9%
Yin2010	Stepwise	19.7%	24.5%	-2.3%
Kan2012	Stepwise	12.0%	0.0%	0.0%
Sha2018	Stepwise	11.0%	-0.51%	0.1%
Yin2010	**Linear**	**3.2%**	**5.4%**	**-0.4%**
Kan2012	**Linear**	**4.8%**	**1.8%**	**-0.1%**
Sha2018	Linear	10.7%	4.8%	-0.5%
Joh2011	Polynomial	-13.5%	-30.6%	2.8%
Kan2012	**Polynomial**	**-2.7%**	**-4.2%**	**0.5%**
Bor2014	**Polynomial**	**0.9%**	**0.3%**	**0.0%**
Sel2020	Polynomial	24.0%	22.0%	-2.3%
Cas2014	Superposition	29.0%	19.8%	-2.1%
Coe2017	Superposition	14.3%	8.4%	-0.9%
Bor2020	Superposition	-8.2%	-11.8%	1.2%

Disregarding the radiation heat transfer in a counterflow flame is not recommended if the formation of species such as carbon monoxide must be accurately captured. The result for the adiabatic scenario (no radiation) has the highest error for this species, with over 10% of overestimation. Even the model of the Optically Thin Approximation, which is the simplest way to account for radiation, has an error of 3.3% while all WSGG models have errors lower than 3% for this case.

There is also a significant advantage in using a WSGG model compared to the OTA as the latter has the highest inaccuracy in predicting the total radiative heat loss of the flame with almost 50% above what was calculated with the LBL method. Also, it appears that accuracy is not correlated entirely with the formulation of a WSGG model but rather the coefficients itself as there is models with good approximation of the LBL with different methods for accounting for the molar ratio.

4.2.2 Dilution of 20% and Strain rate of 20 s^{-1}

4.2.2.1 GG and OTA models

Figure 4.21 compares the LBL integration with the Optically Thin Approximation and the Gray-Gas model for a dilution of 20% of carbon dioxide. The OTA method highly overestimates the total radiative heat loss, as it results in a relative difference of 97.8% to the LBL, while for the GG this error is 28.8%. Therefore, the error associated with the OTA in that quantity almost doubled compared to the base case.

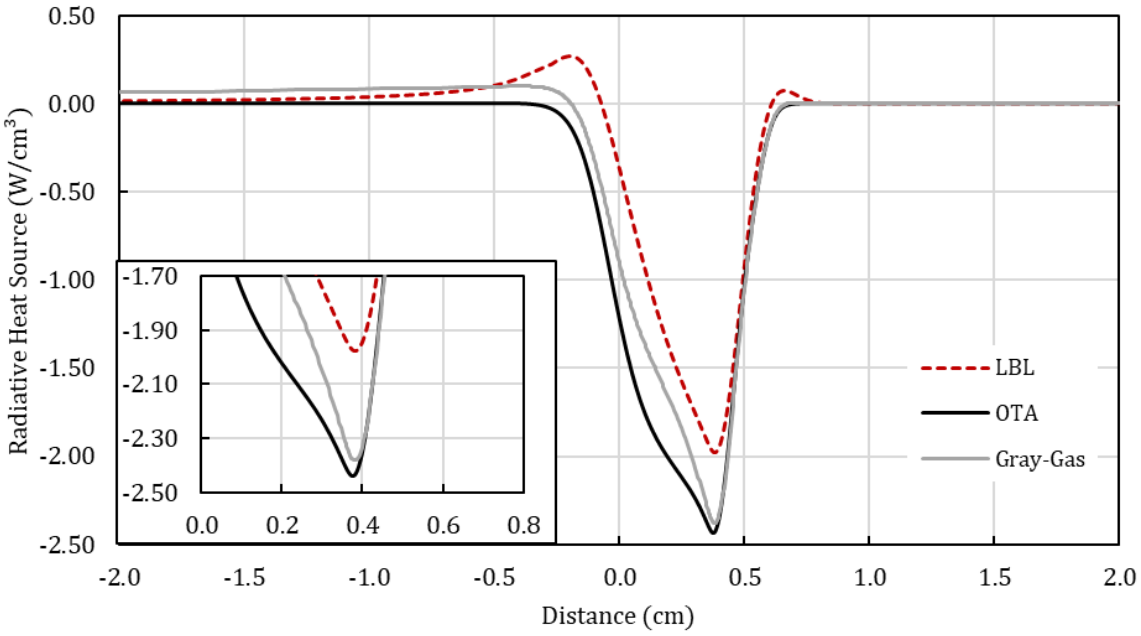

Figure 4.21 – Results of GG and OTA for a 20% dilution and 20 s^{-1} strain rate.

Moreover, it is possible to see that both models cannot correctly capture the curve of the LBL in the zone from -0.5 cm to 0, where there is a reabsorption of radiative heat, which contributes

to the inability to calculate the total heat loss. In terms of the formation of carbon monoxide, both models have had an increase in the inaccuracy of the results compared to the base case, with their results being 5.8% and 3.8% respectively.

4.2.2.2 WSGG formulations with fixed molar ratio of 1:1

Figure 4.22 presents the comparison for the WSGG formulations with a fixed molar ratio of equal parts carbon dioxide and water vapor. All models the maximum value for the radiative heat source, however their results are closer for this case with dilution than the previous one without addition of CO_2. The two best performing models are the Smi1982 and Sha2018 both of them calculates the total radiative heat loss with 0.9% difference from the LBL integration. The former, however, is closer in terms of the maximum value, with 13.9% of error against 27.4% of the latter.

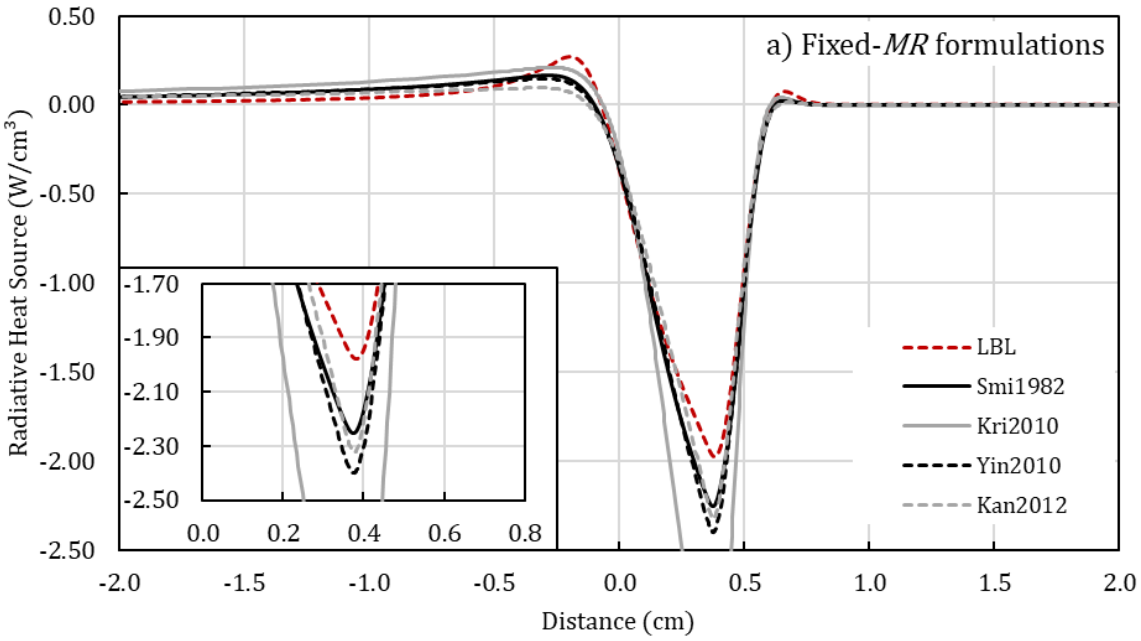

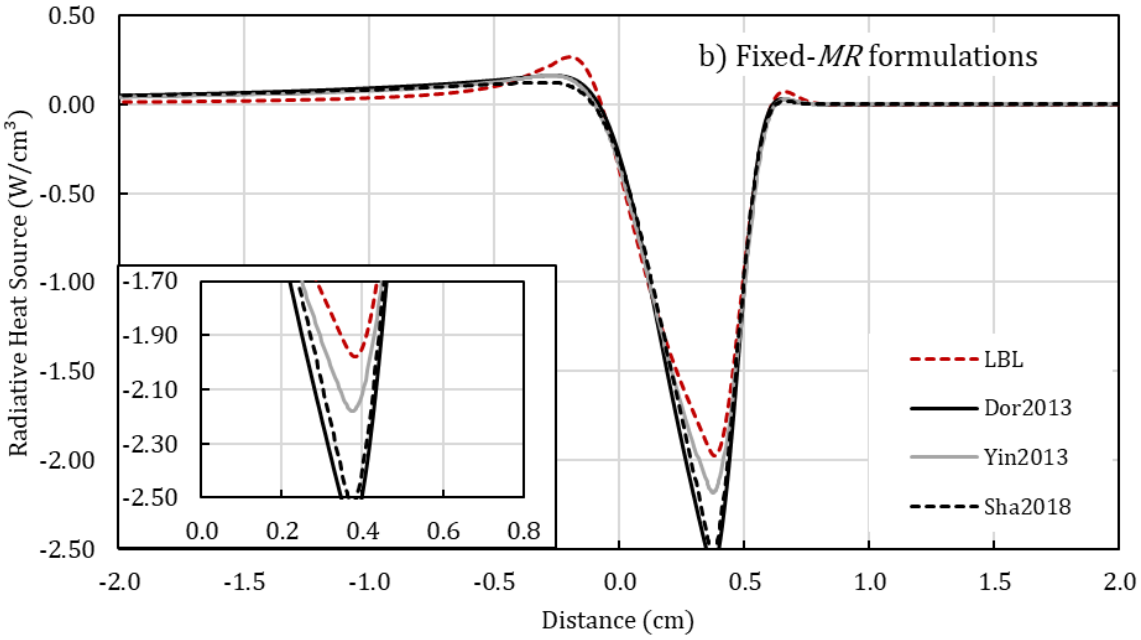

Figure 4.22 – Results of WSGG with molar ratio 1:1 for a 20% dilution and 20 s^{-1} strain rate.

Again, none of the models presented can replicate the behavior of reabsorption correctly. Most models managed to keep the error in CO formation below 3% with exception to the model Kri2010, which has the highest error (7%). It comes naturally because the highest error in the radiative heat loss would lead to the highest temperature difference since it is a coupled calculation where the iterative process would lead to convergence in a different value and therefore to a different formation equilibrium for the species, as the main influence for them is the domain's temperature.

4.2.2.3 WSGG formulations with fixed molar ratio of 2:1

Figure 4.23 illustrates the comparison for the models with a fixed molar ratio of 2 to 1. Although no model can correctly capture the reabsorption region, their approximations of the maximum radiative heat loss are closer to the benchmark than the previous results in this section. All but one have the error for this property below 10%, with the best results from Yin2010 with 0.3% of error.

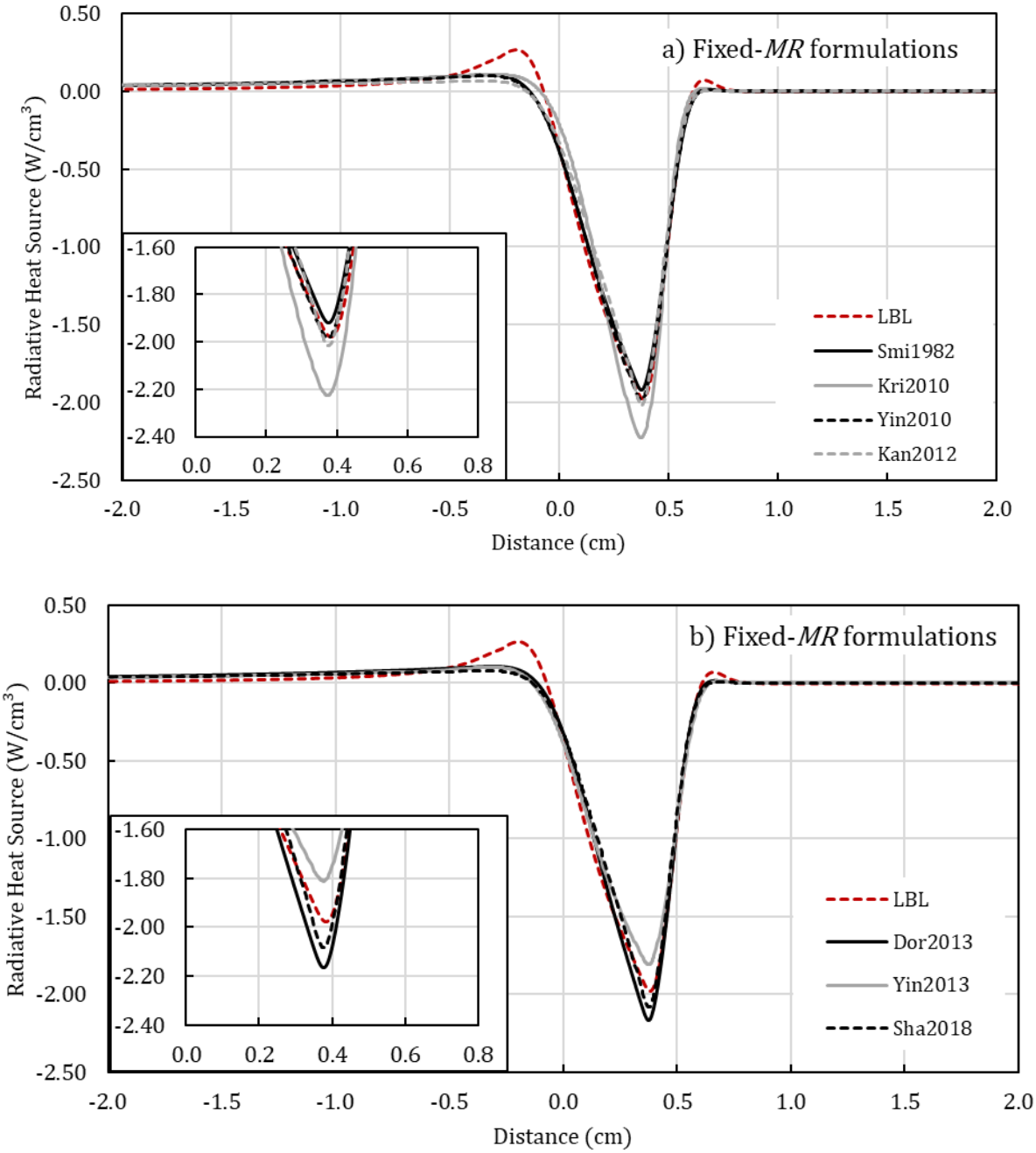

Figure 4.23 – Results of WSGG with molar ratio 2:1 for a 20% dilution and 20 s^{-1} strain rate.

In terms of total radiative heat loss, the best estimation comes from Dor2013 that has an error of 3.5% while the previously mentioned model had 3.8%. Regarding carbon monoxide formation, all models lead to good approximations with errors below 0.7%.

4.2.2.4 WSGG stepwise formulations

Figure 4.24 presents the results for the formulations with the stepwise calculation of the gray gas coefficients. The models Kan2010 and Sha2018 did not manage to attain convergence with the stepwise calculation according to the set up presented in chapter 3. Section 4.4 discuss the limitations of some formulations regarding convergence in setups with dilution of CO_2 in the fuel side. As seen from experimental data available in literature, for this strain rate and dilution of CO_2 a flame does not extinguish due radiative heat loss. Therefore, this results from both models indicates a limitation of them to capture the behavior of counterflow flames with dilution in the fuel side.

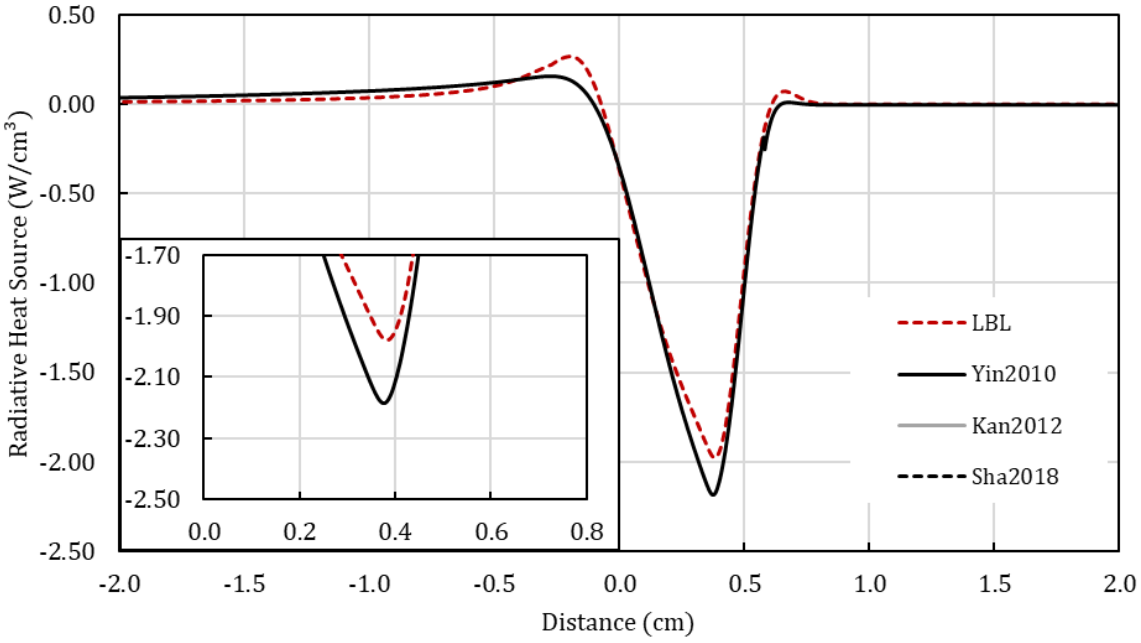

Figure 4.24 – Results of stepwise formulation WSGG for a 20% dilution and 20 s^{-1} strain rate.

The errors for the maximum radiative heat loss for the model of Yin2010 was of 10.5%. Interestingly, this error is roughly the average between the ones presented by the model with fixed molar ratios. However, this value should be lower than the one for molar ratio 2 to 1 as this formulation could account for the variation of this ratio and as seen in Figure 4.3b *MR* is not constant throughout the domain.

4.2.2.5 WSGG linear formulations

The models with this formulation presented a similar behavior as most models from the stepwise formulation. Therefore, for the interpolation scheme, no model managed to converge for this dilution of 20% CO_2 and strain rate of 20 s^{-1}. Again, this is due to limitations in the formulation rather than a case of flame extinction.

4.2.2.6 WSGG polynomial formulations

In Figure 4.25, again some models have not reached convergence for this calculation set up. It was the cases of models Bor2014 and Kan2010.

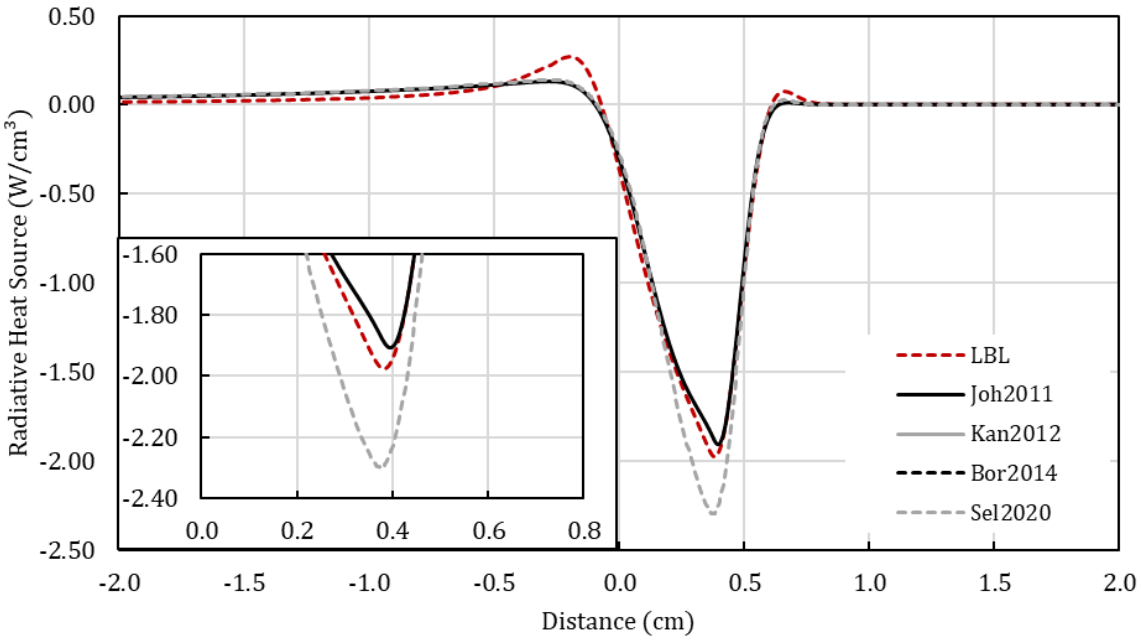

Figure 4.25 – Results of polynomial formulation WSGG for a 20% dilution and 20 s^{-1} strain rate.

Neither of the models could capture the behavior of the LBL integration at the zone between -0.5 cm to 0. This factor affects the total radiative heat loss calculated as the model Yin2010 has an error of 3.5% for the maximum radiative heat loss, but for the total radiative heat loss it increases to 13.1%. The model Sel2020 has the highest error for the maximum radiative heat source with 16.2% but for the total value the error decreases to 1.4%. For carbon monoxide formation, the former has 1.6% while the other has 0.4%.

4.2.2.7 WSGG formulations with superposition coefficients

Figure 4.26 presents the last graph of this section with the models with the superposition formulation for calculating the coefficients of pressure absorption and temperature dependence. The models Cas2014 and Coe2017 are the only ones that can better represent the reabsorption zone as depicted by the benchmark for all models evaluated in this study.

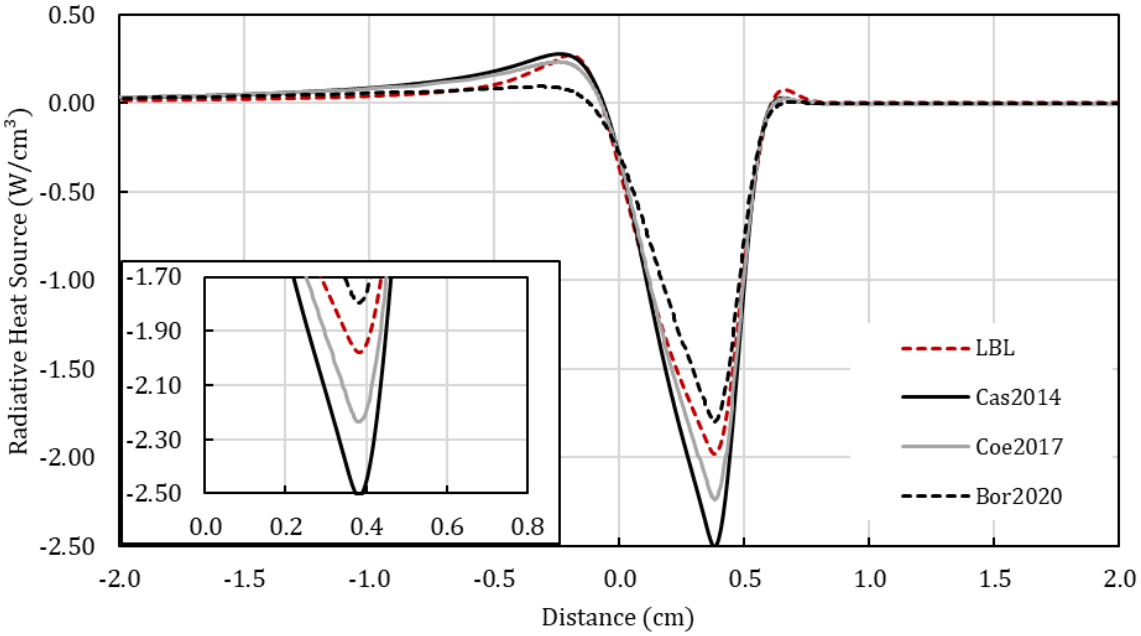

Figure 4.26 – Results of superposition WSGG for a 20% dilution and 20 s^{-1} strain rate.

The errors of maximum and total radiative losses for the Coe2017 are, respectively, 13.1% and 4.4%, while errors of Cas2014 are 26.8% and 3.1%. The other set of coefficients, Bor2020, achieved 9.2% and 16.3% respectively. For the molar fraction of CO, the most accurate model was Coe2017 with 1.1% error.

4.2.2.8 Compiled results

Table 4.2 presents a summary of all results for this set up of calculation in terms of relative error compared to the LBL method. The maximum radiative heat loss, the total radiative heat loss and the maximum value of carbon monoxide molar fraction are shown for the benchmark for reference. Again, it was opted to shown only the models with molar ratio 2:1, since it was seen that the average molar ratio for this case is closer to this value, and they have presented

better results in general compared to the molar ratio of 1:1. In addition, the models that did not convergence in the calculation are not presented.

Table 4.2 – Compiled results for 20% dilution and 20 s^{-1} strain rate. Models with errors below 10% for both maximum and total radiative heat loss are highlighted.

Model	Method	$\dot{Q}_{max}$	Q_{total}	$X_{CO,max}$
LBL	Integration	1.976	0.0721	0.04138
Adiabatic	-	-	-	14.5%
OTA	-	23.2%	97.8%	-5.8%
Gray Gas	1 gas	20.4%	28.8%	-3.8%
Smi1982	**MR 2:1**	**-3.0%**	**-6.2%**	**0.2%**
Kri2010	MR 2:1	12.5%	-7.7%	-0.6%
Yin2010	**MR 2:1**	**0.3%**	**-3.8%**	**-0.1%**
Kan2012	**MR 2:1**	**1.9%**	**-6.2%**	**0.5%**
Dor2013	**MR 2:1**	**9.6%**	**-3.5%**	**-0.6%**
Yin2013	**MR 2:1**	**-8.4%**	**-7.4%**	**0.7%**
Sha2018	**MR 2:1**	**5.4%**	**-6.3%**	**0.2%**
Yin2010	Stepwise	10.5%	-0.7%	-1.4%
Joh2011	Polynomial	-3.5%	-13.1%	0.4%
Sel2020	Polynomial	16.2%	-1.4%	-1.6%
Cas2014	Superposition	26.8%	3.1%	-2.5%
Coe2017	**Superposition**	**13.1%**	**-4.4%**	**-1.1%**
Bor2020	Superposition	-9.2%	-16.3%	1.7%

The result for the adiabatic scenario has the highest error for the CO molar fraction with over 14% of overestimation. All tested models for spectral radiation managed to keep an error below 6% although some of them increased their errors compared to the case with no dilution. The discrepancy between less refined models and the WSGG have increased. It was expected that for this set up the values of WSGG formulations of molar ratio 1:1 to be on par with the 2:1, but although the errors associated with *MR* 1:1 have decreased, so did the errors for *MR* 2:1. This is probably because the region where the molar ratio is locally slightly over 2 is where the highest temperatures are present. Therefore, the radiative quantities are more impactful in that region. The models with best performance are with fixed formulation, and although it was expected that models with varying-*MR* to better perform.

Several models did not attain convergence and this might be due to the addition of CO_2 to the fuel side, that induces a molar ratio of nearly zero in the left side of the domain. These models were not developed with these conditions in mind.

4.2.3 Dilution of 50% and Strain rate of 20 s^{-1}

In this section, none of the stepwise and linear formulation models have attained convergence, and therefore the subsections accounting for their results are left out. Since the average molar ratio is closer to 1 than to 2, models with fixed-*MR* at 1:1 have better performed than the ones with 2:1. Therefore, it was opted to present only the former results.

4.2.3.1 GG and OTA models

In Figure 4.27, the OTA and GG models are compared to the LBL solution for a dilution of 50% of carbon dioxide. As expected from previous section, the error associated with both models increased, with the former reaching 128.1% for total radiative loss, and the latter 33.3% for the same variable.

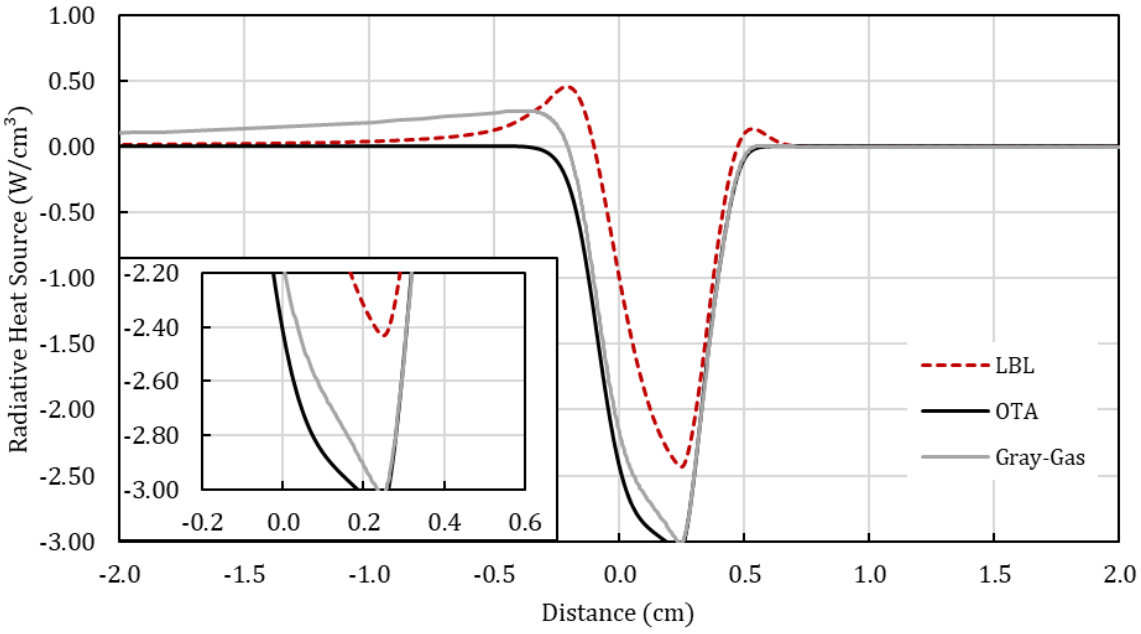

Figure 4.27 – Results of GG and OTA for a 50% dilution and 20 s^{-1} strain rate.

In terms of the maximum radiative heat loss, the errors of both are over the 24%. For the formation of carbon monoxide, the Gray Gas has underestimated this quantity in 7.9% compared to the LBL, and the Optically Thin Approximation, in 10.1%.

4.2.3.2 WSGG formulations with fixed molar ratio of 1:1

Figure 4.28 presents the results for the models with fixed molar ratio at 1:1. Since the content of CO_2 is higher than previous cases, it was seen that these perform better for this case. To some extent, they replicate the reabsorption zone at the fuel side of the flame.

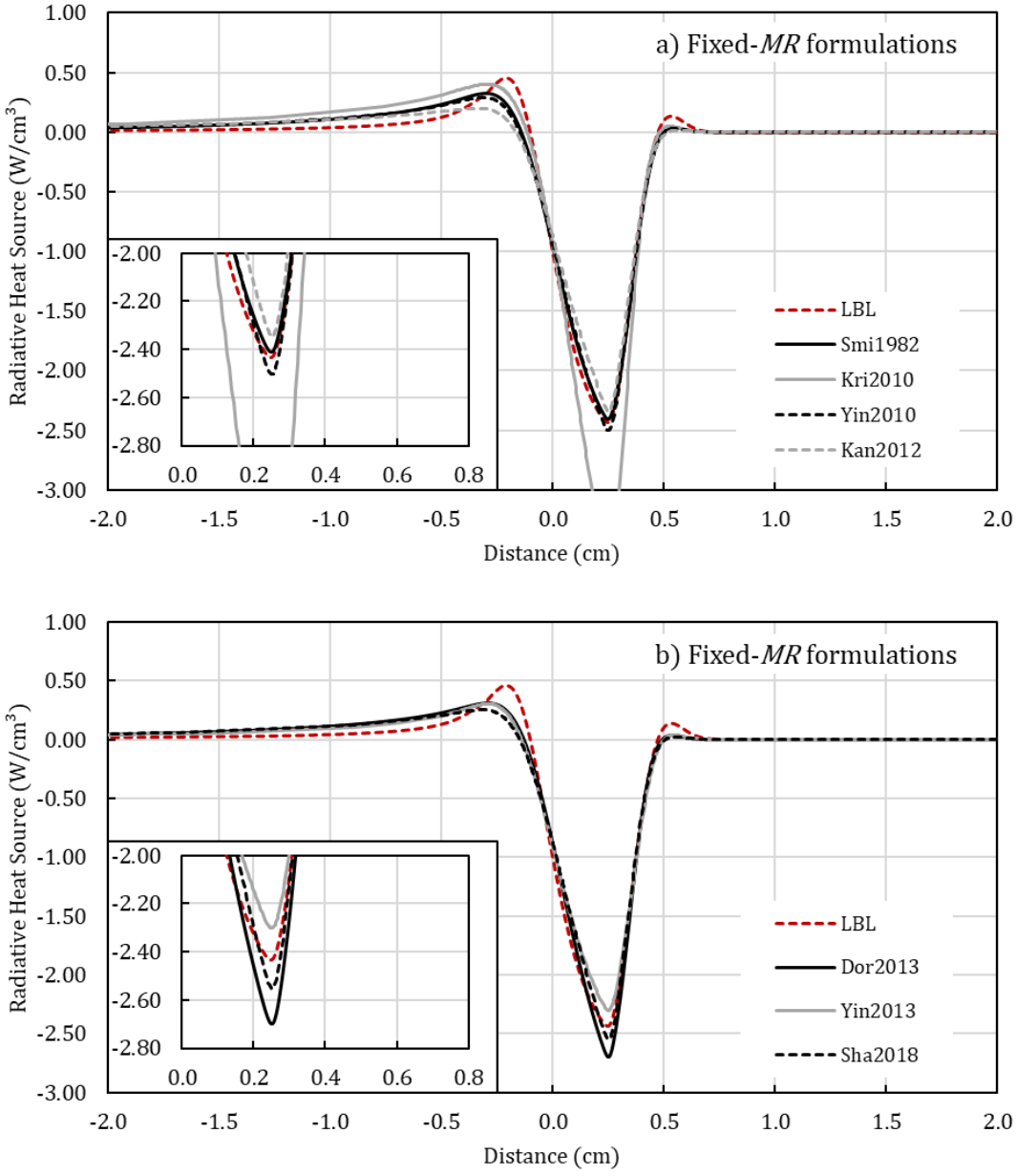

Figure 4.28 – Results of WSGG with molar ratio 1:1 for a 50% dilution and 20 s^{-1} strain rate.

For the maximum source term, the model closer to the reference is the Smi1982, which has an error of 0.9%. The Kri2010 is the most accurate for the total radiative heat loss, with an error of 0.9%; however, this is due to the model overestimating the maximum and minimum values.

4.2.3.3 WSGG polynomial formulations

In Figure 4.29 is seen that only one model with this formulation managed to converge to a result. In comparison with the previous results for the model of Sel2020 it can be noted that its performance improves with higher dilutions.

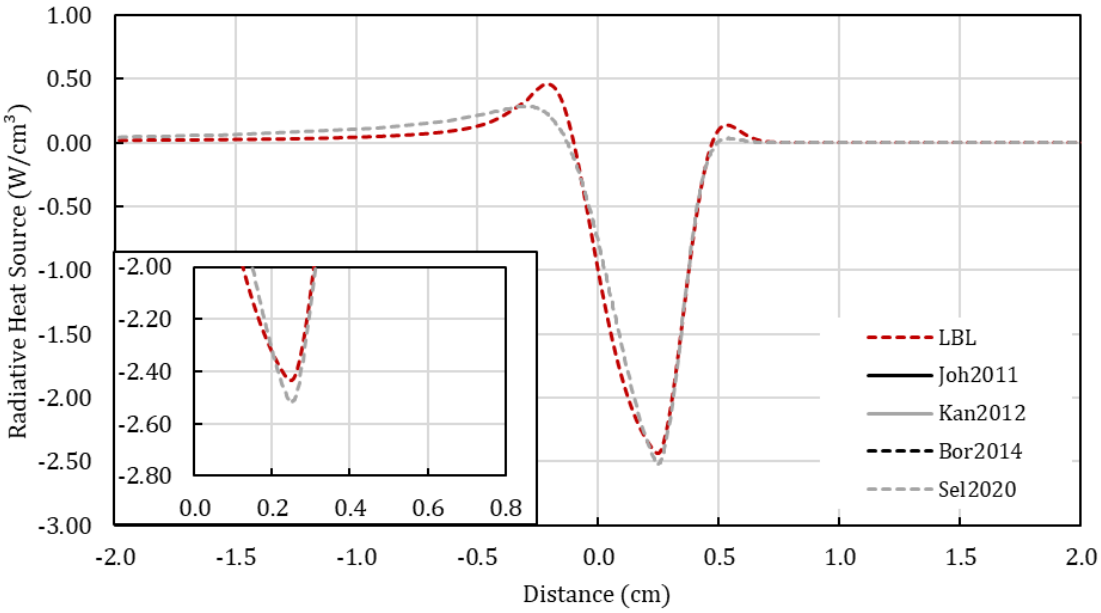

Figure 4.29 – Results of linear formulation WSGG for a 50% dilution and 20 s^{-1} strain rate.

The maximum radiative heat loss was 3.4% higher than the LBL result while the total radiative heat loss was 17.7% lower. For the maximum molar fraction of CO the model only overestimated 0.2% than the benchmark.

4.2.3.4 WSGG superposition method

Figure 4.34 presents the results for the models with the superposition method. With the increasing of dilution, all models have decreased their radiative values relatively to the LBL integration. Therefore, the two models that overestimated the result improved with it while the model that underestimated have increased its error.

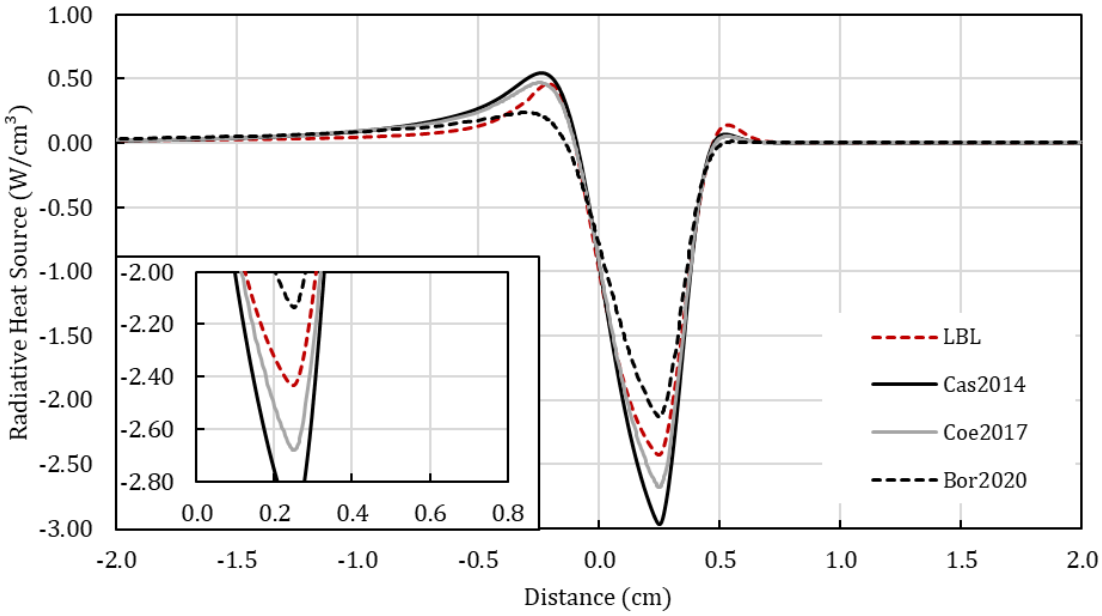

Figure 4.30 – Results of WSGG with superposition formulation for a 50% dilution and 20 s^{-1} strain rate.

The Coe2017 has errors of 10.2% and 6.8% for the maximum and total radiative heat losses respectively, while for Bor2020 these errors are 12.3% and 22.1%. In addition, the former model has the best accuracy for the carbon monoxide formation with 1.0%. While the Cas2014 has the highest error for the maximum radiative heat loss with 22%, for the total value it is 0.1%.

4.2.3.5 Compiled results

In Table 4.3 are summarized the results for dilution of 50% CO_2 and strain rate of 20 s^{-1} in terms of relative error compared to the benchmark. This time, it was opted to show the models with molar ratio 1:1 since it was seen that the average molar ratio for this case is closer to this than to 2:1. In addition, the models with stepwise, interpolation and polynomial formulations that did not converged are not presented here.

The LBL result had an 20% increase for its maximum radiative heat loss compared to the dilution of 20%, but the total heat loss due to emission of the participating species have increased slightly. The molar fraction of carbon monoxide has decreased 17% compared to the previous section.

Table 4.3 – Compiled results for 50% dilution and 20 s^{-1} strain rate. Models with the maximum radiative loss error below 5% were highlighted.

Model	Method	$\dot{Q}_{max}$	Q_{total}	$X_{CO,max}$
LBL	Integration	2.433	0.07383	0.0336
Adiabatic	-	-	-	19.4%
OTA	-	26.1%	128.1%	-10.1%
Gray Gas	1 gas	24.0%	33.3%	-7.9%
Smi1982	**MR 1:1**	**-0.9%**	**-12.8%**	**-0.1%**
Kri2010	MR 1:1	48.0%	-0.9%	-5.4%
Yin2010	**MR 1:1**	**2.9%**	**-12.9%**	**-0.3%**
Kan2012	**MR 1:1**	**-3.6%**	**-17.7%**	**0.9%**
Dor2013	MR 1:1	10.9%	-12.0%	-0.9%
Yin2013	MR 1:1	-5.4%	-16.2%	0.6%
Sha2018	MR 1:1	-8.3%	-15.8%	-0.1%
Sel2020	**Polynomial**	**3.4%**	**-17.7%**	**0.2%**
Cas2014	Superposition	22.0%	-0.1%	-2.4%
Coe2017	Superposition	10.2%	-6.8%	-1.0%
Bor2020	Superposition	-12.3%	-22.1%	2.3%

For a fixed molar ratio formulation, the model that best performed was Smi1982, which could be considered the simplest due to its modeling with only 3 gray gases instead of 4 like the others. For more complex models, both the Sel2020 and Coe2017 appears to present a good compromise for results of the maximum value and total loss together with low error for the species formation.

4.2.4 Dilution of 0% and Strain rate of 10 s^{-1}

The last case in this section is for a lower strain rate than the base case, with 10 s^{-1} and no dilution added to the fuel side. This setup was selected as previous results showed that decreasing the strain rate increases the effect the radiative heat losses have in the equilibrium of the flame. For the fixed-*MR* formulations only the models with molar ratio 2:1 are presented since in previous section it was seen that the error associated with 1:1 molar ratio are higher.

4.2.4.1 GG and OTA models

Figure 4.31 presents the OTA and GG model compared to the LBL integration for the strain rate of 10 s^{-1}. The former has an error of 20.3% and 52.2% for the maximum and total radiative losses respectively, while the latter has errors of 18.1% and 22.4%.

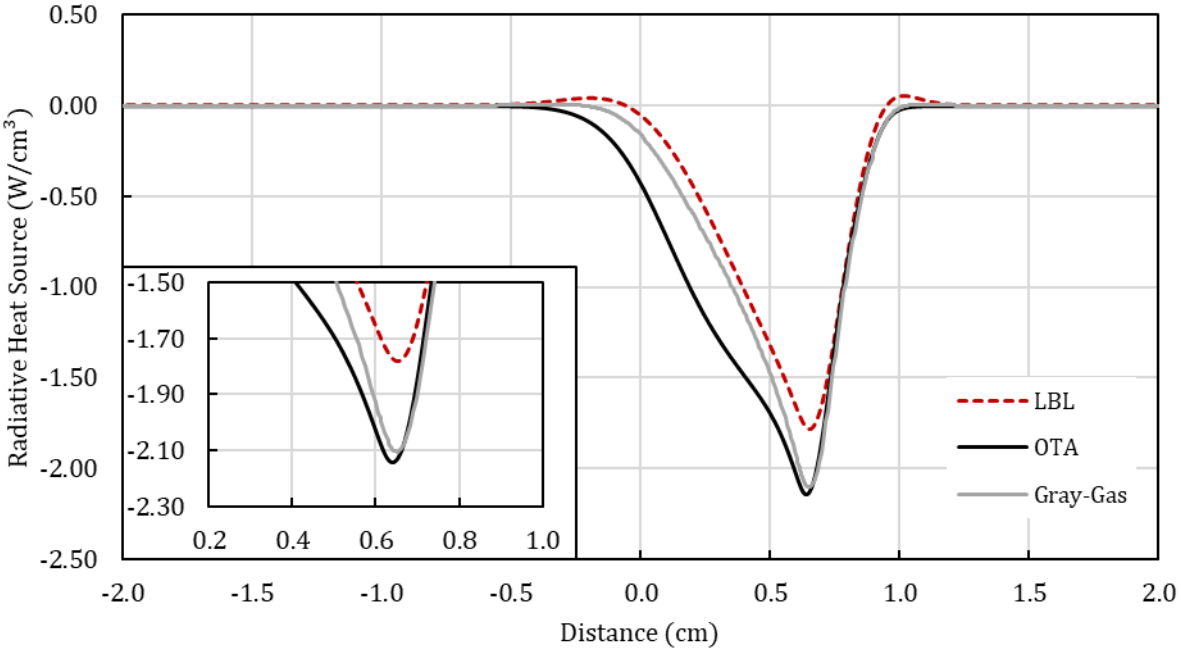

Figure 4.31 – Results of GG and OTA for a 0% dilution and 10 s^{-1} strain rate.

For the formation of carbon monoxide, the OTA and GG have inaccuracies of 7.2% and 3.9% respectively. Therefore, for all these values, the models have worsen compared to the LBL solution.

4.2.4.2 WSGG formulations with fixed molar ratio of 2:1

Since previous results already showed that for no dilution, the molar ratio of 1is not ideal for this case, it was opted to only present the graph of the molar ratio of 2. Figure 4.32 illustrates the models with the fixed coefficients formulation.

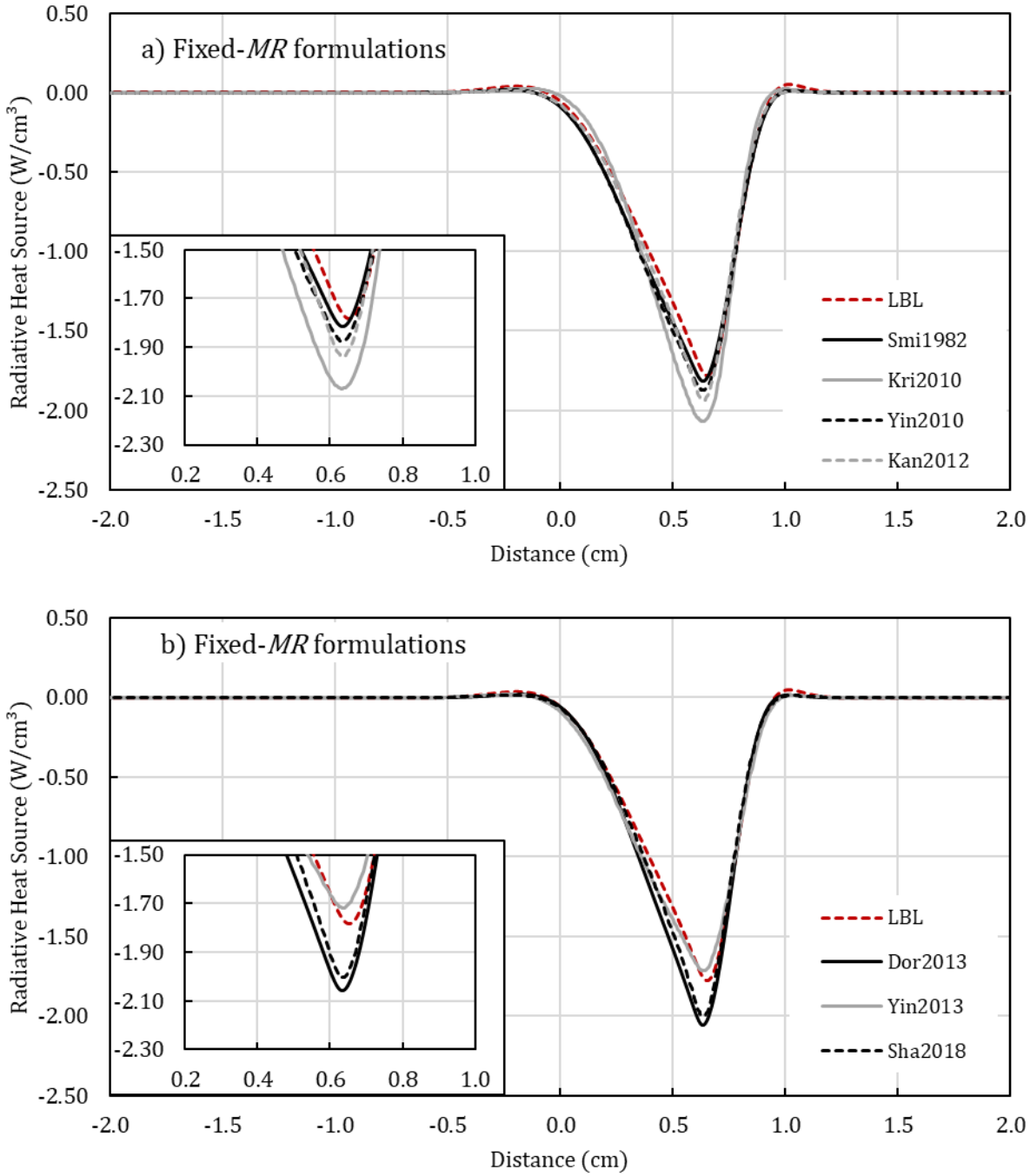

Figure 4.32 – Results of WSGG with molar ratio 2:1 for a 0% dilution and 10 s^{-1} strain rate.

While the model Smi1982 has the best result for the maximum radiative heat loss at 2% error, the Yin2013 has a better estimation of the total value with a 6.3% error. All models lead to prediction of the molar fraction of CO below 3% error. In general, all models improved with a lower strain rate.

4.2.4.3 WSGG stepwise formulations

Figure 4.33 plots the results of the models with the stepwise formulation for this case set up. The model by Sha2018 has the worst results for maximum radiative heat loss with a 9.5% error, while the Kan2012 is closer to the benchmark in the total radiative heat loss with a 0.4% error.

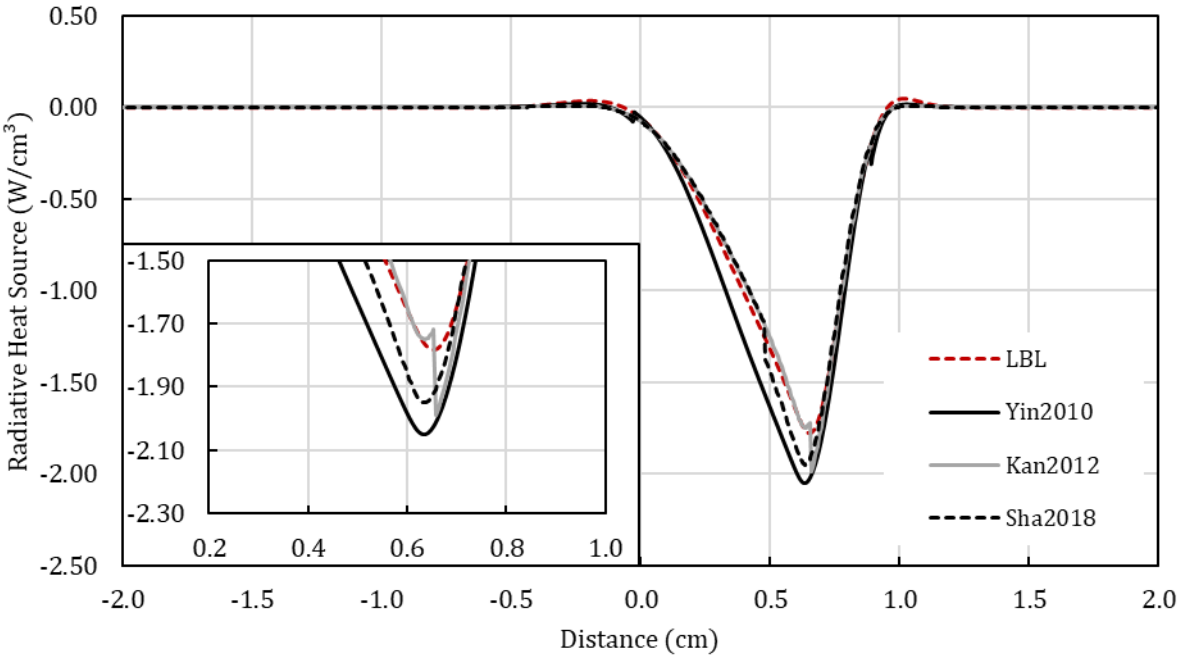

Figure 4.33 – Results of WSGG with stepwise formulation for a 0% dilution and 10 s^{-1} strain rate. Radiative Heat Flux is in the Attachments.

Again, it is possible to see the abrupt changes in the curves due to the way these formulations are structured. The model Yin2010 has the least exact value for the carbon monoxide with 4% discrepancy. Although the maximum value result enhanced for these models with the decrease of the strain rate, for the total value it was the opposite.

4.2.4.4 WSGG linear formulations

Figure 4.34 exhibits the results for the coefficients calculated with the formulation of interpolating different sets of coefficients according to each molar ratio. Contrary to the results from the stepwise formulation, the model with best result for the maximum radiative heat loss

is the Yin2010 with 4.0% closeness to the benchmark solution. Also, the better approximation for the total radiative heat loss with 2.9% and the carbon monoxide with 0.3%.

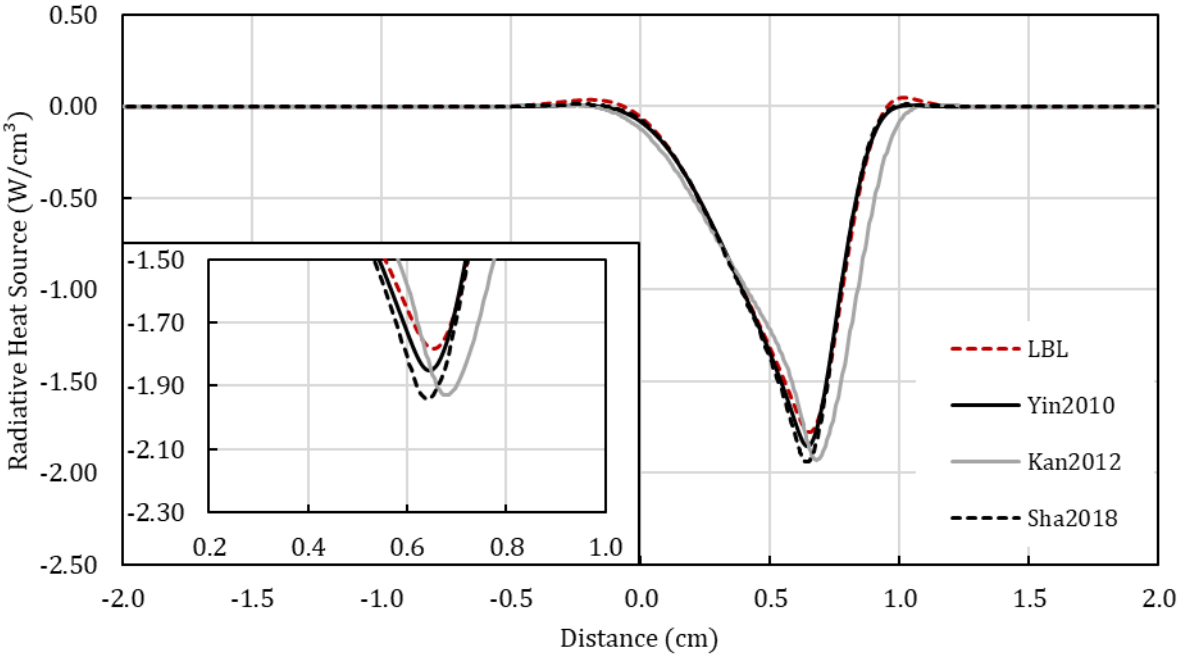

Figure 4.34 – Results of linear formulation WSGG for a 0% dilution and 10 s^{-1} strain rate.

Therefore, decreasing the strain rate improved the results for the Yin2010 model with this formulation while for the other two it worsens. In terms of carbon monoxide formation, the model by Kan2012, is not well indicated in this scenario since its deviation from the benchmark is of 38.9%.

4.2.4.5 WSGG polynomial formulations

Figure 4.35 presents the comparison of the models with the polynomial formulation to the benchmark solution of the LBL. It should be noted that in the close-up image of the maximum value the curve of the LBL is not very noticeable due to the model Bor2014 being well aligned with it. In fact, the difference between both is of 0.4% only.

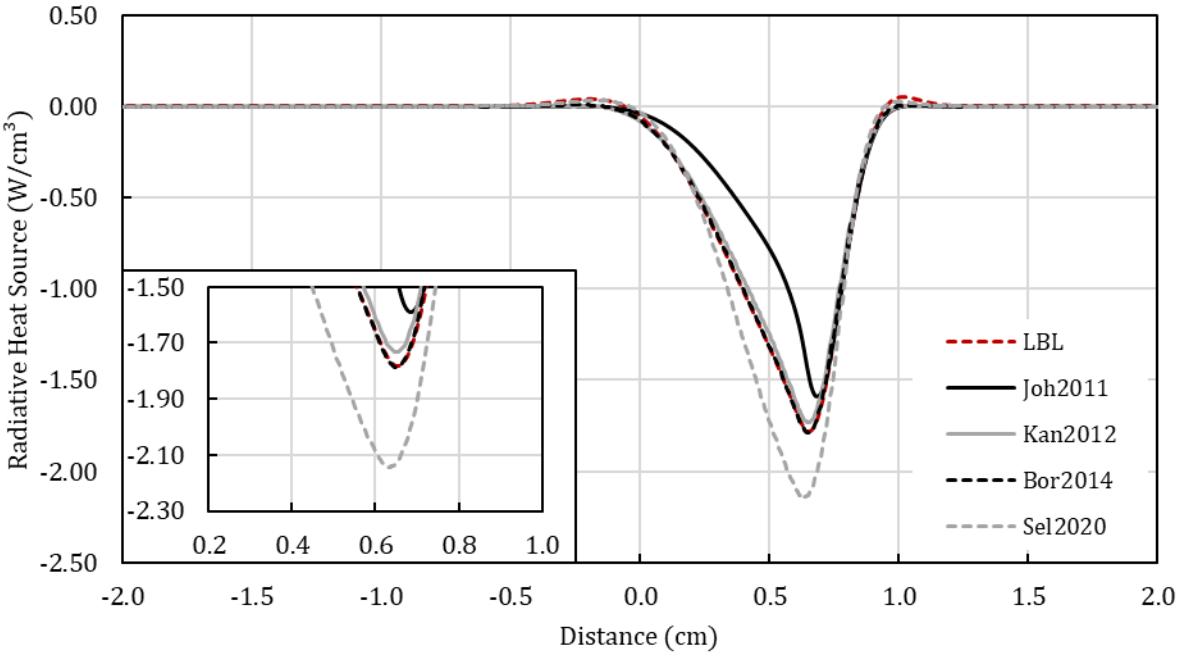

Figure 4.35 – Results of polynomial formulations WSGG for a 0% dilution and 10 s^{-1} strain rate.

The same model also has the best approximation to the total radiative heat loss of the domain with 1.3% deviation from the benchmark. The other three models, although do not have their results as good as this; have improved with the decrease of the strain rate.

4.2.4.6 Superposition WSGG method

Figure 4.36 exhibits the results of the superposition models. The Bor2020 has the closest value of the maximum radiative heat source at 8% error, but the model that better address the total radiative heat loss is the Coe2017 at 8.1% of error.

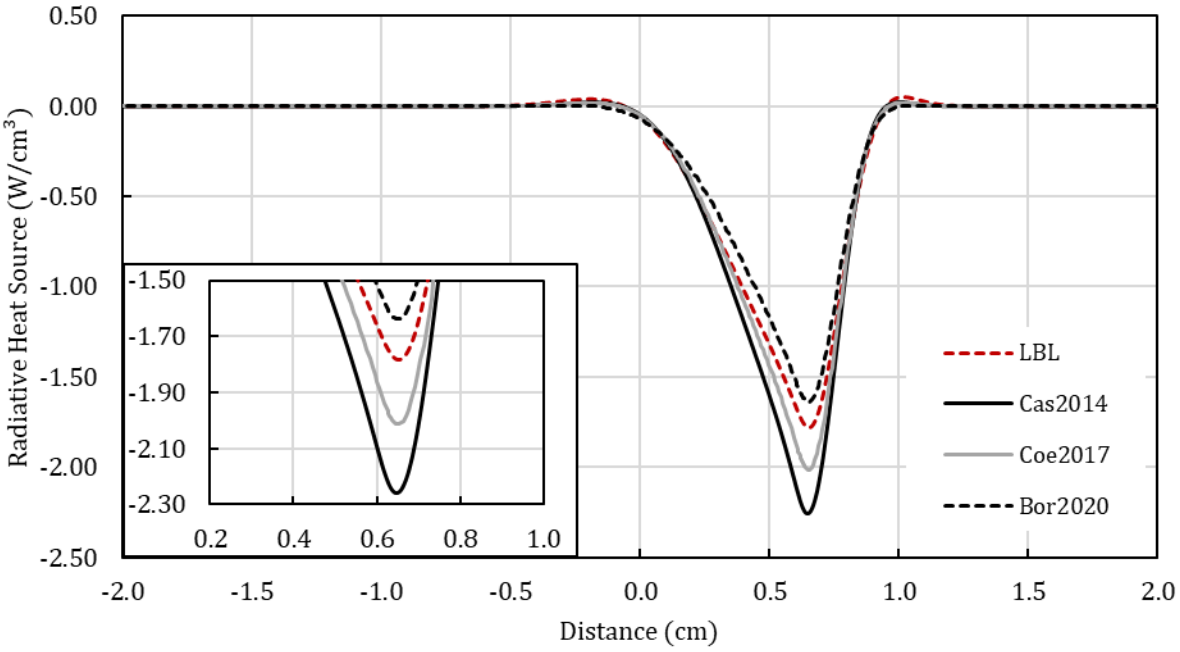

Figure 4.36 – Results of superposition WSGG for a 0% dilution and 10 s^{-1} strain rate.

All three models have had a slight improvement with the reduction of the strain rate in terms of the radiative quantities. However, when looking at the formation of carbon monoxide, it is the opposite. This is due to the temperature difference that is higher in this case, and therefore the reaction rates for the formation of this species is different.

4.2.4.7 Compiled results

Table 4.4 compiles the outcome for this set up of calculation. As with previous tables, the values are presented in relative error compared to the LBL integration. The same with the base case, it was opted to only present the results of fixed-*MR* for ratios of 2 to 1, as these have better results. This is because the average molar ratio of cases with no dilution are closer to 2. In addition, since there is no dilution, all models have attained convergence.

Except for the coefficients proposed by Kan2012 applied to the linear interpolation formulation, the models produce a good approximation for the calculation of species and temperature. Since this case has a lower strain rate than the previous section, the results have in general improved, because the gradients of temperature and reaction rates become less steep with the lowering of the strain rate.

Table 4.4 – Compiled results for 0% dilution and 10 s^{-1} strain rate. Models with maximum and total heat loss below 10% are highlighted.

Model	Method	$\dot{Q}_{max}$	Q_{total}	$X_{CO,max}$
LBL	Integration	1.781	0.0982	0.040
Adiabatic	-	-	-	22.4%
OTA	-	20.3%	52.2%	-7.2%
Gray Gas	1 gas	18.1%	22.4%	-3.9%
Smi1982	**MR 2:1**	**2.0%**	**8.7%**	**-1.3%**
Kri2010	MR 2:1	16.2%	11.2%	-2.8%
Yin2010	MR 2:1	5.3%	11.5%	-1.9%
Kan2012	**MR 2:1**	**8.9%**	**6.5%**	**-1.1%**
Dor2013	MR 2:1	15.4%	13.7%	-2.8%
Yin2013	**MR 2:1**	**-3.5%**	**6.3%**	**-0.7%**
Sha2018	MR 2:1	12.6%	8.5%	-1.7%
Yin2010	Stepwise	15.0%	20.4%	-4.0%
Kan2012	Stepwise	11.7%	0.4%	0.1%
Sha2018	Stepwise	9.5%	3.3%	-0.7%
Yin2010	**Linear**	**4.0%**	**2.9%**	**-0.3%**
Kan2012	Linear	8.3%	17.9%	38.9%
Sha2018	**Linear**	**9.0%**	**5.3%**	**-0.9%**
Joh2011	Polynomial	-10.7%	-26.7%	5.3%
Kan2012	**Polynomial**	**-2.8%**	**-2.5%**	**0.8%**
Bor2014	**Polynomial**	**0.4%**	**1.3%**	**0.0%**
Sel2020	Polynomial	20.4%	18.7%	-4.2%
Cas2014	Superposition	26.8%	18.4%	-4.2%
Coe2017	Superposition	13.0%	8.1%	-1.8%
Bor2020	**Superposition**	**-8.0%**	**-9.6%**	**2.2%**

The models Smi1982 and Yin2010 have appeared to have in general good results for different setups when applied to the fixed-*MR* formulation. Although this formulation does provide a limitation to its applicability since it was not developed for changes in the molar ratio as it is the case for counter flow flames. Models such Kan2012 and Bor2014 have good results in this case, however they present limitations of convergence when there is CO_2 in the fuel side.

4.3 OVERVIEW OF RESULTS

This section is a summary of the results of maximum radiative heat loss and total radiative heat loss. These results are presented in sets of graphs showing the benchmark solution as a red dotted line and the other models according to the legends. There are two overviews, one is for the strain rate of 20 s^{-1} and different dilutions of CO_2 and the other is for no dilution and varying the strain rate of the domain. In this analysis, it was opted to only evaluate 2 models that used a fixed formulation, Smi1982 and Yin2010, because both had the best results in the previous section. Also, since some models from other formulations did not achieved convergence with the increase in dilution, only the models that did converge through all dilutions calculated are presented.

To better analyze the effect of dilution in the results, calculations were carried out for each of the eight WSGG models and the LBL method the case set up with dilutions of 0, 10, 20, 30, 40 and 50%. Figure 4.37 illustrates how these WSGG models compare to the LBL integration as the dilution of CO_2 changes in terms of calculating the maximum radiative heat loss.

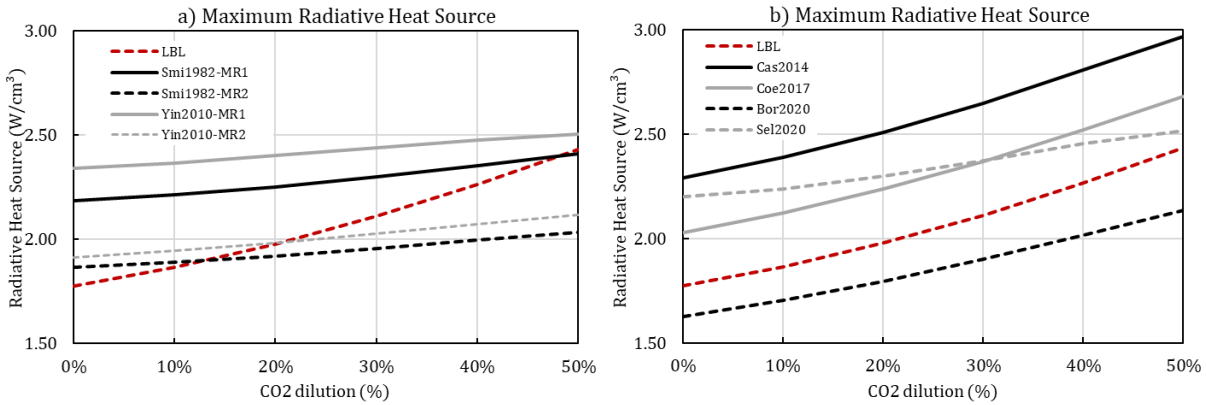

Figure 4.37 – Overview of maximum heat loss by dilution of CO_2.

The models with a fixed molar ratio do not have the same curve slope as the LBL method. Therefore, the same model could at first overestimate and then underestimate the maximum radiative heat loss. The difference between the result from a 2 to 1 model to a 1 to 1 is also relatively high, so trying to combine these formulations in a dilution dependent decision would implicate in an abruptly change the of the heat source term. The accuracy of the model Sel2020, improves as the dilution increases, while the other three capture the benchmark's curve

inclination. The Coe2017 and Bor2020 superposition formulations maintain the error roughly around 10% through all the dilutions calculated.

Figure 4.38 presents the comparison in terms of the total radiative heat loss of the flame to its surrounding. Around the dilution of 10%, the total radiative heat loss is at its lowest value and then this quantity starts to increase again until roughly the 40% dilution mark.

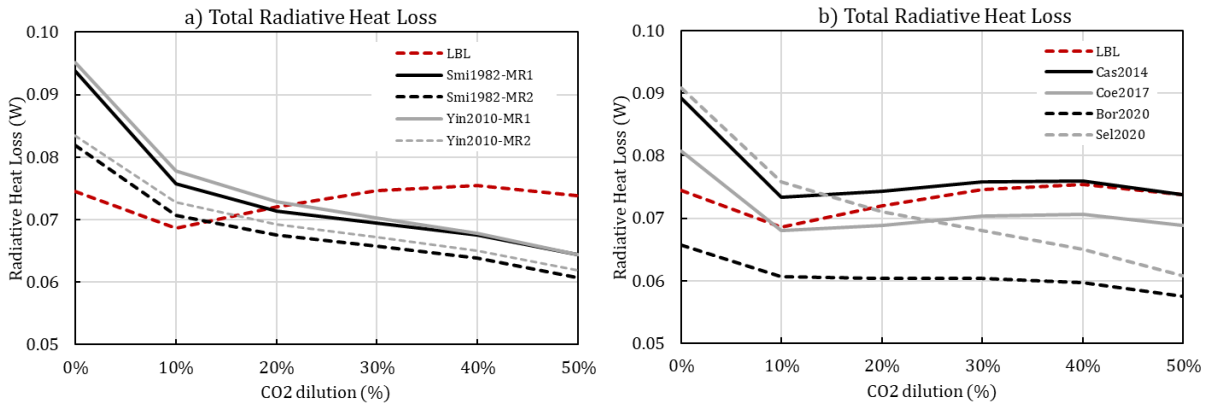

Figure 4.38 – Overview of total heat loss by dilution of CO_2.

Neither one of the models with fixed-*MR* can capture the benchmark behavior, and after the 25% dilution, all models underestimate the total heat loss by the flame. In Figure 4.42b, Sel2020 and Bor2020 models are seen as the least accurate as the curve cannot replicate the behavior of benchmark. This difficulty of the models to replicate the increase in the radiative heat loss is likely due to their incapability to capture the reabsorption zone in the 0.5cm to 0 region, as shown in previous sections. It was seen in the previous figures that in cases of dilution the response of the model was to distribute along the fuel side a portion of the radiative heat source overestimating this absorption and therefore leading to a decrease in the total heat lost.

For an analysis of the effect of different strain rates, each of the selected eight WSGG models and the LBL method are calculated with strain rates of 5, 10, 20, 30, 40 and 60 s^{-1}. Figure 4.43 compares these eight WSGG models with the LBL integration as function of the strain rate for the maximum radiative heat loss.

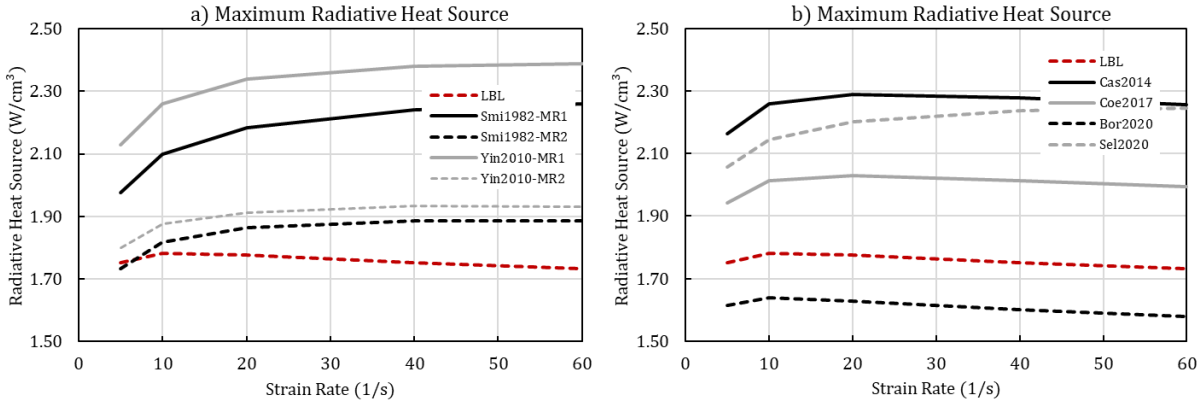

Figure 4.39 – Overview of heat source by strain rate.

The models with fixed molar ratio increase their error in relation to the benchmark as the strain rate increases. It is indicated that this is due to higher gradients as the flame velocity rises. The models with a superposition approach to the calculation of the coefficients seen in Figure 4.43b retain roughly the same accuracy as the strain rate changes, although this difference is around 10% for the two more accurate models. On the other hand, the model with the polynomial formulation has its error proportional to the strain rate.

Figure 4.40 presents the total radiative heat loss calculated by the models and the LBL as function of the flame velocity.

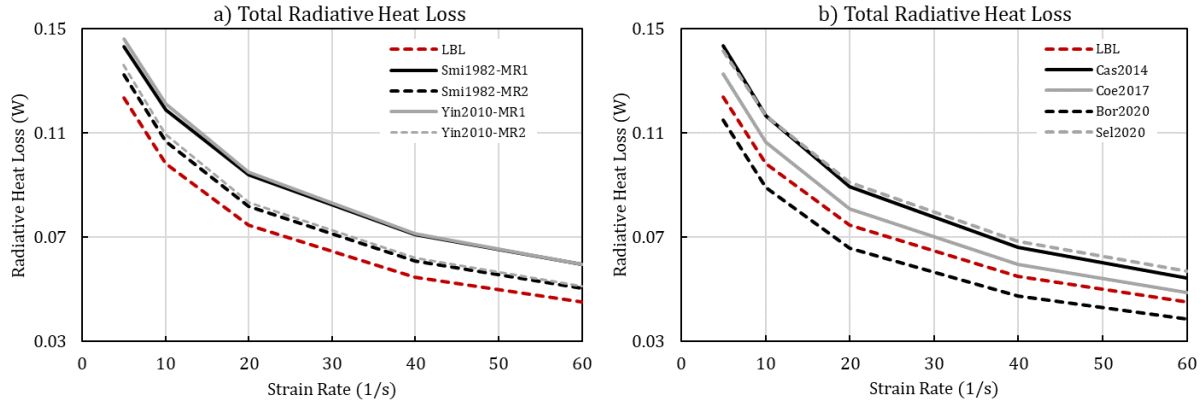

Figure 4.40 – Overview of total heat loss by strain rate.

All models overestimate the total radiative heat loss by the flame. However, all models do accompany the curve behavior of the benchmark. While in Figure 4.44b all models have roughly the same curve inclination as the LBL integration, the superposition models Coe2017 and Bor2020 have closer results to it. In general, although most models present issues correctly

estimating the maximum radiative heat source, they have better results regarding the total radiative heat loss by the flame.

4.4 FLAME EXTINCTION FOR DILUTION OF CO_2

This section compares all models and the LBL solution with the results presented by Bundy et al., 2003. That work assessed with experimental data the critical volume fraction of CO2 required for a counterflow flamejet to extinguish due to radiative losses. Therefore, it was produced results of each model with 0.1% increments in dilution upon each converged calculation. This routine was applied for the strain rates of 5, 10, 20, 24, 28, 30, 32, 40, 60 and 80 s^{-1}. Results from literature are marked as a red "X" in the graphs. Experimental results for strain rates of 5 and 10 s^{-1} were not available.

Figure 4.41 presents the critical carbon dioxide dilution for the LBL integration and the OTA and GG models as well as for the adiabatic case.

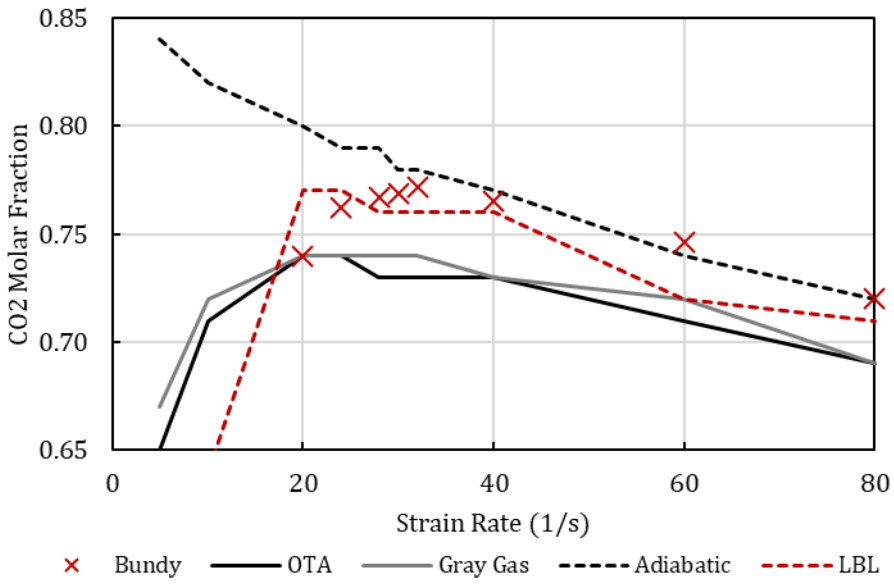

Figure 4.41 – Critical CO_2 required for extinction for LBL, GG, OTA and Adiabatic.

The effect of the radiation is seen in the adiabatic case that can maintain the flame with higher contents of carbon dioxide. The GG and OTA models can reasonably well maintain convergence through different ranges of the strain rate.

Figure 4.46 illustrates the results for the models with the stepwise and linear formulations. Figure 4.46a accounts for the former while Figure 4.46b is for the latter.

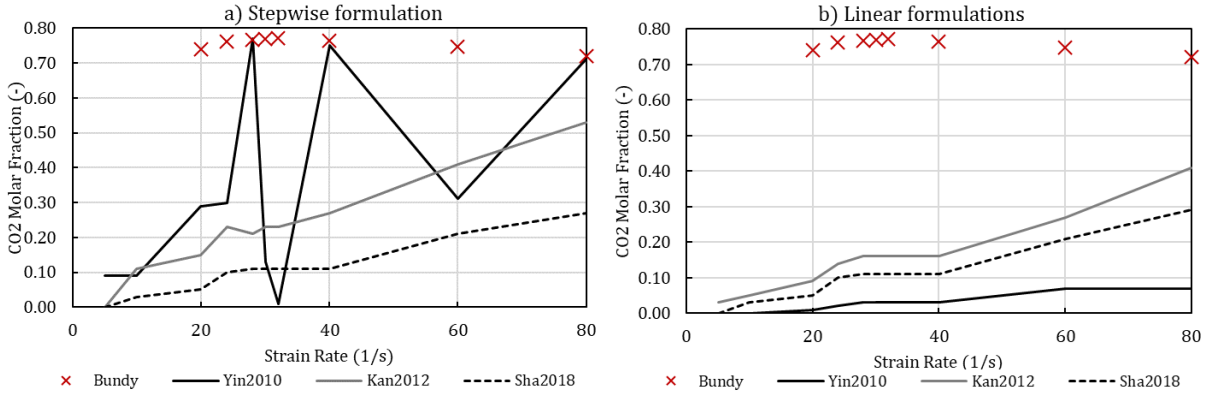

Figure 4.42 – Critical CO_2 required for extinction for WSGG models with stepwise and linear formulations.

As it was seen previously to some extent, these models tend to suffer issues with convergence with the increase in dilution of CO_2. Especially the model Yin2010 with the stepwise formulation that could capture the behavior seem in experimental data for strain rates of 24 and 40 s^{-1} but not for values in between. As shown by Bundy et al., 2003, this region is where the highest critical dilution of CO_2 could be achieved, because is where the counterflow flame has the best stability because the combination of both the radiative and kinetic losses are in its lowest. Therefore, this inability of the model to converge in this region is because it overestimates the radiative heat losses. Furthermore, it can be noted that this effect is also part influence of the strain rate, as increasing it also allows for the models to compute more dilution of carbon dioxide.

Figure 4.47 presents the critical dilution curves for the polynomial models.

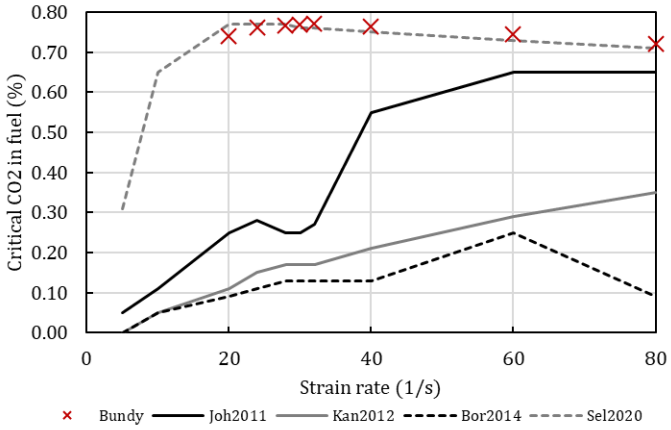

Figure 4.43 – Critical CO_2 required for extinction for polynomial formulation WSGG.

The only model with this formulation that managed to attain convergence and respond like what is expected according to literature is Sel2020. This is likely because of the more robust method for calculating the molar ratio influence while maintaining roughly the same formulation as the other polynomial methods.

Figure 4.48 exhibits the results for the superposition formulations. The model Coe2017 can only converge with roughly 10% CO_2 with a strain rate of 60 s^{-1} and all three models do not converge at all once the strain rate is as high as 80 s^{-1}.

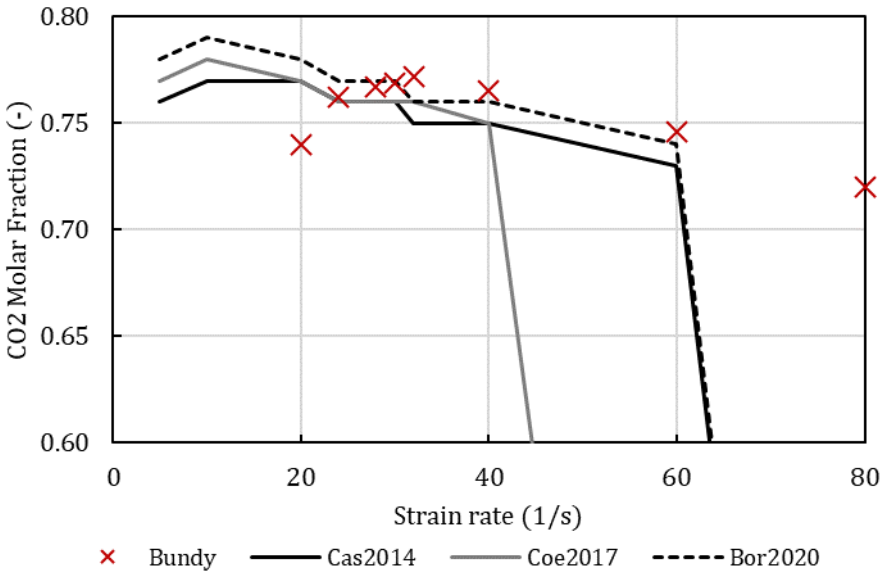

Figure 4.44 – Critical CO_2 required for extinction for superposition WSGG.

Likely due to the method of calculating the coefficients, these models can converge with high values of carbon dioxide in lower strain rates. However, since there were no results presented by Bundy et al., 2003 for this range, these results could be more likely attributed to the robustness of the models and not as much as to a heat balance of the flame.

5. CONCLUSIONS

This work presented a study regarding the radiative spectral modeling in coupled calculations with the chemical reaction and the energy balance for a counter-flow combustion flame of methane and air. The accuracy of several weighted-sum-of-gray-gases models (WSGG), the gray-gas model (GG) and the optically thin approximation (OTA) were evaluated in comparison with the line-by-line integration (LBL) in a wide range of flame velocities and CO_2 dilution of the fuel using the CHEM1D software. The main quantities observed in this study were the maximum radiative heat loss, the total radiative heat loss and the maximum value for the molar fraction of carbon monoxide. After an assessment of the accuracy of the models, their capacity to replicate data available in literature regarding the critical dilution of CO_2 that leads to a flame extinction was evaluated.

At first, the models were compared with the LBL method at a strain rate of 20 s^{-1} and no dilution of CO_2 where it could be seen that WSGG correlations for a molar ratio of 1:1 had larger error with those of 2:1 having better results. Varying-*MR* formulations with more had better results, especially the model proposed by Bordbar et al., 2014, which presented errors below 1%. The WSGG showed good results when considering the molar fraction of CO, with no correlation above 3% inaccuracy.

Then dilution of carbon dioxide at the fuel side was introduced, which diminished the average molar ratio of the domain, improving the results of both sets of models with “fixed” molar ratio correlations for dilutions of up to 20% and for higher values only the 1:1 models were in agreement to the reference. However, several of the models with varying-*MR* correlations could not attain a convergence of the calculation, with only the models by Selhorst et al., 2020 and those that use the superposition method managing to achieve results. This is likely could be firstly because the fuel side of the domain with dilution has high values of partial pressure of carbon dioxide and close to zero molar ratio, which is a scenario outside the range of application of these formulations. Secondly, because the high gradients of temperature and species concentration combined with the DOM method and the increased quantity of coefficients for the fitting of these models cannot reach convergence in the specified residual criteria. One could consider relaxing the criteria, but tests made with the criteria up to 10^{-5} (originally the cases were with 10^{-7}) were performed and yet convergence was not achieved for all dilutions. Increasing further this relaxation would be a compromise at the results themselves. On the other hand, results without accounting for radiative losses could lead to errors of almost 20% in the prediction of the carbon monoxide.

After this, the effect of decreasing the strain rate (or the flame velocity) was considered. In general, the WSGG models improved with this change, indicating that the gradients of temperature and species formation have great impact in the overall performance of the model. The GG and OTA models presented an opposite trend, where the errors for predicting radiative quantities increased with lower strain rates.

Next, for selected models that had better results, it was shown an overview of the main quantities in observation at this work as function of the dilution of CO_2 and then as of the strain rate. In the case of the dilution of CO_2, it was possible to see that only the correlations with the superposition formulation were capable of accurately following the behavior of the LBL integration for the maximum radiative heat loss and total radiative heat loss, in special the correlations proposed by Coelho et al., 2017. For this and the one proposed by Bordbar et al., 2020, the inaccuracy when calculating the maximum radiative heat source was in all cases around the 12% and for the total radiative heat loss was around 10%. Therefore, these correlations presented good robustness and predictability.

Finally, the critical dilution of CO_2 that each varying-*MR* correlation can account for in its calculation before not being able to attain convergence was studied. Besides the LBL and the simpler models, the only WSGG correlation that could adequately converge with CO_2 contents on par of what is presented in literature was the Selhorst et al., 2020. Although the superposition model had stable errors through the previous parts of this study, they cannot converge well in higher strain rates. On the other hand, the other correlations have shown that they increase robustness with higher strain rates, although values are still far from what was expected from literature.

In general, most WSGG correlations evaluated in this work have attained reasonable results with estimations of the maximum radiative heat source around 10%, the total radiative heat loss below 20% and the maximum molar fraction of carbon monoxide below 5%. Some correlations even presented very good results that would be below 5% for any of these observed quantities in some scenarios. However, the main issue presented in this study was the difficulty of correlations to combine robustness with accuracy and predictability. In other words, there is no correlation that is universally adequate to each, and all cases presented, with variations of strain rate and fuel dilution.

The formulation that has the better compromise between these three factors are that of the superposition method, where the influence of water vapor and carbon dioxide are calculated separately then combined for calculating the coefficients. Especially the correlations proposed by Coelho et al., 2017 and Bordbar et al., 2020. Although these do not manage to reach

convergence in higher strain rates, a case could be made as for higher flames velocities the radiation is a less preeminent form of heat loss.

5.1 SUGGESTIONS FOR FURTHER WORKS

After considering the findings, this work proposes the following further research:

- Implementation and assessment of the Spectral-Line Weighted-Sum-of-Gray-Gases (SLW) model, which allows for further detailing in the treatment of the radiation spectrum, gases mixtures, and non-isothermal and non-homogeneous media, and therefore is expected to provide better results in comparison.
- Evaluation of the accuracy of the models in cases of dilution of N_2, which also has experimental data available in literature for comparison. To do such assessment would be necessary also to implement a new chemistry model that would detail reaction steps of the N_2.
- Evaluation of the formation of NO_x in cases with or no dilution of CO_2 or N_2. As with the previous suggestion, this would require a new chemistry model that contains the reaction steps of N_2.
- Consider WSGG correlations that evaluate the effects of soot formation. Soot is product mainly present in incomplete combustion, which is presented in diffusion flames.

REFERENCES

Bidi, M., Hosseini, R., and Nobari, M.R.H. Numerical analysis of methane-air combustion considering radiation effect, **Energy Conversion and Management**, vol. 49, p. 3634-3647, 2008.

Bordbar, M.H., Wĕcel, G., and Hyppänen, T. A line by line based weighted sum of gray gases model of inhomogeneous CO_2-H_2O mixture in oxy-fired combustion, **Combustion and Flame**, vol. 161, p. 2435-2445, 2014.

Bordbar, M.H., Fraga, G.C., and Hostikka, S. An extended weighted-sum-of-gray-gases model to account for all CO_2-H_2O molar fraction ratios in thermal radiation, **International Communications in Heat and Mass Transfer**, vol. 110, 2020.

Bundy, M., Hamins, A., and Ki Yong Lee. Suppression limits of low strain rate non-premixed methane flames, **Combustion and Flame**, vol 133, p. 299-310, 2003.

Cassol, F., Brittes, R., França, F.H.R., and Ezeyoke, O.A. Application of the weighted-sum-of-gray-gases model for media composed of arbitrary compositions of H_2O, CO_2 and soot, **International Journal of Heat and Mass Transfer**, vol. 79, p. 796-806, 2014.

Celik, I., Ghia, U., and Roache, P.J. Procedure of Estimation and Reporting of Uncertainty Due to Discretization in CFD Applications, **Journal of Fluids Engineering**, vol. 130, 2008.

Centeno, F.R., da Silva, C.V., Brittes, R., and França, F.H.R. Numerical simulations of the radiative transfer in a 2D axisymmetric turbulent non-premixed methane-air flame using up-to-date WSGG and gray-gas models, **Journal of the Brazilian Society of Mechanical Sciences and Engineering**, vol. 37, 2015.

Chan, S.H., Yin, J.Q., and Shi, B.J. Structure and extinction of methane-air flamelet with radiation and detailed chemical kinetic mechanism, **Combustion and Flame**, vol 112 (3), p. 445-456, 1998.

Chandrasekhar, S. **Radiative Transfer**. Dover Publications, 1960.

Coelho, F.R. **Geração de Novas Correlações da Soma-Ponderada-de-Gases-Cinza para H_2O e CO_2 em Alta Pressão**. Dissertação de Mestrado, Universidade Federal do Rio Grande do Sul, 2017.

Da Silva, F.N.R. **Numerical Study of Radiative Heat Loss on Near-Extinction Laminar Non-Premixed Flames employing Detailed Chemistry and the FGM Method**. Master's Dissertation, Universidade Federal do Rio Grande do Sul, 2020.

De Goey, L.P.H., and Boonkkamp, J.H.M.T. A flamelet description of premixed laminar flames and the relation with flame stretch, **Combustion and Flame**, vol. 119(3), p. 253-271, 1999.

Dorigon, L.J., Duciak, G., Brittes, R., Cassol, F., Galarça, M., and França, F.H.R. WSGG correlations based on HITEMP2010 for computation of thermal radiation in non-isothermal, non-homogeneous H_2O/CO_2 mixtures, **International Journal of Heat and Mass Transfer**, vol.64, p. 863-873, 2013.

Hoerlle, C. **Estudo Numérico de Chamas Laminares Difusivas de CH4 Diluído com CO2 Empregando Mecanismos Cinéticos Globais e a Técnica Flamelet-Generated Manifold**. Master's thesis, Universidade Federal do Rio Grande do Sul, Porto Alegre, Brasil, 2015.

Howell, J., Menguc, M., and Siegel, R. **Thermal Radiation Heat Transfer**. CRC Press, 2016.

Incropera, F., DeWitt, D., Bergman, T., and Lavine, A. **Fundamentals of Heat and Mass Transfer**. Wiley, 2008.

Johansson, R., Leckner, B., Andersson, K., and Johsson, F. Account for variations in the H_2O to CO_2 molar ratio when modelling gaseous radiative heat transfer with the weighted-sum-of-gray-gases model, **Combustion and Flame**, vol. 158(5), p. 893-901, 2011.

Kanganwanpongpan, T., França, F.H., da Silva, R.C., Schneider, P.S., and Krautz, H.J. New correlations for the weighted-sum-of-gray-gases model in oxy-fuel conditions based on HITEMP2010 database, **International Journal of Heat and Mass Transfer**, vol. 55(25), p. 7419-7433, 2012

Krishnamoorthy, G. A new weighted-sum-of-gray-gases model for CO_2-H_2O gas mixtures, **International Communications in Heat and Mass Transfer**, vol. 37, p. 1182-1186, 2010.

Modest, M.F. **Radiative Heat Transfer**, 2nd edition, McGraw-Hill, New York, 2003.

Roache, P.J. Perspective: a method for uniform reporting of grid refinement studies, **Journal of Fluids Engineering**, vol. 116, p. 405-413, 1994.

Rothman, L.S., Rinsland, C.P., Goldman, A., Massie, S.T., Edwards, D.P., and Flaud, J.-M et al. The HITRAN Molecular Spectroscopic Database and HAWKS (HITRAN Atmospheric Workstation): 1996 edition, **Journal of Quantitative Spectroscopy and Radiative Transfer**, vol. 60(5), p. 665-710, 1996.

Rothman, L.S., Gordon, I.E., Barber, R.J., Dothe, H., Gamache, R.R., Goldman, A., Perevalov, V.I., Tashkun, S.A., and Tennyson, J. HITEMP, the high-temperature molecular spectroscopic database, **Journal of Quantitative Spectroscopy & Radiative Transfer**, vol. 111, p. 2139-2150, 2010.

Selhorst, A.H.B. **New WSGG correlation accounting for variations on the mole ratio and the partial pressure of the participating species.** Master's Dissertation, Universidade Federal do Rio Grande do Sul, 2020.

Shan, S., Qian, B., Zhou, Z., Wang, Z., and Cen, K. New pressurized WSGG model and the effects of pressure on the radiation heat transfer of H_2O/CO_2 gas mixtures, **International Journal of Heat and Mass Transfer**, vol. 121, p. 999-1010, 2018.

Smith, T.F., Shen, Z.F., and Friedman, J.N. Evaluation of coefficients for weighted sum of gray gases model, **Journal of Heat Transfer**, vol. 104, p. 602-608, 1982.

Smooke, M.D. and Giovangigli, V. Formulation of the Premixed and Nonpremixed Test Problems, **Lecture Notes in Physics**, vol. 384, 1991.

Somers, B. **The simulation of flat flames with detailed and reduced chemical models**. Eindhoven University of Technology, 1994.

Wang, A., and Modest, M.F. Photon Monte Carlo simulation for radiative transfer in gaseous media represented by discrete particle fields, **Journal of Heat Transfer**, vol. 128 (10), p. 1041-1049, 2006.

Yin, C., Johansen, L.C.R., Rosendahl, L.A., and Kaer, S.K. New Weighted Sum of Gray Gases Model Applicable to Computational Fluid Dynamics (CFD) Modeling of Oxy-Fuel Combustion: Derivation, Validation, and Implementation, **Energy Fuels**, vol. 24, p. 6275-6282, 2010.

Yin, C. Refined Weighted Sum of Gray Gases Model for Air-Fuel Combustion and Its Impacts, **Energy Fuels**, vol. 27 (8), p. 4258-4269, 2013.